# CAPTURING DYNAMICS OF MARINE INORGANIC CARBON FLUXES FROM DIURNAL TO DECADAL TIMESCALES

By
Sophie Ning-Shin Chu

B.S. Chemical Engineering
Columbia University in the City of New York, 2009

Submitted in partial fulfillment of the requirements for the degree of
Doctor of Philosophy
at the
MASSACHUSETTS INSTITUTE OF TECHNOLOGY
and the
WOODS HOLE OCEANOGRAPHIC INSTITUTION

February 2017



Author _____
Joint Program in Oceanography/Applied Ocean Science & Engineering
Massachusetts Institute of Technology
& Woods Hole Oceanographic Institution
February 9, 2017

Certified by _____
Zhaohui Aleck Wang
Woods Hole Oceanographic Institution
Thesis Supervisor

Accepted by _____
Shuhei Ono
Chair, Joint Committee for Chemical Oceanography
Massachusetts Institute of Technology
& Woods Hole Oceanographic Institution

# Capturing dynamics of inorganic carbon fluxes from diurnal to decadal timescales

By
Sophie N. Chu

Submitted to the MIT-WHOI Joint Program in Oceanography and Applied Ocean Science and Engineering, in partial fulfillment of the requirements for the degree of Doctor of Philosophy in Chemical Oceanography

**Abstract**

The marine carbon cycle plays an important role in regulating Earth's climate. The vastness of the open ocean and the large variability in the coastal ocean provide obstacles to accurately quantify storage and transport of inorganic carbon within marine ecosystems and between marine and other earth systems.

Thus far, the open ocean has been the only true net sink of anthropogenic carbon dioxide ($C_{anthro}$) emissions. However, ocean storage of $C_{anthro}$ is not uniformly distributed. Changes in water chemistry in the Northeast Pacific were quantified to estimate the amount of $C_{anthro}$ stored in this region over the last decade. This additional $C_{anthro}$ was found to cause acidification and aragonite saturation horizon shoaling at rates towards the higher end of those found in Pacific and Atlantic Ocean basins, making the Northeast Pacific one of the most sensitive regions to the invasion of anthropogenic carbon dioxide.

Due to large variability in biogeochemical signals in coastal oceans, it is challenging to accurately assess carbon fluxes across different boundaries, such as tidal exchange between coastal wetlands and coastal oceans. Coastal salt marshes have been suggested to be a large net $CO_2$ sink, thus designated as a type of "blue carbon." However, accurate and dynamic estimates of carbon fluxes to and from tidal marshes are still premature, particularly carbon fluxes from marshes to the coastal ocean via tidal exchange, often referred to as marsh lateral fluxes. In this thesis, lateral total alkalinity (TA) and dissolved inorganic carbon (DIC) export fluxes were realistically quantified using high frequency time-series, in situ data. High-resolution fluxes permitted a closer look at how marsh generated TA and DIC are being exported over diurnal, spring-neap, and seasonal scales. I investigated the best way to capture variability of marsh exports via traditional bottle sampling and assessed uncertainties associated with different sampling strategies. Marsh TA and DIC exports significantly modified buffering capacity of coastal waters. This work contains the first realistic estimate of TA exports from a tidal salt marsh. Accurate estimates of DIC and TA fluxes indicate the significance of salt marshes to the coastal carbon and alkalinity budgets.

Thesis supervisor: Zhaohui Aleck Wang
Title: Associate Scientist, Woods Hole Oceanographic Institution

# Acknowledgements

I would like to express my sincere gratitude to my thesis advisor, Aleck Wang, for guiding me through my PhD journey. His high expectations pushed me to succeed in ways beyond what I thought I could achieve. I greatly appreciate the advice and thoughtfulness of my thesis committee Kevin Kroeger, Harry Hemond, and Dan McCorkle who have all contributed to my thesis. Thank you Dan for always checking in on me even before joining my committee. My defense chair Scott Doney also provided me with assistance on the first chapter of my thesis. Bernhard Peucker-Ehrenbrink who was the Education Coordinator and valued student input regarding the Joint Program. I also had the pleasure of having Bernhard, Scott, and Dan as teachers and would like to them them as well as all of the scientists who taught classes and the TAs who had to grade our homework. Thank you to WHOI Academic Programs Office and EAPS Education Office as well as Joint Program administrators for helping the program be successful.

I would like to recognize everyone who has helped with instrumentation, and collecting or analyzing data for this thesis. Thank you to Al Bradley and Fritz Sonnichsen for patience and determination in getting the CHANOS to work. Thank you to members of Kevin's lab at USGS who helped with field work at Sage Lot Pond especially Meagan Gonneea for undertaking the planning and organizing, Jennifer O'Keefe Suttles, Adrian Mann, and Sandy Brosnahan. Big thank you to Neil who helped me understand how to calculate water fluxes. I would also like to thank the *R/V New Horizon* captain and crew as well as everyone who participated on that cruise. Thank you to Gareth Lawson and Amy Maas for providing me opportunities to join on the *R/V Tioga* and become an expert at identifying pteropods. Thank you to volunteers and summer students for their help in collecting and analyzing salt marsh samples.

I am incredibly grateful to members of the Wang lab, especially Katherine Hoering who showed me the ropes when I first came to the lab, Kate Morkeski for taking on the CHANOS and for housing me, and Zoe Sandwith for helping with whatever was asked of her and for Maggie.

Thank you to the largest chemistry cohort in JP history (?), especially Winn, Nick, Emily, Sarah, and Jamie for providing me with support and friendship, particularly when food was involved. To Julie and Isabela, forever my Harvard/Wilson roommates.

To Nicholas, who has been by my side through the ups and downs of this PhD, thank you for your patience and understanding. To my family, my mom and dad and my two older sisters, who always believed in me and provided unwavering support and encouragement, thank you for everything.

The work in this thesis was supported by the National Science Foundation Graduate Research Fellowship Program, Link Foundation Ocean Engineering and Instrumentation Ph.D. Fellowship, WHOI Academic Programs Office, MIT PAOC Houghton Fund, MIT Student Assistance Fund, WHOI Innovative Technology Award (PI: Wang), National Institute of Science and Technologies (NIST no. 60NANB10D024, PIs: Camilli, Wang), USGS LandCarbon Program, USGS Coastal and Marine Geology Program, NSF (OCE-1233654, PI: Wang; OCE-1041068 PIs: Lawson, Wang, Wiebe, Lavery; OCE-1459521 PIs: Wang, Kroeger, Gonneea), and NOAA Science Collaborative (NA09NOS4190153, PIs: Leschen, Roth, Surgeon-Rogers, Tang, Kroeger, Ganju, Moseman-Valtierra, Abdul-Aziz, Emmett-Mattox, Emmer, Crooks, Megonigal, Walker, Weidman).

## Table of contents

**List of Figures**

**Chapter 2 Figures**



**Chapter 3 Figures**



**Chapter 4 Figures**

**List of Tables**

**Chapter 2 Tables**



**Chapter 3 Tables**



**Chapter 4 Tables**

# Chapter 1

# Introduction

## 1.1 Overview

The marine carbon cycle plays an important role in regulating Earth's climate. The concentration of carbon dioxide ($CO_2$) in the atmosphere has a large effect on climate due to its ability to act as a greenhouse gas to trap heat (Arrhenius, 1896). The atmosphere, terrestrial biosphere, and ocean act as the main carbon reservoirs where carbon is transferred, transformed, and stored over varying time scales. From 1750 to 2013, cumulative $CO_2$ emissions of 580 $\pm$ 70 Pg C were released to the atmosphere from fossil fuel burning, cement manufacture, and land use change (Ciais et al., 2013; Le Quéré et al., 2015). Less than half of those emissions have accumulated in the atmosphere while the remainder has been absorbed by the ocean and land. While it is clear that the ocean has been a net sink for anthropogenic carbon dioxide emissions, there still exist large uncertainties regarding how and where this carbon is stored in the ocean and how it will affect marine ecosystems and evolve under future climate change. Using directly measured ocean interior observations to estimate decadal scale inventory changes will improve our ability to monitor changes in ocean carbon storage in the future.

The coastal ocean plays a disproportionately large role in the marine carbon cycle (Cai et al., 2006; Cai 2011; Bauer et al., 2013). While the ocean as a whole is clearly a

significant sink for anthropogenic $CO_2$, the role of the coastal ocean as a net sink or source of atmospheric $CO_2$ has been controversial topic, where the magnitude and even sign of net $CO_2$ flux has been debated (Smith and Mackenzie 1987; Smith and Hollibaugh 1993; Gattuso et al., 1998; Wollast 1998; Borges 2005; Borges et al., 2005; Chen and Borges 2009). More recently, Bauer et al. (2013) has suggested that while continental shelves and wetlands act as $CO_2$ sinks, estuaries as well as lakes and rivers act as $CO_2$ sources. The magnitude of these sinks and sources and how they interact across boundaries are based on limited data and still carry large uncertainties. In this work, I quantified the TA and DIC fluxes due to tidal exchange from coastal salt marshes to coastal oceans, or marsh lateral fluxes. These fluxes vary greatly over diurnal, tidal, seasonal, and annual timescales and require high-frequency measurements at these timescales to capture this variability.

This thesis aims to examine and quantify the temporal variability of inorganic carbon fluxes that occur in the open ocean and coastal salt marshes to evaluate the role of different marine systems as a carbon sink or source to the atmosphere or adjacent water bodies. In this thesis, I will specifically address the following questions to improve the current understanding of inorganic carbon cycling in the coastal and open oceans:

1) How did the Northeast Pacific Ocean contribute to the oceanic carbon sink and how did seawater chemistry change over this region in the last decade?

2) How can salt marsh lateral fluxes to the coastal carbon cycle be quantified and sampled more accurately to help assess whether or not salt marshes act as carbon sinks?

3) How do lateral fluxes of inorganic carbon and alkalinity from salt marshes impact coastal water chemistry and the coastal carbon cycle?

### 1.2 Northeast Pacific carbon sink

For Chapter 2, I sought to contribute the scientific understanding of the ocean's role as a sink for anthropogenic carbon dioxide ($C_{anthro}$). Oceans have already absorbed a quarter to a third of the total carbon emissions from fossil fuel burning, land use change, and cement manufacture (Sabine et al., 2004; Khatiwala et al., 2009; Ciais et al., 2013). Since the beginning of the industrial era, atmospheric $pCO_2$ has increased from 280 ppm to over 400 ppm (Scripps, 2016). By 2100, atmospheric $CO_2$ levels are projected to reach near 1000 ppm under a business-as-usual scenario (IPCC, 2014). This increase in $CO_2$ in the atmosphere and subsequent absorption by the ocean has already and will continue to have multifaceted impacts on seawater chemistry and marine ecosystems through several direct and indirect pathways such as ocean warming, deoxygenation, ocean acidification, and the shoaling of the aragonite saturation horizon, among others.

Storage of anthropogenic carbon in the ocean is a major driver of change in seawater chemistry, but it is not evenly distributed across ocean basins. Despite being the largest ocean basin, the Pacific only stores about 18% of the global ocean inventory of anthropogenic $CO_2$ (Feely et al., 2001). The Northeast Pacific is located at the end of the ocean meridional overturning circulation and is a region containing particularly low concentrations of $C_{anthro}$ due to both the lack of significant deep-water formation and slow circulation that limit the transport $C_{anthro}$ into the ocean interior (Stuiver et al.,

1983; Reid 1997; Sabine et al., 2002). Being at the end of the ocean conveyor belt also causes the Northeast Pacific waters to have naturally high dissolved inorganic carbon (DIC) concentrations, low pH, low buffering capacity, and a relatively shallow aragonite saturation horizon compared to other ocean basins. These conditions cause the water column to be close to calcium carbonate undersaturation and sensitive to future chemical changes.

An extended multiple linear regression (eMLR) (Friis et al., 2005; Tanhua et al., 2007) approach was applied to data collected from two cruises along a repeated hydrographic line, P17, in the Northeast Pacific in 2001 and 2012 to estimate the change in the anthropogenic $CO_2$ inventory over the decade. The eMLR method is ideal for estimating changes in $C_{anthro}$ using data from reoccupations of cruise transects over decadal scales. It can provide a realistic change in DIC by removing isopycnal heave at seasonal and interannual scales (Doney et al., 2007; Levine et al., 2008; Wanninkhof et al., 2010). The eMLR method has several advantages over other $C_{anthro}$ methods in that it does not require any assumptions of preindustrial concentrations or require water mass ages. The method does, however, assume that the relationships between the chosen regression parameters do not change substantially for the time period over which the eMLR is applied.

It is increasingly important to quantify the ocean's ability to absorb and store anthropogenic carbon dioxide as storage capacity is expected to slow down due to the increase of temperature and decrease of buffering capacity (Levitus 2005; Sabine et al.,

2004). The storage rate estimate made from this study can be incorporated into the global inventory of $C_{anthro}$ storage rate data to allow for further analysis of the uptake and storage capacity of the ocean and its role in the global carbon cycle.

### 1.3 Salt marsh carbon and alkalinity exports

Coastal ecosystems are important ecologically and economically. Coastal oceans, though they cover a small surface area, represent some of the largest carbon fluxes in the global ocean (Borges 2005; Borges et al., 2005; Cai et al., 2006; Cai 2011). However, despite their biogeochemical significance, large variability and limited sampling over spatiotemporal scales make it difficult to characterize and accurately quantify fluxes being transferred from the land to the coast and the coast to the open ocean. The variability of biogeochemical fluxes are due in part to the relatively shallow water column of coastal regions compared to the open ocean that allows for tight coupling between sediments, water, and atmosphere. Fundamental to understanding coastal systems is being able to make measurements at an appropriate timescale to the processes being studied. Because of the complex dynamics of coastal fluxes, high frequency measurements are necessary to capture variability.

Wetlands, in particular, are regions of high productivity that laterally export dissolved and particulate carbon to adjacent coastal waters (Duarte et al., 2005; Cai 2011). It has been suggested that wetlands are likely a $CO_2$ sink due to high rates of plant production, burial, and organic carbon export (Woodwell et al., 1973; Hopkinson 1988; Bouillon et al., 2008, Bauer et al., 2013). However, the net $CO_2$ sink in wetlands is

difficult to quantify because of the lack of accurate estimates of surface area and a complete budget of carbon fluxes into and out of wetlands. The export from wetlands via tidal exchange is particularly challenging to assess as it varies on time scales ranging from minutes to tidal to annual and inter-annual.

Intertidal salt marshes are among the most productive ecosystems with an average net ecosystem production greater than 1500 g C $m^{-2}$ $yr^{-1}$ (Duarte et al., 2005). Salt marshes have been designated as important carbon sinks that sequester $CO_2$ into their underlying sediments as well as their living and non-living plant biomass (Chmura et al., 2003; Duarte et al., 2005; Mcleod et al., 2011). In addition to storing carbon, studies have suggested that through tidal exchange, salt marshes export organic carbon, nutrients and more recently, inorganic carbon (Morris and Whiting 1986; Cai and Wang 1998; Raymond et al., 2000; Wang and Cai 2004; Wang et al., 2016). It has been suggested that salt marshes are also an important source of alkalinity, which is generated in marsh sediments by anaerobic respiration processes including sulfate reduction and subsequent pyrite burial (Howarth and Teal 1979; Giblin and Howarth 1984; Giblin 1988; Giblin and Wieder 1992; Hu and Cai 2011). However, there has not yet been an estimate of lateral alkalinity export from salt marshes based on direct measurements. In Chapter 3, bottle samples and measured physical and biogeochemical parameters from high frequency, in situ sensors were used to constrain an empirical model to estimate high-resolution lateral fluxes of TA over tidal and seasonal scales following a similar method used to estimate DIC export in Wang et al. (2016) at the same location. These

high-resolution instantaneous flux estimates were used to evaluate tidal and seasonal signals in order to determine when the largest amount of alkalinity export occurs and to provide insight into how marshes are producing and exporting TA throughout the year. An analogous empirical approach was used to estimate the salt marsh DIC export to investigate the relationship between DIC and TA export in regards to the importance of aerobic and anaerobic respiration processes. Estimates of TA export from salt marshes are critical to help evaluate how salt marshes contribute buffering capacity to the coastal ocean, which is increasingly important to understand as tidal wetlands are being rapidly destroyed by deforestation, urbanization and climate change (Woodroffe 1995; Duarte et al., 2005; Silliman et al., 2009; Hopkinson et al., 2012).

In Chapter 4, in-situ high frequency DIC data measured by a state-of-the-art sensor called CHANnelized Optical Sensor (CHANOS), revealed intricacies of carbon cycling never before studied. Previous studies of DIC export typically relied on bottle sampling periods of hourly to half a tidal cycle over monthly to seasonal intervals, and thus required large interpolation between sampling events (Capone et al., 1983; Morris and Whiting 1986; Neubauer and Anderson 2003; Wang and Cai 2004). These studies from salt and freshwater marshes along the U.S. east coast from Virginia to Georgia reported a DIC export of ~150-200 g C $m^{-2}$ $yr^{-1}$. Wang et al. (2016) reported a revised estimate of 414 g C $m^{-2}$ $yr^{-1}$, more than twice the previous export, using an empirical model approach with high frequency data similar to that used in Chapter 3 of this thesis. This indicates the importance of using high frequency to estimate fluxes in coastal

habitats. Scaled up to U.S. East Coast marsh area, this export is one of the largest marsh fluxes and a major term of the East Coast carbon budget, greater than riverine dissolved organic carbon or DIC export. DIC fluxes estimated from direct sensor measurements in Chapter 4 were used to verify the DIC fluxes reported in Chapter 3. Such verification is critical to help to establish acceptable methods to constrain carbon fluxes exported from tidal wetlands. With high frequency, direct measurements, it was possible to fully characterize timescales over which the DIC export occurred in order to inform best sampling strategies to capture true dynamics of carbon exports from tidal wetlands.

**References**


Arrhenius, Svante (1896). "On the Influence of Carbonic Acid in the Air Upon the Temperature of the Ground." Philosophical Magazine 41: 237-76.

Bauer, J. E., W. J. Cai, P. A. Raymond, T. S. Bianchi, C. S. Hopkinson, and P. A. G. Regnier. 2013. The changing carbon cycle of the coastal ocean. Nature 504: 61-70.

Borges, A. V. 2005. Do we have enough pieces of the jigsaw to integrate CO2 fluxes in the coastal ocean? Estuaries 28: 3–27. doi:10.1007/BF02732750

Borges, A. V., B. Delille, and M. Frankignoulle (2005), Budgeting sinks and sources of CO2 in the coastal ocean: Diversity of ecosystems counts, Geophys. Res. Lett., 32(14), n/a-n/a, doi:10.1029/2005GL023053.

Bouillon, S., and others. 2008. Mangrove production and car- bon sinks: A revision of global budget estimates. Global Bio- geochem. Cycles 22: GB2013, doi:10.1029/2007GB003052

Cai, W. J. 2011. Estuarine and coastal ocean carbon paradox: CO2 sinks or sites of terrestrial carbon incineration? Annu. Rev. Mar. Sci. 3: 123-145.

Cai, W. J., Dai, M., & Wang, Y. (2006). Air - sea exchange of carbon dioxide in ocean margins: A province - based synthesis. Geophysical Research Letters, 33(12).

Capone, D. G., D. D. Reese, and R. P. Kiene. 1983. Effects of metals on methanogenesis, sulfate reduction, carbon- dioxide evolution, and microbial biomass in anoxic salt-marsh sediments. Appl. Environ. Microbiol. 45: 1586–1591.

Chen, C. T. A., and A. V. Borges. 2009. Reconciling opposing views on carbon cycling in the coastal ocean: Continental shelves as sinks and near-shore ecosystems as sources of atmospheric CO2. Deep-Sea Research II 56: 578-590.

Chmura, G. L., S. C. Anisfeld, D. R. Cahoon, and J. C. Lynch. 2003. Global carbon sequestration in tidal, saline wetland soils. Global Biogeochem. Cy. **17**. doi: 1029/2002GB00191.

Ciais, P., Sabine, C., Bala, G., Bopp, L., Brovkin, J., & Thornton, P. (2013). IPCC, 2013: Climate Change 2013: The Physical Science Basis. Contribution of Working Group I to the Fifth Assessment Report of the Intergovernmental Panel on Climate Change.

Doney, S. C., S. Yeager, G. Danabasoglu, W. G. Large, and J. C. McWilliams (2007), Mechanisms governing interannual variability of upper ocean temperature in a global hindcast simulation, J. Phys. Oceanogr., 37, 1918–1938, doi:10.1175/JPO3089.1.

Duarte, C. M., J. J. Middelburg, and N. Caraco. 2005. Major role of marine vegetation on the oceanic carbon cycle. Biogeosciences 2: 1-8.

Feely, R. A., C. L. Sabine, T. Takahasi, and R. Wanninkhof (2001), Uptake and storage of carbon dioxide in the ocean: The global CO2 survey, Oceanography, 14(4), 18–32, doi:10.5670/oceanog.2001.03.

Friis, K., A. Ko€rtzinger, J. P€atsch, and D. W. R. Wallace (2005), On the temporal increase of anthropogenic CO2 in the subpolar North Atlantic, Deep Sea Res., Part I, 52(5), 681–698, doi:10.1016/j.dsr.2004.11.017.

Gattuso, J. P., Frankignoulle, M., & Wollast, R. (1998). Carbon and carbonate metabolism in coastal aquatic ecosystems. Annual Review of Ecology and Systematics, 405-434.

Giblin, A. E. 1988. Pyrite Formation in Marshes during Early Diagenesis. Geomicrobiol. J. 6: 77-97.

Giblin, A. E., and R. W. Howarth. 1984. Porewater Evidence for a Dynamic Sedimentary Iron Cycle in Salt Marshes. Limnol. Oceanogr. 29: 47-63.

Giblin, A. E., and R. K. Wieder. 1992. Sulfur cycling in marine and freshwater wetlands. In R. W. Howarth, J. W. Stewart, and M. V. Ivanov [eds.], Sulphur cycling on the Continents. SCOPE.

Herrmann, M. and others 2015. Net ecosystem production and organic carbon balance of U.S. East Coast estuaries: A synthesis approach. Global Biogeochem. Cy. 29: 96-111.

Hopkinson, C. S. 1988. Patterns of organic carbon exchange between coastal ecosystems—the mass balance approach in salt marsh ecosystems. In B.-O. Jansson [ed.], Coastal- offshore ecosystem interactions. Lecture notes on coastal and estuarine studies. Springer.

Hopkinson, C. S., W. J. Cai, and X. P. Hu. 2012. Carbon sequestration in wetland dominated coastal systems - a global sink of rapidly diminishing magnitude. Curr Opin Env Sust **4:** 186-194.

Howarth, R. W., and J. M. Teal (1979), Sulfate reduction in a New England Salt Marsh, Lim, 24(6), 999–1013.

Hu, X. P., and W. J. Cai. 2011. An assessment of ocean margin anaerobic processes on oceanic alkalinity budget. Global Biogeochem. Cy. 25. doi: doi:10.1029/2010GB003859.

IPCC (2014), Climate Change 2014: Synthesis Report. Contribution of Working Groups I, II and III to the Fifth Assessment Report of the Intergovernmental Panel on Climate Change, edited by Core Writing Team, R. K. Pachauri and L. A. Meyer, IPCC, Geneva, Switzerland, 151 pp.

Khatiwala, S., F. Primeau, and T. Hall (2009), Reconstruction of the history of anthropogenic CO(2) concentrations in the ocean., Nature, 462(7271), 346–349, doi:10.1038/nature08526.

Le Quéré, C., T. Takahashi, E. T. Buitenhuis, C. Ro€denbeck, and S. C. Sutherland (2010), Impact of climate change and variability on the global oceanic sink of CO2, Global Biogeochem. Cycles, 24, GB4007, doi:10.1029/2009GB003599.

Levine, N. M., S. C. Doney, R. Wanninkhof, K. Lindsay, and I. Y. Fung (2008), Impact of ocean carbon system variability on the detection of temporal increases in anthropogenic CO2, J. Geophys. Res., 113, C03019, doi:10.1029/2007JC004153.

Levitus, S., J. Antonov, and T. Boyer (2005), Warming of the world ocean, 1955-2003, Geophys. Res. Lett., 32, L02604, doi:10.1029/ 2004GL021592.

Mcleod, E., Chmura, G. L., Bouillon, S., Salm, R., Björk, M., Duarte, C. M., ... & Silliman, B. R. (2011). A blueprint for blue carbon: toward an improved

understanding of the role of vegetated coastal habitats in sequestering CO2. Frontiers in Ecology and the Environment, 9(10), 552-560.

Morris, J. T., and G. J. Whiting. 1986. Emission of Gaseous Carbon-Dioxide from Salt-Marsh Sediments and Its Relation to Other Carbon Losses. Estuaries **9:** 9-19.

Neubauer, S. C., and I. C. Anderson. 2003. Transport of dissolved inorganic carbon from a tidal freshwater marsh to the York River estuary. Limnol. Oceanogr. 48: 299-307.

Raymond, P. A., J. E. Bauer, and J. J. Cole. 2000. Atmospheric CO2 evasion, dissolved inorganic carbon production, and net heterotrophy in the York River estuary. Limnol. Oceanogr. **45:** 1707-1717.

Raymond, P. A., and C. S. Hopkinson. 2003. Ecosystem modulation of dissolved carbon age in a temperate marsh-dominated estuary. Ecosystems 6: 694-705.

Reid, J. L. (1997), On the total geostrophic circulation of the pacific ocean: Flow patterns, tracers, and transports, Prog. Oceanogr., 39, 263– 352, doi:10.1016/S0079-6611(97)00012-8.

Sabine, C. L., R. A. Feely, R. M. Key, J. L. Bullister, F. J. Millero, K. Lee, T.-H. Peng, B. Tilbrook, T. Ono, and C. S. Wong (2002), Distribution of anthropogenic CO2 in the Pacific Ocean, Global Biogeochem. Cycles, 16(4), 1083, doi:10.1029/2001GB001639.

Sabine, C. L., et al. (2004), The oceanic sink for anthropogenic CO2, Science, 305(5682), 367–371, doi:10.1126/science.1097403. Sabine, C. L., R. A. Feely, F. J. Millero, A. G. Dickson, C. Langdon, S. Mecking, and D. Greeley (2008), Decadal changes in Pacific carbon, J. Geo- phys. Res., 113, C07021, doi:10.1029/2007JC004577.

Silliman, Brian R., Edwin Grosholz, and Mark D. Bertness. 2009. Human impacts on salt marshes: a global perspective. Univ of California Press.

Smith, S. V., and J. T. Hollibaugh. 1993. Coastal Metabolism and the oceanic organic-carbon balance. Rev. Geophys. 31: 75-89.

Smith, S. V., & Mackenzie, F. T. (1987). The ocean as a net heterotrophic system: implications from the carbon biogeochemical cycle. Global Biogeochemical Cycles, 1(3), 187-198.

Stuiver, M., P. D. Quay, and H. G. Ostlund (1983), Abyssal water carbon-14 distribution and the age of the world oceans, Science, 219(4586), 849–51, doi:10.1126/science.219.4586.849.

Tanhua, T., A. Ko€rtzinger, K. Friis, D. W. Waugh, and D. W. R. Wallace (2007), An estimate of anthropogenic CO2 inventory from decadal changes in oceanic carbon content, Proc. Natl. Acad. Sci. U. S. A., 104(9), 3037–3042, doi:10.1073/pnas.0606574104.

Wang, Z. A., and W. J. Cai. 2004. Carbon dioxide degassing and inorganic carbon export from a marsh-dominated estuary (the Duplin River): A marsh CO2 pump. Limnol. Oceanogr. 49: 341-354.

Wang, Z. A., Kroeger, K. D., Ganju, N. K., Gonneea, M. E. and Chu, S. N. (2016), Intertidal salt marshes as an important source of inorganic carbon to the coastal ocean. Limnol. Oceanogr., 61: 1916–1931. doi:10.1002/lno.10347

Wanninkhof, R., S. C. Doney, J. L. Bullister, N. M. Levine, M. Warner, and N. Gruber (2010), Detecting anthropogenic CO2 changes in the interior Atlantic Ocean between 1989 and 2005, J. Geophys. Res., 115, C11028, doi:10.1029/2010JC006251.

Woodroffe CD. 1995. Response of tide-dominated mangrove shorelines in northern Australia to anticipated sea-level rise. Earth Surf Proc Land 20: 65–85.

Woodwell GM, Rich PH, Hall CAS. 1973. Carbon in estuaries. In Carbon and the Biosphere, ed. GM Woodwell, EV Pecan. U.S. Atomic Comm., Springfield, Virg.

# Chapter 2

# Changes in anthropogenic carbon storage in the Northeast Pacific in the last decade

This chapter was originally published in Journal of Geophysical Research: Oceans in 2016 and is reprinted with permission from the publisher, AGU Publications. 

Chu, S. N., Z. A. Wang, S. C. Doney, G. L. Lawson, and K. A. Hoering (2016), Changes in anthropogenic carbon storage in the Northeast Pacific in the last decade, J. Geophys. Res. Oceans, 121, 4618–4632, doi:10.1002/ 2016JC011775.

## 2.1 Abstract

In order to understand the ocean's role as a sink for anthropogenic carbon dioxide ($CO_2$), it is important to quantify changes in the amount of anthropogenic $CO_2$ stored in the ocean interior over time. From August to September 2012, an ocean acidification cruise was conducted along a portion of the P17N transect (50°N 150°W to 33.5°N 135°W) in the Northeast Pacific. These measurements are compared with data from the previous occupation of this transect in 2001 to estimate the change in the anthropogenic $CO_2$ inventory in the Northeast Pacific using an extended multiple linear regression (eMLR) approach. Maximum increases in the surface waters were 11 μmol $kg^{-1}$ over 11 years near 50°N. Here, the penetration depth of anthropogenic $CO_2$ only reached ~300 m depth, whereas at 33.5°N, penetration depth reached ~600 m. The average increase of the depth-integrated anthropogenic carbon inventory was 0.41 ± 0.12 mol $m^{-2}$ $yr^{-1}$ across the transect. Lower values down to 0.20 mol $m^{-2}$ $yr^{-1}$ were observed in the northern part of the transect near 50°N and increased up to 0.55 mol $m^{-2}$ $yr^{-1}$ toward 33.5°N. This increase in anthropogenic carbon in the upper ocean resulted in an average pH decrease of 0.002 ± 0.0003 pH units $yr^{-1}$ and a 1.8 ± 0.4 m $yr^{-1}$ shoaling rate of the aragonite saturation horizon. An average increase in apparent oxygen utilization of 13.4 ± 15.5 μmol $kg^{-1}$ centered on isopycnal surface 26.6 kg $m^{-3}$ from 2001 to 2012 was also observed.

## 2.2 Introduction

The ocean plays a significant role in regulating Earth's carbon cycle by absorbing about one-quarter to one-third of the total anthropogenic carbon dioxide ($CO_2$) released into the atmosphere by fossil fuel burning and land use changes (Le Quéré et al., 2010; Sabine et al., 2004). Global surface ocean $pCO_2$ increases at a similar rate as atmospheric $CO_2$ at ~ 2 ppm $yr^{-1}$ based on long-term time series observations at various locations in the ocean (Bates et al., 2014; Takahashi et al., 2009). Yet, on local scales, physical, chemical, and biological processes can lead to variability in surface water $CO_2$ levels, causing disequilibrium of $CO_2$ between the surface ocean and the atmosphere.

As the oceanic storage capacity potentially slows down due to the increase of temperature and decrease of buffer capacity (Levitus et al., 2005; Sabine et al., 2004), it becomes increasingly important to characterize and quantify the ocean's ability to absorb and store anthropogenic carbon dioxide ($C_{anthro}$). However, making estimates of $C_{anthro}$ is inherently difficult because it cannot be directly measured. The anthropogenic signal is relatively small compared to the large natural background and variability of the marine inorganic carbon system. In the 1990s, the World Ocean Circulation Experiment Hydrographic Program (WOCE/WHP) and Joint Global Ocean Flux Study (JGOFS) began conducting extensive surveys with high quality, seawater carbonate system measurements. Subsequently, the Climate Variability and Predictability Program (CLIVAR) Repeat Hydrography/$CO_2$ Program (http://ushydro.ucsd.edu/) and Global Ocean Ship-Based Hydrographic Investigations Program (GO-SHIP; http://www.go-

ship.org) began reoccupying several of the WOCE hydrographic lines (Talley et al., 2016). These observations target direct assessments of $C_{anthro}$ uptake and storage in the ocean, which allow us to examine the changing role of the ocean in the global carbon cycle under climate change.

Despite being the largest ocean basin, the Pacific only stores about 18% of the global ocean inventory of anthropogenic $CO_2$ ($C_{anthro}$) (Feely et al., 2001). The Pacific Ocean covers almost half of the total ocean area and therefore has the potential to experience significant changes in carbon cycling as climate continues to change. The Northeast Pacific, located at the end of the ocean meridional overturning circulation, is a region with particularly low concentrations of $C_{anthro}$. Both the lack of significant deep-water formation and slow meridional circulation limit the transport $C_{anthro}$ into the ocean interior (Reid, 1997; Sabine et al., 2002; Stuiver et al., 1983). As a result, the Pacific generally has much shallower $C_{anthro}$ penetration and lower $C_{anthro}$ storage compared to the Atlantic. In the North Atlantic, deep water formation and relatively fast ventilation allows anthropogenic $CO_2$ to almost reach the bottom (~5000 m) (Gruber et al., 1996; Körtzinger et al., 1999; Wanninkhof and McGillis, 1999).

Several categories of methods are used to estimate $C_{anthro}$, including back calculation methods to estimate $\Delta C^*$ (Brewer, 1978; Chen and Millero, 1979; Gruber et al., 1996), tracer-based methods (Hall et al., 2004; Waugh et al., 2006), and model-based approaches (Khatiwala et al., 2009; Pardo et al., 2014). The various advantages and disadvantages to these methods are discussed in Sabine and Tanhua (2010). In this

paper, we use the extended multiple linear regression (eMLR) approach (Friis et al., 2005; Tanhua et al., 2007) to estimate the change in $C_{anthro}$ between two data sets collected along the CLIVAR P17N transect in the Northeast Pacific. The eMLR method is well-suited to estimate changes in $C_{anthro}$ for reoccupation of cruise transects over decadal scales, assuming that the relationships between the chosen regression parameters do not change substantially for the time period over which the eMLR is applied. An advantage of the eMLR method is that it does not require any assumptions of preindustrial concentrations. Recent studies in the South Pacific and Pacific sector of the Southern Ocean use the eMLR technique (Waters et al., 2011; Williams et al., 2015), but few studies have made DIC data-based estimates of the change in $C_{anthro}$ storage in the Northeast Pacific with the exceptions of Peng et al. (2003) at 30°N, 152°W from 1973 to 1991 and Sabine et al. (2008) at P16N from 1991/1992 to 2006, from 200 to 1600 km west of the P17 transect.

The Northeast Pacific waters have naturally high dissolved inorganic carbon (DIC) concentrations, low pH, low buffering capacity, and a relatively shallow aragonite saturation horizon compared to other ocean basins. Even though this region does not currently hold a large amount of $C_{anthro}$, the system is already close to calcium carbonate undersaturation, which may have significant biological and ecological consequences. Therefore, studying how $C_{anthro}$ storage changes in the Northeast Pacific is as important as understanding uptake in higher storage areas such as the North Atlantic. In this paper, we report the results from a 2012 cruise along a northern segment of the

WOCE/CLIVAR P17 transect in the Northeast Pacific and evaluate changes in $C_{anthro}$ and the carbonate system from 2001 to 2012. This is the first estimate of $C_{anthro}$ using direct DIC measurements in the Northeast Pacific. We compare the decadal changes in $C_{anthro}$ and carbonate chemistry at P17 with other Pacific regions and other ocean basins, and examine the corresponding mechanisms that may cause observed within-basin and between-basin differences. The storage rate estimate made from this study should be incorporated into the global inventory of $C_{anthro}$ storage rate data to allow for further analysis of the uptake capacity of the ocean and its role in the global carbon cycle.

## 2.3 Data and Methods

### 2.3.1 Data collection and sample analysis

Data were collected during a research cruise aboard the R/V New Horizon (cruise number NH1208) from 9 August to 18 September 2012 along a northern portion (33.5-50°N) of the WOCE/CLIVAR P17N cruise track (Figure 1). This cruise was part of a broader effort designed to investigate how the carbonate chemistry in the Atlantic and Pacific Oceans affects the abundance, distribution, species composition, shell condition and vertical migratory behavior of thecosomatous pteropods. Stations were at every 0.5° latitude and ~0.8° longitude from 50°N 150°W to 41°N 135°W and every 0.5° latitude along 135°W from 41°N to 33.5°N. Deep station casts were conducted every 2° latitude from 50 to 43°N, 1.5° latitude from 43 to 35.5°N and 1° latitude for the remaining stations. Sampling depths were chosen to match similar water column coverage from

previous WOCE/CLIVAR cruises. Vertical sample spacing ranged from 20 m near the surface to 250 m below 1000 m.

A 24 position, 10 L bottle Rosette Niskin package equipped with a Conductivity-Temperature-Depth sensor (CTD, Seabird SBE 911plus) and a SBE43 dissolved oxygen (DO) sensor was used to collect discrete seawater samples for analysis of total dissolved inorganic carbon (DIC), total alkalinity (TA), pH, DO, nutrients (nitrate, phosphate, and silicate), and salinity. Seawater samples were collected for pH, DIC, TA, and nutrients at all 34 stations for all sampling depths. Salinity and DO samples were collected at all stations at every third depth for calibrations of the conductivity and DO sensors on the CTD Rosette. Samples for DO were collected first from the Niskin bottles, followed by pH, DIC/TA (in the same bottle), nutrients, and salinity. Standard protocols were followed for sampling procedures (Dickson et al., 2007). DIC and TA samples were collected into 250 ml Pyrex borosilicate bottles after being filtered with a 0.45 μm in-line capsule filter (Farrwest Environmental Supply, Texas). Each sample was poisoned with 100 μL of a saturated mercuric chloride solution for preservation (Dickson et al., 2007) and sealed with a ground-glass stopper coated with APIEZON®-L grease and was secured with a rubber band applied to the bottle top.

DIC was analyzed using an Apollo SciTech DIC auto-analyzer (Model AS-C3), which uses a nondispersive infrared (NDIR) method. The sample is acidified with a 10% phosphoric acid in 10% sodium chloride solution, and $CO_2$ is purged with high purity nitrogen gas and measured by a LI-COR 7000 infrared analyzer. Certified Reference

Material (CRM) from Dr. A. Dickson at Scripps Institution of Oceanography was used to calibrate the DIC auto-analyzer at least once daily. In addition, CRM was measured as a sample every few hours to gauge and correct any potential drift. The precision and accuracy of the instrument was ~ ±2.0 μmol $kg^{-1}$. The average absolute difference of duplicates was 5.4 ± 4.5 μmol $kg^{-1}$ (N=29). The larger standard deviation of duplicates may be a result of sampling, storage, or other sources of error.

TA was measured with an Apollo SciTech alkalinity auto-titrator (Model AS-ALK2), a Ross combination pH electrode and a pH meter (ORION 3 Star) to perform a modified Gran titration (Wang and Cai, 2004). The electrode and concentration of hydrochloric acid was calibrated every day. The CRMs were also measured as samples every few hours to correct any potential small drift. The average absolute difference of duplicate samples was 2.7 ± 2.1 μmol $kg^{-1}$ (N=28), which is similar to the accuracy and precision of the instrument, about ± 2.0 μmol $kg^{-1}$.

Seawater pH samples were collected directly into 10 cm cylindrical optical cells via silicone tubing and thermostated to 25.0 ± 0.1°C for at least an hour before measurement. Samples were analyzed using an Agilent 8453 UV-VIS spectrophotometer and meta-cresol purple (m-CP) as the indicator (Dickson et al., 2007). Sample pH was measured on the total scale. Measurements of pH were corrected for indicator perturbation and indicator impurity (Clayton and Byrne, 1993; Dickson et al., 2007; Liu et al., 2011; Yao et al., 2007). The average of combined corrections was 0.0026 ± 0.0046.

The average absolute difference of duplicates (N=28) was 0.0014 ± 0.0010, which is similar to the instrument accuracy and precision of 0.002 and 0.001, respectively.

The nutrient samples were filtered through 0.2 μm filters, collected into vials that had been cleaned with 10% hydrochloric acid and were immediately frozen after collection. Samples were analyzed at the University of California at Santa Barbara Marine Science Institute. Nutrient data from NH1208 were found to have relatively larger scatter than the previous P17N cruise data. This may be due to storage issues that involved freezing and possible melting of samples. Further details regarding analysis procedures for DO and salinity can be found in the supporting information (SI).

Bottle samples were assigned WOCE quality flags. Property-property plots were also examined to check for any aberrant data points. Samples in the near surface were allowed more variability in flagging. Data below 1000 m were also compared against 2001 CLIVAR data and strong deviations were noted.

### 2.3.2 Internal consistency

The seawater inorganic carbon system can be described by four measurable parameters: DIC, TA, pH and fugacity of $CO_2$ or $fCO_2$. Any pair of carbon parameters can be used to define the remaining parameters based on $CO_2$ equilibrium relationships. To test for internal consistency within the measured DIC, TA, and pH data, carbonate system parameters were calculated using the CO2SYS program by Pierrot et al. (2006) with constants from Mehrbach et al. (1973) as refit by Dickson and Millero (1987). Crossover-corrected DIC (details described in section 2.4), TA, and pH data were used in

CO2SYS calculations to compare with measured values in order to determine offsets and outliers. In this case, DIC was calculated from measured TA and pH to compare with measured DIC values. The mean residual (calculated – measured value) for DIC (N=562) was 0.5 ± 9.0 μmol $kg^{-1}$ (one standard deviation). There was good agreement over the entire water column and residuals were randomly distributed, suggesting there were no significant systematic errors in the data. The mean difference was within required accuracies for $C_{anthro}$ calculation, while the variation of this data set was somewhat higher than the previous CLIVAR P17N DIC data, which had an internal consistency for DIC of 3.2 ± 6.6 μmol $kg^{-1}$. This had a limited effect on $C_{anthro}$ estimates, since the eMLR method should remove most of the random scattering in the data set by comparing estimated means (Tanhua et al., 2007; Wanninkhof et al., 2010).

### 2.3.3 Selection of previous CLIVAR data

The NH1208 cruise occupied a portion of the CLIVAR P17N cruise track, which was previously occupied in 25 July to 28 August 2001 by a CLIVAR cruise. For the 2001 CLIVAR cruise (data from CLIVAR and Carbon Hydrographic Office (CCHDO) http://cchdo.ucsd.edu/cruise/49NZ200107_1), there were 78 stations. Discrete samples were taken for salinity, DO, nutrients, DIC, and TA. Salinity, DO, and nutrients were taken at every station for every depth. pH, DIC, and TA samples were taken at every other station. The data from the stations that overlap in latitude for the two cruises were used to quantify the total changes of seawater chemistry over the decade. The overlapping sections include stations 1-32 for NH1208, corresponding to stations 28-73

for CLIVAR. CLIVAR sampled every 0.5° latitude from 33.5-41°N at 135°W for 36 depths to 4000-5000 m and then every 0.3° latitude, 0.5° longitude from 41-50°N. The duplicate DIC, TA, and pH samples were within acceptable limits for accuracy and precision. CLIVAR data were not seasonally corrected for the eMLR analysis because of similar timings between the 2001 (July-August) and 2012 (August-September) cruises. The CLIVAR carbonate data quality was also confirmed by Certified Reference Materials (Dickson, 2001; Feely et al., 2001).

### 2.3.4 Deep crossover analysis

To remove biases between the 2012 and 2001 data sets, the deep isopycnal crossover analysis method (Lamb et al., 2002) was used at the overlapping stations. This method assumes that Pacific Deep Water with a residence time of ~500 years (Stuiver et al., 1983) does not experience significant changes over decadal timescales. Shallow depths are subject to changes due to seasonal variability of biological processes and penetration of $C_{anthro}$, which can vary the relationships between carbon parameters over different periods of time. For the CLIVAR occupation, crossover analyses have already been conducted and adjustments have been made according to PACIFic ocean Interior CArbon (PACIFICA) (Suzuki et al., 2013) (Table 1). PACIFICA adjustments are recommended based on calibration procedures, CRM analyses, precision of replicates, deep-water crossover analyses and internal consistency. Estimated accuracy after PACIFICA adjustments was ±4 μmol $kg^{-1}$ for DIC and ±6 μmol $kg^{-1}$ for TA.

To make adjustments to the NH1208 2012 cruise data, data from >2000 m were used for the crossover analysis. It should be noted that NH1208 has fewer data points below 2000 m than CLIVAR 2001, which might affect comparison statistics. Salinity and oxygen, along with carbonate system parameters and nutrients were compared using potential density referenced to 3000 dbar ($\sigma_3$). The data from each of the CLIVAR and NH1208 cruise occupations of this portion of P17N (2001 and 2012) were plotted against $\sigma_3$ and fit by a second-order polynomial (supporting information Figure S1). Only data with acceptable quality flags were used in the crossover analysis. Oxygen, silicate, phosphate, DIC, and TA required corrections (Table 1).

### 2.3.5 Extended multiple linear regression

The eMLR method is a derivative of the MLR introduced by Wallace (1995) that develops an empirical relationship to characterize DIC variability using chemical and hydrographic parameters (Friis et al., 2005). The original MLR method uses data sets from the same region from two different time periods and derives a MLR for one period, usually the earlier period. Those coefficients are applied to data from the later period and then the difference between the calculated and observed DIC for the later period is taken as the change in anthropogenic $CO_2$ between the two time periods, $\Delta C_{anthro}$. In the eMLR method, MLRs are created separately for two periods using the same sets of regression model variables, and the difference of the coefficients applied to data from one of the time periods, usually the later period, is used to calculate $\Delta C_{anthro}$.

The eMLR was conducted on the water column from 100 to 1000 m depth and the entire transect as a whole. The eMLR was only applied to data from 100 to 1000 m due to the fewer number of data points below 1000 m for the 2012 NH1208 cruise. The top 100 m of the water column was not included in the fit to exclude apparent trends due to complex, seasonally varying surface processes in the mixed layer, such as high biological production and air-sea exchange, which may affect eMLR results. Surface values (0-100 m) were estimated based on the assumption that $fCO_2$ in the surface water changes at the same rate as $fCO_2$ in the atmosphere (Sabine et al., 2008; Waters et al., 2011).

The eMLR was not separated by potential density bins or by latitudinal ranges due to the limited data availability caused by removing flagged nutrient data as mentioned previously. Calculating MLRs by potential density bins is useful in removing errors introduced by isopycnal heave at seasonal and decadal scales (Doney et al., 2007; Levine et al., 2008; Wanninkhof et al., 2010). However, our analysis did not show significantly large errors by applying one MLR to the entire transect for both years.

The coefficients of the eMLR regressions on DIC for the two time periods are shown in Table 2. The best set of parameters to characterize DIC was apparent oxygen utilization (AOU), salinity (S), potential temperature ($\vartheta$), and silicate (Si). This set of parameters was chosen based on reducing the error of the fit while taking into consideration data quality. AOU, salinity, and potential temperature were tested in models with one or a combination of nutrients. Among the nutrients, silicate was found

to improve the fit the most while adding phosphate and/or nitrate led to minimal improvement. The RMSE of 10.0 μmol $kg^{-1}$ is similar to the uncertainty in the internal consistency calculations (9.1 μmol $kg^{-1}$). No significant systematic trends were found when plotting residuals (model-observation) against potential density, latitude, and depth (supporting information Figure S2).

Total alkalinity was not included in the MLR because it did not significantly improve the MLR fit and there was a co-linearity found between TA and salinity. In addition, contribution to changes in DIC due to calcium carbonate precipitation or dissolution were negligible in that there was no significant difference in salinity-normalized total alkalinity compared on isopycnals between the two cruises.

## 2.4 Results

### 2.4.1 Latitudinal distribution of geochemical features along P17N

The salinity and density fields show strong upper-ocean vertical stratification in the northern part of the transect in the subpolar gyre where colder, fresher water is dominant in the surface (Figure 2a). The transition zone between the subpolar and subtropical gyres can be defined by the outcrops of isohaline 33.0 and 33.8 (Roden, 1991), which are found here at 42°N and 34°N, respectively. This indicates that the 2012 cruise did not extend into the waters of the subtropical gyre. Depth profiles of salinity show only subpolar gyre and transition zone salinity structure, with low salinity in the surface that increases with depth. Subtropical gyre salinity depth profiles have high salinity in surface waters with a clear presence of the North Pacific Intermediate Water

(NPIW) salinity minimum and slight increase of salinity with depth below (Talley, 1993), neither of which are seen in Figure 2a. The potential density contours shown in Figure 2 shoal from the southern part of the transect toward the northern part. The shallow isopycnals in the northern latitudes are caused by wind-driven upwelling where there is outcropping of the isopycnals. It is evident that water movement is primarily along isopycnals (Gruber et al., 1996; Iselin, 1939; Quay et al., 2007) as shown by horizontal distribution patterns of all parameters in Figure 2 that generally follow the isopycnals.

AOU is mostly negative near the surface along P17N (Figure 2b), indicating oxygen supersaturation due to summer heating and greater net community production (Broecker and Peng, 1982; Shulenberger and Reid, 1981). In the southern part of P17N, there is an area of AOU of 250 μmol $kg^{-1}$ and greater between 500 and 1500 m that gradually expands to 350 – 2000 m at the northern part of the transect. This AOU horizon corresponds to an oxygen concentration of ~50 μmol $kg^{-1}$, used here as the upper limit definition of an oxygen minimum zone (OMZ). A combination of weak ventilation and high oxygen utilization allows for the formation of OMZs, an area that is also accompanied by high DIC.

The vertical structure of DIC shows low concentrations in surface waters and increasing concentrations with depth (Figure 2c). The lowest DIC values of <2000 μmol $kg^{-1}$ in the surface waters are partially due to elevated biological productivity converting DIC into organic carbon that subsequently sinks from the upper ocean. Surface DIC

concentration is slightly higher in the colder, fresher water of the northern latitudes than the southern part of the transect. Additionally, there is shoaling of high DIC water at depth along isopycnals in the northern latitudes due to upwelling and outcropping of old and deep water. The middepth water in this region is especially rich in DIC and nutrients due to the accumulation of products from remineralization. The distribution patterns of AOU and DIC are correlated because similar processes such as circulation, air-sea exchange, solubility, and biological activities modulate both AOU and DIC.

The ability of seawater to buffer $CO_2$ entering the ocean can be described by the Revelle Factor $\left(\mathrm{RF} = \frac{\partial \ln [CO_2]}{\partial \ln \mathrm{DIC}}\right)$ (Broecker et al., 1979; Egleston et al., 2010; Revelle and Suess, 1957). A lower RF represents a larger buffer capacity for a parcel of water. An increase in $pCO_2$ or DIC for a water parcel tends to increase the parcel's Revelle Factor and make it less able to absorb more $CO_2$. Currently, the RF across ocean basins varies between 9 and 15 and has increased by approximately one unit since preindustrial times (Egleston et al., 2010; Sabine et al., 2004). In general, the Northeast Pacific region has a higher than average RF within the mixing zone because these older waters have higher DIC and lower pH. Figure 2d shows that the surface RF varied from 11 to 13, with the higher surface values found in the northern part of the transect, where the water is the coldest and freshest. For a given increase of surface $pCO_2$, the southern part of the transect would absorb more $CO_2$ and thus experience a larger increase in DIC than the northern part, assuming other system factors remain constant.

Physical, biological, and anthropogenic changes along P17N can be examined by directly subtracting gridded parameters of 2001 from 2012. Changes in physical processes, such as circulation and frontal movement can cause changes in salinity, AOU, and DIC. AOU and DIC can also be influenced by ventilation and biological processes. In addition, DIC changes can be attributed to invasion of anthropogenic $CO_2$. Between 2001 and 2012, changes in salinity along P17N are almost completely confined to the upper 300 m (Figure 3a). A salinity increase of ~0.4 units is found from 125 to 300 m from 36 to 48.5°N, with an especially large increase up to 0.6 units in the top 50 m from 37.5 to 39.5°N. There is fresher water in the subpolar gyre as shown by the decrease in salinity of 0.1-0.3 units near 50°N. The changes in surface salinity along P17N agree with the overall reported surface ocean trends from 1950 to 2008, where evaporation-dominated areas experienced salinity increases and precipitation-dominated areas experienced salinity decreases (Durack and Wijffels, 2010). Multiple studies have reported freshening in the North Pacific Ocean, primarily in the upper 100 m. The pattern differs in shallow subsurface waters. Boyer et al. (2005) and Durack and Wijffels (2010) both find a salinity increase in subpolar North Pacific at 50°N at 150 m, which agree with the subsurface salinity increase along P17N.

Changes in AOU are seen from the surface to ~600 m. In the upper 100 m, there are mostly decreases of 10-20 μmol $kg^{-1}$ over the transect with a more intense area of decrease up to 40 μmol $kg^{-1}$ near 50°N (Figure 3b). For 100-600 m, the overall pattern in ΔAOU shows an increase in concentrations from 2001 to 2012. Since the 1970s, a

decrease in overturning circulation has been reported in the subpolar North Pacific (Deutsch et al., 2006; McPhaden and Zhang, 2002; Mecking et al., 2008; Sabine et al., 2008). Reduced circulation in addition to warming (data not shown) would lead to greater stratification that would result in deoxygenation, an increase in AOU, and an intensification as well as expansion of the OMZ. Most of the large AOU changes are seen between the 26 and 27 kg $m^{-3}$ isopycnals. This is consistent with data along the 26.6 kg $m^{-3}$ isopycnal, which is the densest isopycnal to outcrop in the open North Pacific in climatological data (Mecking et al., 2008). It is the upper-most isopycnal involved in the formation of NPIW and serves as an interface between ventilated waters and indirectly or non-locally ventilated deeper waters. By averaging ΔAOU for isopycnals 26.55-26.65 kg $m^{-3}$, centered on 26.6 kg $m^{-3}$ (Figure 3b), the mean AOU increase from 2001 to 2012 was +13.4 ± 15.5 μmol $kg^{-1}$. Changes in AOU and in situ $O_2$ should be similar in magnitude though opposite in sign because potential temperature and salinity variations are relatively small along isopycnals (Mecking et al. 2008). Mean deoxygenation between 2001 and 2012 calculated from in situ dissolved $O_2$ concentration changes was –12.8 ± 13.9 μmol $kg^{-1}$ centered on the same isopycnal 26.6 kg $m^{-3}$. Mean ΔAOU and $\Delta O_2$ are also comparable to an expected deoxygenation of –7.6 ± 0.1 μmol $kg^{-1}$, based on the rate of 0.68-0.70 μmol $kg^{-1}$ $yr^{-1}$ found on isopycnals 26.5 and 26.7 kg $m^{-3}$ reported at Ocean Station Papa (50°N, 145°W) (Falkowski et al., 2011; Whitney et al., 2007).

Changes in DIC are seen throughout the whole water column. Down to 600m, ΔDIC patterns are similar in sign and somewhat larger in magnitude to those of ΔAOU,

with additional unmatched temporal differences in DIC below 600 m. The similarities between the ΔDIC and ΔAOU distributions is expected due to remineralization and circulation processes that affect the distribution of both parameters similarly, leading to co-varying patterns between the two (Figures 3b and 3c). The difference between the ΔDIC and ΔAOU distributions is likely attributed to $C_{anthro}$ affecting DIC but not AOU. However, it seems that the factors affecting AOU changes account for a majority of the DIC changes, which agrees with (Sabine et al., 2008) finding that changes in AOU account for 80% of total DIC change in the North Pacific.

### 2.4.2 Distribution of decadal changes of anthropogenic carbon dioxide along P17N

From 2001 to 2012, across the P17N transect, $\Delta C_{anthro}$ values at the surface have a range of 7 – 11 μmol $kg^{-1}$ (Figure 4). Such a range is similar to an expected 13-17 μmol $kg^{-1}$ increase in surface water DIC based on a growth rate of 1.36 ± 0.16 μatm $yr^{-1}$ in surface seawater $pCO_2$ measured at Station P (50°N, 145°W) (Wong et al., 2010). The coarse transition between the top 100 m and the rest of the water column is due to separate treatment of the surface layer as mentioned previously. The penetration depth of $\Delta C_{anthro}$, roughly defined by the +2.5 μmol $kg^{-1}$ isoline, is at approximately 700 – 1000 m in the southern part of the transect, shoaling to approximately 400 m in the subpolar gyre at 50°N, likely reflecting prevailing upwelling patterns that compress the anthropogenic signal near the surface ocean. Because there is no deep-water formation in the Northeast Pacific, $C_{anthro}$ does not penetrate into the deep ocean in this region. In the

upper thermocline (~300 m), $\Delta C_{anthro}$ decreases equatorward along isopycnal surfaces, consistent with thermocline ventilation pathways.

The distribution pattern of $\Delta C_{anthro}$ can be partially verified by comparison to measured anthropogenic chlorofluorocarbon (CFC), trichlorofluoromethane (CFC-11), from a previous WOCE cruise in 1993 along P17N (Figure 4b). The CFC data show similar patterns to the $\Delta C_{anthro}$ in terms of the north-south gradients along isopycnal surfaces in the upper 300 m. Vertically, CFC penetration reaches ~400 m and is almost uniform with latitude, except at the very northern part of the transect. Considering the different input histories and chemical properties between anthropogenic $CO_2$ and CFCs and the different time frame between Figures 4a and 4b, their difference in distribution patterns is expected. Nevertheless, the similarity of the distribution between $\Delta C_{anthro}$ and CFCs suggests the results of the eMLR-derived $\Delta C_{anthro}$ in this study are reasonable.

### 2.4.3 Change in anthropogenic $CO_2$ water column inventory

Using $C_{anthro}$ surface values (0-100 m) based on the assumption of surface ocean-atmosphere equilibrium, the average increase in $\Delta C_{anthro}$ column inventory across P17N based on the eMLR analysis was $+0.41 \pm 0.12$ ($1\sigma$) mol $m^{-2}$ $yr^{-1}$. There are at least two other methods that can be used to estimate surface layer $\Delta C_{anthro}$, one of which is to include surface values in the eMLR (Friis et al., 2005; Wanninkhof et al., 2010). While we did not include the surface values in our eMLR, we applied eMLR coefficients to the surface data to estimate surface $\Delta C_{anthro}$ calculated an average column inventory of $+0.39 \pm 0.09$ mol $m^{-2}$ $yr^{-1}$. Secondly, if eMLR-calculated $\Delta C_{anthro}$ values at 100 m were

extrapolated to the surface (Brown et al., 2010), the column inventory would be +0.43 ± 0.12 mol $m^{-2}$ $yr^{-1}$. Therefore, using different methods of estimating the $\Delta C_{anthro}$ surface values do not significantly affect the end result. To calculate the column inventory, negative $\Delta C_{anthro}$ values were set to zero. Depth profiles were interpolated using a piecewise cubic hermite interpolation (Tanhua et al., 2007, 2010). Then with trapezoidal integration, the column-integrated $\Delta C_{anthro}$ was calculated at each station. Stations that had insufficient data (less than two depths of data) were not included. The uncertainty reported here is the standard deviation of the average change in column inventory across P17N and thus includes regional variations. The storage rate across the transect shows a general decrease from +0.55 mol C $m^{-2}$ $yr^{-1}$ at 34°N to +0.20 mol C $m^{-2}$ $yr^{-1}$ at 50°N with significant latitudinal variability (Figure 5). As the high latitude waters experience an upwelling regime with surface divergence and lateral transport of $C_{anthro}$ in the subpolar gyre, there is expected lower accumulation of $C_{anthro}$ near the surface at the northern stations (Sabine et al., 2004). The higher change in column inventory in the lower latitudes transitioning toward the subtropical surface waters, similarly, is consistent with a convergent, downwelling regime where anthropogenic carbon and CFCs are transported downward along isopycnal surfaces into the ocean interior.

The storage rate calculated using eMLR is similar to simulation results from the Community Earth System Model (CESM) (Doney et al., 2009a, 2009b). The storage rate from the CESM ranges from +0.21 to +0.43 with an average rate of +0.38 ± 0.06 mol $m^{-2}$ $yr^{-1}$. The average storage rate calculated by the two methods agree within

uncertainties and follow a similar latitudinal pattern with higher rates in the southern half of the transect decreasing to lower rates in the northern half of the transect. The eMLR results show higher degree of variation along the transect. The overall agreement between these two different methods suggests that the results from the eMLR method are robust.

## 2.5 Discussion

### 2.5.1 Anthropogenic carbon storage rates

Two other observational, DIC data-based studies have estimated $\Delta C_{anthro}$ near P17N. Peng et al. (2003) used a MLR method at 30°N, 152°W and data from Geochemical Ocean Section Study (GEOSECS) 1973 and WOCE/JGOFS 1991 to estimate an average rate of 1.3 ± 0.5 mol C $m^{-2}$ $yr^{-1}$. Sabine et al. (2008) estimated an average rate of 0.25 mol $m^{-2}$ $yr^{-1}$ along the WOCE/CLIVAR P16N transect (0-56°N, 152°W), west of P17N, between 1991/1992 and 2006 based on an eMLR method (Figure 6). The earlier estimate by Peng et al. (2003) is likely to be an overestimate due to systematic biases in the GEOSECS DIC data (Quay et al., 2007; Sabine and Tanhua, 2010).

Differences in the application of the eMLR may partially explain the differences in the estimated $\Delta C_{anthro}$ between P16 and P17. The P16 study (Sabine et al., 2008) was conducted on data from 1991/1992 and 2006 using a somewhat different eMLR approach. They first calculated total DIC change ($\Delta C_{total}$) and carbon change calculated from AOU ($\Delta C_{AOU}$) using separate eMLRs but with the same regression parameters:

potential temperature, salinity, silicate, and phosphate. Then they computed $\Delta C_{anthro}$ by correcting the $\Delta C_{total}$ for $DC_{AOU}$, assuming an organic matter C:$O_2$ stoichiometry of 117/170 (Anderson and Sarmiento, 1994), where the AOU correction reduces the $\Delta C_{total}$ substantially, by up to 80%. Sabine et al. (2008) argue that the ΔAOU patterns primarily reflect variations in circulation rather than export, but to some extent any resulting changes in remineralized carbon in the subsurface should already be captured by the two eMLRs through the variations of phosphate that contribute to both the AOU and total DIC regressions. Here we used AOU as an eMLR regression parameter for the P17N $\Delta C_{anthro}$, in part because of the poor quality of the phosphate data from NH1208. Therefore, a direct comparison to the Sabine et al. two-step eMLR approach is not possible. Note, though, that the small-scale patterns in ΔAOU and ΔDIC (Figures 3b and 3c) are largely removed from $\Delta C_{anthro}$ (Figure 4a), suggesting that to some degree AOU trends are adequately captured in our approach.

With these caveats in mind, Figure 6 shows a comparison from this study to the results from Sabine et al. (2008) for P16N. At 50°N, where the two transects are closest, there is similarity between the two storage rates at 0.20 and 0.18 mol $m^{-2}$ $yr^{-1}$ for P17 and P16, respectively. As the transects separate, so do the estimated storage rates, with the P17 storage rates increasing to 0.54 mol $m^{-2}$ $yr^{-1}$ at 33.5°N, while for P16 the rate is ~0.34 mol $m^{-2}$ $yr^{-1}$. Given the uncertainty associated with P16 and P17 calculations of 0.2 and 0.12 mol $m^{-2}$ $yr^{-1}$, respectively, these differences are likely not statistically significant. Future studies could delve deeper into these technique driven differences. Besides

methodological reasons that could cause these differences, P17 is further east than P16 by 2-17° in longitude and is subject to slightly different currents and water masses. Comparing these rates to those in the Northwest Pacific, average storage rates are reported as 0.4 ± 0.1 – 0.5 ± 0.2 mol $m^{-2}$ $yr^{-1}$ (Murata et al., 2009; Wakita et al., 2013), which are not significantly different from the P16N and P17N values (Sabine et al., 2002, 2008). Further observation and analysis are needed to fully understand the spatial distribution of $DC_{anthro}$ across the Pacific.

Estimated $C_{anthro}$ storage rates in the Pacific are lower than the rates at similar latitudes in the North Atlantic. North Atlantic storage rates ranging from 0.6-2.2 mol $m^{-2}$ $yr^{-1}$ are consistent with the higher cumulative $C_{anthro}$ inventory for the basin (Friis et al., 2005; Quay et al., 2007; Sabine and Tanhua, 2010; Tanhua et al., 2007). The average storage rate across P17N of 0.41 ± 0.12 mol $m^{-2}$ $yr^{-1}$ agrees within uncertainty to 0.63 ± 0.16 mol $m^{-2}$ $yr^{-1}$ estimated from Quay et al. (2007) for the entire North Atlantic. However, taking a closer look at specific latitudes that overlap with our P17N transect, the P17N storage rate is significantly lower than 1.2 ± 0.3 and 2.2 ± 0.7 mol $m^{-2}$ $yr^{-1}$, found in the Atlantic at 20-40°N and 40-65°N, respectively (Friis et al., 2005; Tanhua et al., 2007). The high inventory and storage rate are mainly the result of deep-water formation in the North Atlantic, which drives the transport of $C_{anthro}$ into the ocean interior (Khatiwala et al., 2013; Mikaloff Fletcher et al., 2006). With no deep-water formation and upwelling in the Northeast Pacific, $C_{anthro}$ penetration and accumulation is limited.

### 2.5.2 Anthropogenic $CO_2$ effects on carbonate chemistry

Since the beginning of the industrial era, atmospheric $CO_2$ has increased from ~280 ppm to over 400 ppm (http://www.esrl.noaa.gov/gmd/ccgg/trends/weekly.html). By 2100, atmospheric $CO_2$ levels are projected to reach near 1000 ppm under a business-as-usual scenario (IPCC, 2014). This could lead to irreversible damage to Earth's marine ecosystems through a myriad of effects, which can be partially gauged by monitoring of the rate of ocean acidification and the shoaling rate of the aragonite saturation horizon ($\Omega_a = 1$).

To evaluate the effect of the increase in $C_{anthro}$ on the carbonate system of this region, the results from the eMLR were used to calculate changes in pH ($\Delta$pH) and aragonite saturation state ($\Delta\Omega_a$) as a result of $\Delta C_{anthro}$. pH and $\Omega_a$ were first calculated for 2012, using measured DIC and TA. To calculate pH and $\Omega_a$ for 2001, an expected 2001 DIC value was obtained by subtracting eMLR-calculated $\Delta C_{anthro}$ from the 2012 DIC value. This expected DIC was then used with the 2012 TA value to calculate expected pH and $\Omega_a$. It is assumed that any TA change between the 2001 and 2012 is due to natural variability, therefore, using TA from 2012 for 2001 calculations should remove natural variability of TA and the change in pH and $\Omega_a$ between 2001 and 2012 would be solely due to increase in $C_{anthro}$.

The decadal change in pH ($\Delta$pH, Figure 7a) or the ocean acidification rate in this region has similar patterns to the $\Delta C_{anthro}$, as $\Delta C_{anthro}$ is the sole driving force for the ocean acidification rate calculated here. The estimated pH decrease can be translated to

an acidification rate of 0.0008 – 0.004 pH units $yr^{-1}$ in the upper 100 m, with an average rate of ~0.002 ± 0.0009 pH units per year. Such rates are slightly higher than the rates of 0.0016 ± 0.0001 – 0.0018 ± 0.0001 pH units per year estimated for HOT, Station ALOHA, and P16N in the North Pacific (Bates et al., 2014; Byrne et al., 2010; Dore et al., 2009; Takahashi et al., 2014). Ocean acidification in the Northwest Pacific has been estimated to occur at a rate of 0.0015 ± 0.0005 – 0.002 ± 0.0007 units per year (Ishii et al., 2011; Midorikawa et al., 2010). These differences in ocean acidification rates are consistent with those differences in $\Delta C_{anthro}$ previously described.

The distribution of $\Delta\Omega_a$ also follows the pattern of ocean acidification rates (Figure 7). The decrease of $\Omega_a$ due to increases in $C_{anthro}$ has resulted in a shoaling of the aragonite saturation horizon ($\Omega_a = 1$) by 10 – 35 m with an average of ~19.6 m over 11 years, or ~1.8 ± 0.4 m $yr^{-1}$. At 50°N, $\Omega_a = 1$ is near 125 m, the shallowest depth over the transect. At this rate, the entire water column in the northern part of the P17N will become undersaturated in 50-90 years. The mean rate of shoaling in this region agrees, within uncertainties, with those reported by Feely et al. (2012) for P16N at 0.81 ± 0.71 m $yr^{-1}$ and P16S at 2.01 ± 0.80 m $yr^{-1}$. The change in saturation state at P17N translates to a decrease of -0.40 ± 0.07 % $yr^{-1}$ at 100 m, which is less than -1.24 ± 0.29 % $yr^{-1}$ reported at 100 m for the Northeast Pacific region by Jiang et al. (2015). However, the P17N rate is faster than -0.27 ± 0.03 to -0.28 ± 0.04 % $yr^{-1}$ previously reported for the HOT and ALOHA, and agrees within uncertainty to 0.34 ± 0.04 % $yr^{-1}$ at P16N (Bates et al., 2014; Dore et al., 2009; Feely et al., 2012; Takahashi et al., 2014). Comparing to

the North Atlantic, where acidification rates range from 0.0017 ± 0.0001 to 0.0020 ± 0.0004 pH units $yr^{-1}$ and decreases in aragonite saturation state from 0.26 ± 0.02 to 0.34 ± 0.07 % $yr^{-1}$, this study suggests that P17N is among the most sensitive regions to ocean acidification in terms of high rates of pH decrease and fast shoaling of the aragonite saturation horizon.

### 2.6 Conclusions

The data from a 2012 cruise along P17N show significant changes in salinity, AOU, and DIC, relative to a 2001 CLIVAR occupation of the transect, which primarily reflect changes in circulation but also reveal deoxygenation and invasion of anthropogenic carbon dioxide in the water column of the Northeast Pacific. An extended multiple linear regression was used to estimate an increase of 7-11 μmol $kg^{-1}$ anthropogenic $CO_2$ concentration in surface waters with a strong northward increase near the surface. The penetration depth of $C_{anthro}$ decreases northward from 600 m at 33.5°N to 300 m at 50°N. As a result, $C_{anthro}$ storage rates up to 0.55 mol $m^{-2}$ $yr^{-1}$ were found in the southern portion of the transect, which decrease gradually to 0.20 mol $m^{-2}$ $yr^{-1}$ at the northern part of the transect with an average of 0.41 ± 0.12 mol $m^{-2}$ $yr^{-1}$. The increase in anthropogenic $CO_2$ in the Northeast Pacific resulted in a mean acidification rate of -0.002 ± 0.0009 pH units $yr^{-1}$ and a mean shoaling of the aragonite saturation horizon of 1.8 ± 0.4 m $yr^{-1}$. These rates may be slightly higher than other estimates of anthropogenic carbon storage, acidification and shoaling rates in the Pacific. The Northeast Pacific is considered the end of the ocean conveyor belt. Waters found here

are old, and have high DIC content and high Revelle Factors, or low buffering capacity. This causes the aragonite saturation horizon to be already quite shallow (near 125 m) compared to other regions of the ocean. As such, the Northeast Pacific is among the most sensitive regions to changes in carbonate chemistry under ocean acidification. Even though this region may not be known for its strong uptake of anthropogenic carbon, it still has the potential to store a significant amount. This study has shown that the $C_{anthro}$ storage in the region is still increasing and that it is important to continue to monitor such changes in this region to understand its variability across time and space as well as the potential biological and ecosystem impacts of rising $CO_2$.

**Acknowledgements**

All data presented in this paper can be found at the NSF Biological and Chemical Oceanography Data Management Office (BCO-DMO) (http://www.bco-dmo.org). The authors would like to thank the Captain and crew of the R/V New Horizon, and to thank all the scientists, students, and volunteers who participated in the research expeditions. We would also like to express our gratitude to Amy Maas, Leocadio Blanco Bercial, Peter Wiebe, Nancy Copley, Alex Bergan, Taylor Crockford, Robert Nick Tuttle, Elliot Roberts, and Kelly Brugler for their sampling and analysis support. Thank you to Harry Hemond, Dan McCorkle, and Kevin Kroeger for their guidance. This work was funded by the National Science Foundation Ocean Acidification Program (OCE-1041068), National Institute of Standards and Technology (NIST-60NANB10D024), and NSF Graduate Research Fellowship Program.

**References**


Anderson, L. A., and J. L. Sarmiento (1994), Redfield ratios of remineralization determined by nutrient data analysis, Global Biogeochem. Cycles, 8(1), 65–80, doi:10.1029/93GB03318.

Bates, N. R., Y. M. Astor, M. J. Church, K. Currie, J. E. Dore, M. Gonzalez-Davila, L. Lorenzoni, F. Muller-Karger, J. Olafsson, and J. M. Santana-Casiano (2014), A Time-Series View of Changing Surface Ocean Chemistry Due to Ocean Uptake of Anthropogenic $CO_2$ and Ocean Acidification, Oceanography, 27(1), 126–141, doi:10.5670/oceanog.2014.16

Boyer, T. P., S. Levitus, J. I. Antonov, R. A. Locarnini, and H. E. Garcia, (2005), Linear trends in salinity for the World Ocean, 1955–1998, Geophys. Res. Lett., 32. L01604, doi:10.1029/2004GL021791.

Brewer, P. G. (1978), Direct observation of the oceanic CO2 increase, Geophys. Res. Lett., 5(12), 997–1000, doi:10.1029/GL005i012p00997.

Broecker, W. S., and T. H. Peng (1982), Tracers in the Sea, 690 pp., Lamont-Doherty Geol. Obs. Palisades, N. Y.

Broecker, W. S., T. Takahashi, H. J. Simpson, and T. H. Peng (1979), Fate of Fossil Fuel Carbon Dioxide and the Global Carbon Budget, Science, 206(4417), 409–418, doi:10.1126/science.206.4417.409.

Brown, P. J., D. C. E. Bakker, U. Schuster, and A. J. Watson (2010), Anthropogenic carbon accumulation in the subtropical North Atlantic, J. Geophys. Res., 115, C04016, doi:10.1029/2008JC005043.

Byrne, R. H., S. Mecking, R. A. Feely, and X. Liu (2010), Direct observations of basin-wide acidification of the North Pacific Ocean, Geophys. Res. Lett., 37, L02601, doi:10.1029/2009GL040999.

Chen, C.-T. A., and F. J. Millero (1979), Gradual increase of oceanic $CO_2$, Nature, 277, 205–206, doi:10.1038/277205a0.

Clayton, T. D., and R. H. Byrne (1993), Spectrophotometric seawater pH measurements: Total hydrogen ion concentration scale calibration of m-cresol purple and at-sea results, Deep Sea Res., Part I, 40(10), 2115–2129, doi:10.1016/0967-0637(93)90048-8.

Deutsch, C., S. Emerson, and L. Thompson (2006), Physical-biological interactions in North Pacific oxygen variability, J. Geophys. Res., 111, C09S90, doi:10.1029/2005JC003179.

Dickson, A., C. Sabine, and J. Christian (2007), Guide to best practices for ocean $CO_2$ measurement, PICES Special Publication 3, 191 pp.

Dickson, A. G. (2001), Reference materials for oceanic $CO_2$ measurements, Oceanography, 14(4), 21–22.

Dickson, A. G., and F. J. Millero (1987), A comparison of the equilibrium constants for the dissociation of carbonic acid in seawater media, Deep Sea Res. Part A, 34(10), 1733–1743, doi:10.1016/0198-0149(87)90021-5.

Doney, S. C., S. Yeager, G. Danabasoglu, W. G. Large, and J. C. McWilliams (2007), Mechanisms governing interannual variability of upper ocean temperature in a global hindcast simulation, J. Phys. Oceanogr., 37, 1918–1938, doi:10.1175/JPO3089.1.

Doney, S. C., I. Lima, R. A. Feely, D. M. Glover, K. Lindsay, N. Mahowald, J. K. Moore, and R. Wanninkhof (2009a), Mechanisms governing interannual variability in upper-ocean inorganic carbon system and air-sea $CO_2$ fluxes: Physical climate and atmospheric dust, Deep Sea Res. Part II, 56(8-10), 640–655, doi:10.1016/j.dsr2.2008.12.006.

Doney, S. C., I. Lima, J. K. Moore, K. Lindsay, M. J. Behrenfeld, T. K. Westberry, N. Mahowald, D. M. Glover, and T. Takahashi (2009b), Skill metrics for confronting global upper ocean ecosystem-biogeochemistry models against field and remote sensing data, J. Mar. Syst., 76(1-2), 95–112, doi:10.1016/j.jmarsys.2008.05.015.

Dore, J. E., R. Lukas, D. W. Sadler, M. J. Church, and D. M. Karl (2009), Physical and biogeochemical modulation of ocean acidification in the central North Pacific, Proc. Natl. Acad. Sci. U. S. A., 106(30), 12235–12240, doi:10.1073/pnas.0906044106.

Durack, P. J., and S. E. Wijffels (2010), Fifty-Year trends in global ocean salinities and their relationship to broad-scale warming, J. Clim., 23(16), 4342–4362, doi:10.1175/2010JCLI3377.1.

Egleston, E. S., C. L. Sabine, and F. M. M. Morel (2010), Revelle revisited: Buffer factors that quantify the response of ocean chemistry to changes in DIC and alkalinity, Global Biogeochem. Cycles, 24, GB1002, doi:10.1029/2008GB003407.

Falkowski, P. G. et al. (2011), Ocean deoxygenation: Past, present, and future, Eos Trans. AGU, 92(46), 409–410, doi:10.1029/2011EO460001.

Feely, R. A., C. L. Sabine, T. Takahasi, and R. Wanninkhof (2001), Uptake and Storage of Carbon Dioxide in the Ocean: The Global $CO_2$ Survey, Oceanography, 14(4), 18–32, doi:10.5670/oceanog.2001.03.

Feely, R. A., C. L. Sabine, R. H. Byrne, F. J. Millero, A. G. Dickson, R. Wanninkhof, A. Murata, L. A. Miller, and D. Greeley (2012), Decadal changes in the aragonite and calcite saturation state of the Pacific Ocean, Global Biogeochem. Cycles, 26, GB3001, doi:10.1029/2011GB004157.

Friis, K., A. Körtzinger, J. Pätsch, and D. W. R. Wallace (2005), On the temporal increase of anthropogenic $CO_2$ in the subpolar North Atlantic, Deep Sea Res. Part I, 52(5), 681–698, doi:10.1016/j.dsr.2004.11.017.

Gruber, N., J. L. Sarmiento, and T. F. Stocker (1996), An improved method for detecting anthropogenic $CO_2$ in the oceans, Global Biogeochem. Cycles, 10(4), 809–837, doi:10.1029/96GB01608.

Hall, T. M., D. W. Waugh, T. W. N. N. Haine, P. E. Robbins, and S. Khatiwala (2004), Estimates of anthropogenic carbon in the Indian Ocean with allowance for mixing and time-varying air-sea $CO_2$ disequilibrium, Global Biogeochem. Cycles, 18, GB1031, doi:10.1029/2003GB002120.

IPCC (2014), Climate Change 2014: Synthesis Report. Contribution of Working Groups I, II and III to the Fifth Assessment Report of the Intergovernmental Panel on Climate Change, edited by Core Writing Team, R. K. Pachauri and L. A. Meyer, IPCC, Geneva, Switzerland, 151 pp.

Iselin, C. O. (1939), The influence of vertical and lateral turbulence on the characteristics of the waters at mid-depths, Eos Trans. AGU, 20(3), 414–417, doi:10.1029/TR020i003p00414.

Ishii, M., N. Kosugi, D. Sasano, S. Saito, T. Midorikawa, and H. Y. Inoue (2011), Ocean acidification off the south coast of Japan: A result from time series observations of $CO_2$ parameters from 1994 to 2008, J. Geophys. Res., 116, C06022, doi:10.1029/2010JC006831.

Jiang, L., R. A. Feely, B. R. Carter, D. J. Greeley, D. K. Gledhill, and K. M. Arzayus (2015), Global Biogeochemical Cycles saturation state in the global oceans, Global Biogeochem. Cycles, 29, 1656–1673, doi:10.1002/2015GB005198.

Khatiwala, S., F. Primeau, and T. Hall (2009), Reconstruction of the history of anthropogenic $CO_2$ concentrations in the ocean., Nature, 462(7271), 346–349, doi:10.1038/nature08526.

Khatiwala, S., et al. (2013), Global ocean storage of anthropogenic carbon, Biogeosciences, 10(4), 2169–2191, doi:10.5194/bg-10-2169-2013.

Körtzinger, A., M. Rhein, and L. Mintrop (1999), Anthropogenic $CO_2$ and CFCs in the North Atlantic Ocean - A comparison of man-made tracers, Geophys. Res. Lett., 26(14), 2065–2068, doi:10.1029/1999GL900432.

Lamb, M. F., et al. (2002), Consistency and synthesis of Pacific Ocean $CO_2$ survey data, Deep Sea Res., Part II, 49(1-3), 21–58, doi:10.1016/S0967-0645(01)00093-5.

Le Quéré, C., T. Takahashi, E. T. Buitenhuis, C. Rödenbeck, and S. C. Sutherland (2010), Impact of climate change and variability on the global oceanic sink of $CO_2$, Global Biogeochem. Cycles, 24, GB4007, doi:10.1029/2009GB003599.

Levine, N. M., S. C. Doney, R. Wanninkhof, K. Lindsay, and I. Y. Fung (2008), Impact of ocean carbon system variability on the detection of temporal increases in anthropogenic $CO_2$, J. Geophys. Res., 113, C03019, doi:10.1029/2007JC004153.

Levitus, S., J. Antonov, and T. Boyer (2005), Warming of the world ocean, 1955-2003, Geophys. Res. Lett., 32, L02604, doi:10.1029/2004GL021592.

Liu, X., M. C. Patsavas, and R. H. Byrne (2011), Purification and characterization of meta-cresol purple for spectrophotometric seawater ph measurements, Environ. Sci. Technol., 45(11), 4862–4868, doi:10.1021/es200665d.

McPhaden, M. J., and D. Zhang (2002), Slowdown of the meridional overturning circulation in the upper Pacific Ocean, Nature, 415(6872), 603–608, doi:10.1038/415603a.

Mecking, S., C. Langdon, R. A. Feely, C. L. Sabine, C. A. Deutsch, and D. H. Min (2008), Climate variability in the North Pacific thermocline diagnosed from oxygen measurements: An update based on the U.S. CLIVAR/$CO_2$ Repeat Hydrography cruises, Global Biogeochem. Cycles, 22, GB3015, doi:10.1029/2007GB003101.

Mehrbach, C., C. H. Culberson, J. E. Hawley, and R. M. Pytkowicz (1973), Measurement of the apparent dissociation constants of carbonic acid in seawater at atmospheric pressure, Limnol. Oceanogr., 18(6), 897–907, doi:10.4319/lo.1973.18.6.0897.

Midorikawa, T., M. Ishii, S. Saito, D. Sasano, N. Kosugi, T. Motoi, H. Kamiya, A. Nakadate, K. Nemoto, and H. Y. Inoue (2010), Decreasing pH trend estimated from 25-yr time series of carbonate parameters in the western North Pacific, Tellus, Ser. B, 62(5), 649–659, doi:10.1111/j.1600-0889.2010.00474.x.

Mikaloff Fletcher, S. E. et al. (2006), Inverse estimates of anthropogenic $CO_2$ uptake, transport, and storage by the ocean, Global Biogeochem. Cycles, 20, GB2002, doi:10.1029/2005GB002530.

Murata, A., Y. Kumamoto, K. I. Sasaki, S. Watanabe, and M. Fukasawa (2009), Decadal increases of anthropogenic $CO_2$ along 149??E in the western North Pacific, J. Geophys. Res., 114, C04018, doi:10.1029/2008JC004920.

Pardo, P. C., F. F. Pérez, S. Khatiwala, and A. F. Ríos (2014), Anthropogenic $CO_2$ estimates in the Southern Ocean: Storage partitioning in the different water masses, Prog. Oceanogr., 120, 230–242, doi:10.1016/j.pocean.2013.09.005.

Peng, T. H., R. Wanninkhof, and R. A. Feely (2003), Increase of anthropogenic $CO_2$ in the Pacific Ocean over the last two decades, Deep Sea Res. Part II, 50(22-26), 3065–3082, doi:10.1016/j.dsr2.2003.09.001.

Pierrot, D., E. Lewis, and D. W. R. Wallace (2006), MS Excel program developed for $CO_2$ system calculations, ORNL/CDIAC-105a, Carbon Dioxide Inf. Anal. Cent., Oak Ridge Natl. Lab., U.S. Dep. Energy, Oak Ridge, Tennessee, doi:10.3334/CDIAC/otg.CO2SYS_XLS_CDIAC105a.

Quay, P., R. Sonnerup, J. Stutsman, J. Maurer, A. Körtzinger, X. A. Padin, and C. Robinson (2007), Anthropogenic $CO_2$ accumulation rates in the North Atlantic Ocean from changes in the 13C/12C of dissolved inorganic carbon, Global Biogeochem. Cycles, 21, GB1009, doi:10.1029/2006GB002761.

Reid, J. L. (1997), On the total geostrophic circulation of the pacific ocean: Flow patterns, tracers, and transports, Prog. Oceanogr., 39, 263–352, doi:10.1016/S0079-6611(97)00012-8.

Revelle, R., and H. E. Suess (1957), Carbon Dioxide Exchange Between Atmosphere and Ocean and the Question of an Increase of Atmospheric $CO_2$ during the Past Decades, Tellus, 9(1), 18–27, doi:10.1111/j.2153-3490.1957.tb01849.x.

Roden, G. I. (1991), Subarctic-subtropical transition zone of the North Pacific: Large-scale aspects and mesoscale structure, Biol. Oceanogr. Fish. North Pacific, 105, 1–38.

Sabine, C. L., and T. Tanhua (2010), Estimation of anthropogenic $CO_2$ inventories in the ocean, Annu. Rev. Mar. Sci., 2, 175–198, doi:10.1146/annurev-marine-120308-080947.

Sabine, C. L., R. A. Feely, R. M. Key, J. L. Bullister, F. J. Millero, K. Lee, T.-H. Peng, B. Tilbrook, T. Ono, and C. S. Wong (2002), Distribution of anthropogenic $CO_2$ in

the Pacific Ocean, Global Biogeochem. Cycles, 16(4), 1083, doi:10.1029/2001GB001639.

Sabine, C. L., et al. (2004), The Oceanic Sink for Anthropogenic $CO_2$, Science, 305(5682), 367–371, doi:10.1126/science.1097403.

Sabine, C. L., R. A. Feely, F. J. Millero, A. G. Dickson, C. Langdon, S. Mecking, and D. Greeley (2008), Decadal changes in Pacific carbon, J. Geophys. Res., 113, C07021, doi:10.1029/2007JC004577.

Schlitzer, R. (2015), Ocean Data View, ODV. [Available at odv.awi.de.]

Shulenberger, E., and J. L. Reid (1981), The Pacific shallow oxygen maximum, deep chlorophyll maximum, and primary productivity, reconsidered, Deep Sea Res., Part A, 28(9), 901–919, doi:10.1016/0198-0149(81)90009-1.

Stuiver, M., P. D. Quay, and H. G. Ostlund (1983), Abyssal water carbon-14 distribution and the age of the world oceans, Science, 219(4586), 849–51, doi:10.1126/science.219.4586.849.

Suzuki, T. et al. (2013), PACIFICA data synthesis project, ORNL/CDIAC-159, NDP-092, Carbon Dioxide Inf. Anal. Cent., Oak Ridge Natl. Lab., U.S. Dep. Energy, Oak Ridge, Tenn., doi:10.3334/CDIAC/OTG.PACIFICA_NDP092.

Takahashi, T., et al. (2009), Climatological mean and decadal change in surface ocean $pCO_2$, and net sea-air $CO_2$ flux over the global oceans, Deep Sea Res. Part II, 56(8-10), 554–577, doi:10.1016/j.dsr2.2008.12.009.

Takahashi, T., S. C. Sutherland, D. W. Chipman, J. G. Goddard, and C. Ho (2014), Climatological distributions of pH, $pCO_2$, total $CO_2$, alkalinity, and $CaCO_3$ saturation in the global surface ocean, and temporal changes at selected locations, Mar. Chem., 164, 95–125, doi:10.1016/j.marchem.2014.06.004.

Talley, L. D. (1993), Distribution and Formation of North Pacific Intermediate Water, J. Phys. Oceanogr., 23(3), 517–537, doi:10.1175/1520-0485(1993)023<0517:dafonp>2.0.co;2.

Talley, L. D., et al. (2016), Changes in Ocean Heat, Carbon Content, and Ventilation: A Review of the First Decade of GO-SHIP Global Repeat Hydrography, Annu. Rev. Mar. Sci., 8(1), 185-215, doi:10.1146/annurev-marine-052915-100829.

Tanhua, T., A. Körtzinger, K. Friis, D. W. Waugh, and D. W. R. Wallace (2007), An estimate of anthropogenic $CO_2$ inventory from decadal changes in oceanic carbon content., Proc. Natl. Acad. Sci. U. S. A., 104(9), 3037–3042, doi:10.1073/pnas.0606574104.

Tanhua, T., S. van Heuven, R. M. Key, A. Velo, A. Olsen, and C. Schirnick (2010), Quality control procedures and methods of the CARINA database, Earth Syst. Sci. Data, 2(1), 35–49, doi:10.3334/CDIAC/otg.CARINA.SO.V1.0.

Wakita, M., et al. (2013), Ocean acidification from 1997 to 2011 in the subarctic western North Pacific Ocean, Biogeosciences, 10(12), 7817–7827, doi:10.5194/bg-10-7817-2013.

Wallace, D. W. R. (1995), Monitoring global ocean carbon inventories, OOSDP Background Rep., 5, 54.

Wang, Z. A., and W.-J. Cai (2004), Carbon dioxide degassing and inorganic carbon export from a marsh-dominated estuary (the Duplin River): A marsh $CO_2$ pump, Limnol. Oceanogr. Methods, 49(2), 341–354, doi:10.4319/lo.2004.49.2.0341.

Wanninkhof, R., and W. R. McGillis (1999), A cubic relationship between air-sea $CO_2$ exchange and wind speed, Geophys. Res. Lett., 26(13), 1889–1892, doi:10.1029/1999GL900363.

Wanninkhof, R., S. C. Doney, J. L. Bullister, N. M. Levine, M. Warner, and N. Gruber (2010), Detecting anthropogenic $CO_2$ changes in the interior Atlantic Ocean between 1989 and 2005, J. Geophys. Res., 115, C11028, doi:10.1029/2010JC006251.

Waters, J. F., F. J. Millero, and C. L. Sabine (2011), Changes in South Pacific anthropogenic carbon, Global Biogeochem. Cycles, 25, GB4011, doi:10.1029/2010GB003988.

Waugh, D. W., T. M. Hall, B. I. McNeil, R. Key, and R. J. Matear (2006), Anthropogenic $CO_2$ in the oceans estimated using transit time distributions, Tellus, Ser. B, 58(5), 376–389, doi:10.1111/j.1600-0889.2006.00222.x.

Whitney, F. A., H. J. Freeland, and M. Robert (2007), Persistently declining oxygen levels in the interior waters of the eastern subarctic Pacific, Prog. Oceanogr., 75(2), 179–199, doi:10.1016/j.pocean.2007.08.007.

Williams, N. L., R. A. Feely, C. L. Sabine, A. G. Dickson, J. H. Swift, L. D. Talley, and J. L. Russell (2015), Quantifying Anthropogenic Carbon Inventory Changes in the Pacific Sector of the Southern Ocean, Mar. Chem., 174, 147–160, doi:10.1016/j.marchem.2015.06.015.

Wong, C. S., J. R. Christian, S. K. Emmy Wong, J. Page, L. Xie, and S. Johannessen (2010), Carbon dioxide in surface seawater of the eastern North Pacific Ocean (Line P), 1973-2005, Deep Sea Res. Part I, 57(5), 687–695, doi:10.1016/j.dsr.2010.02.003.

Yao, W., X. Liu, and R. H. Byrne (2007), Impurities in indicators used for spectrophotometric seawater pH measurements: Assessment and remedies, Mar. Chem., 107(2), 167–172, doi:10.1016/j.marchem.2007.06.012.

**Figure 1.** Northeast Pacific study region showing the segment of the P17N transect occupied by the present study (cruise NH1208) in 2012. For NH1208, there were 34 water-column sampling stations; 22 (white circles) were sampled to 1000 m at 15 depths while the rest (black squares) were sampled to 3000 m at 24 depths. Color scale shows sea surface temperature from a 1 month satellite composite of Aqua MODIS data centered at 16 August 2012.

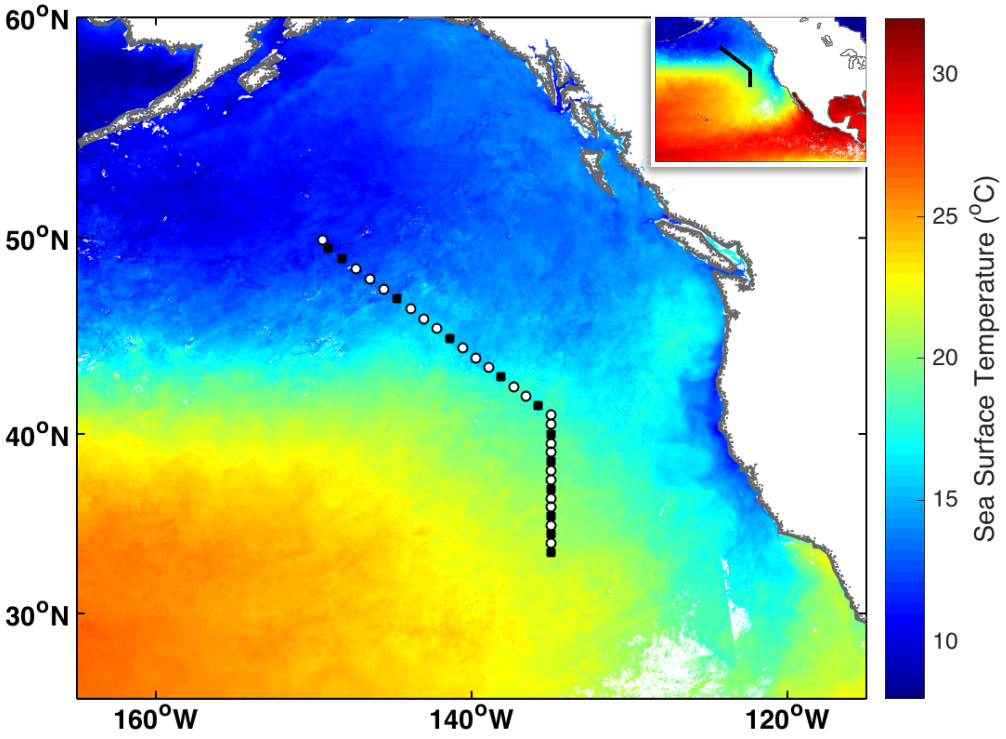

**Figure 2**. Latitudinal sections from the 2012 occupation of P17N for salinity, AOU, DIC, and Revelle Factor (calculated from DIC and TA) overlaid with potential density contours. The sections are gridded on 1° by 50 m grids with Data-Interpolating Variational Analysis (DIVA) software in Ocean Data View (Schlitzer, 2015).

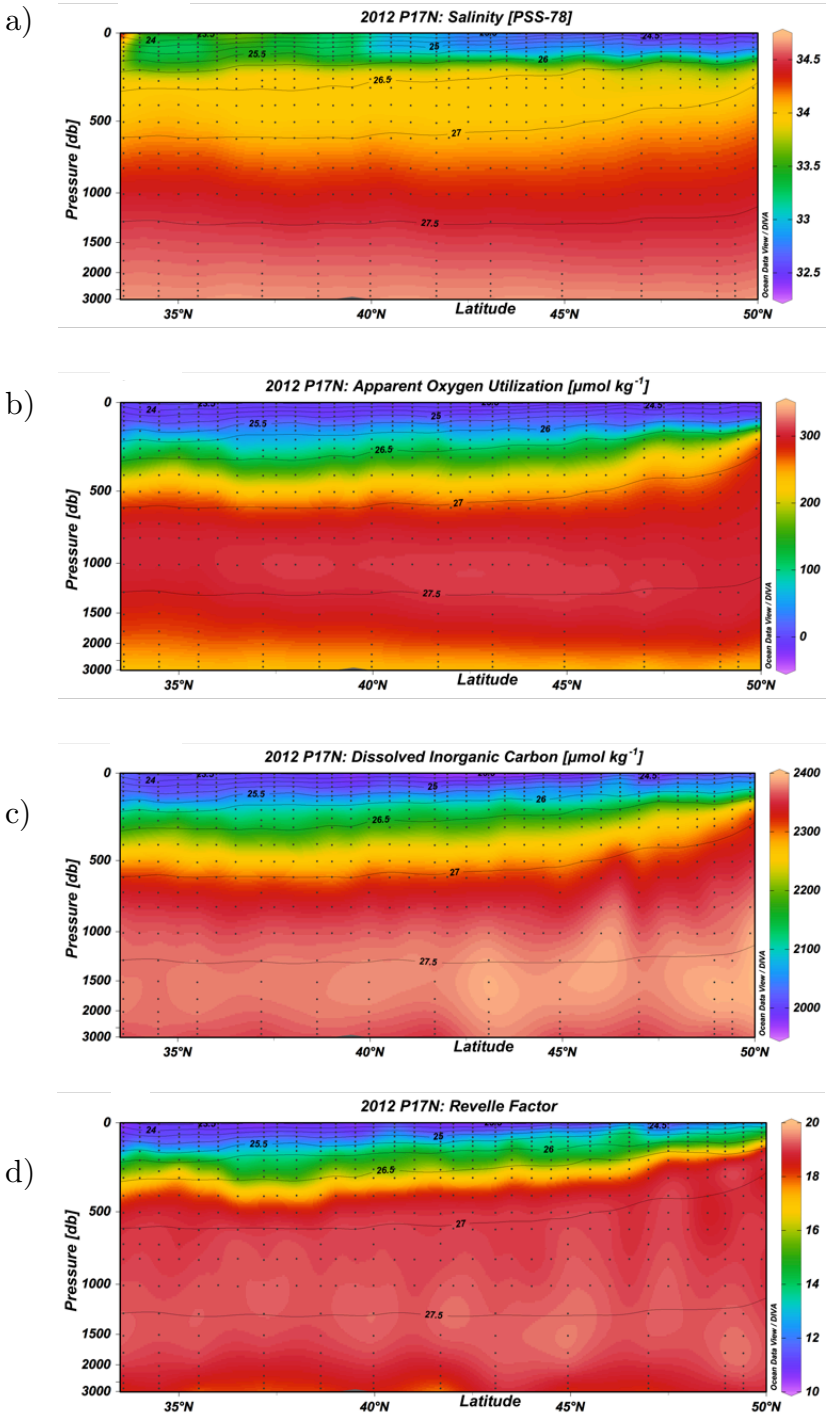

**Figure 3**. Differences between repeat occupations of P17N from 2001 CLIVAR and 2012 NH1208 for salinity, AOU, and DIC overlaid with potential density contour lines.

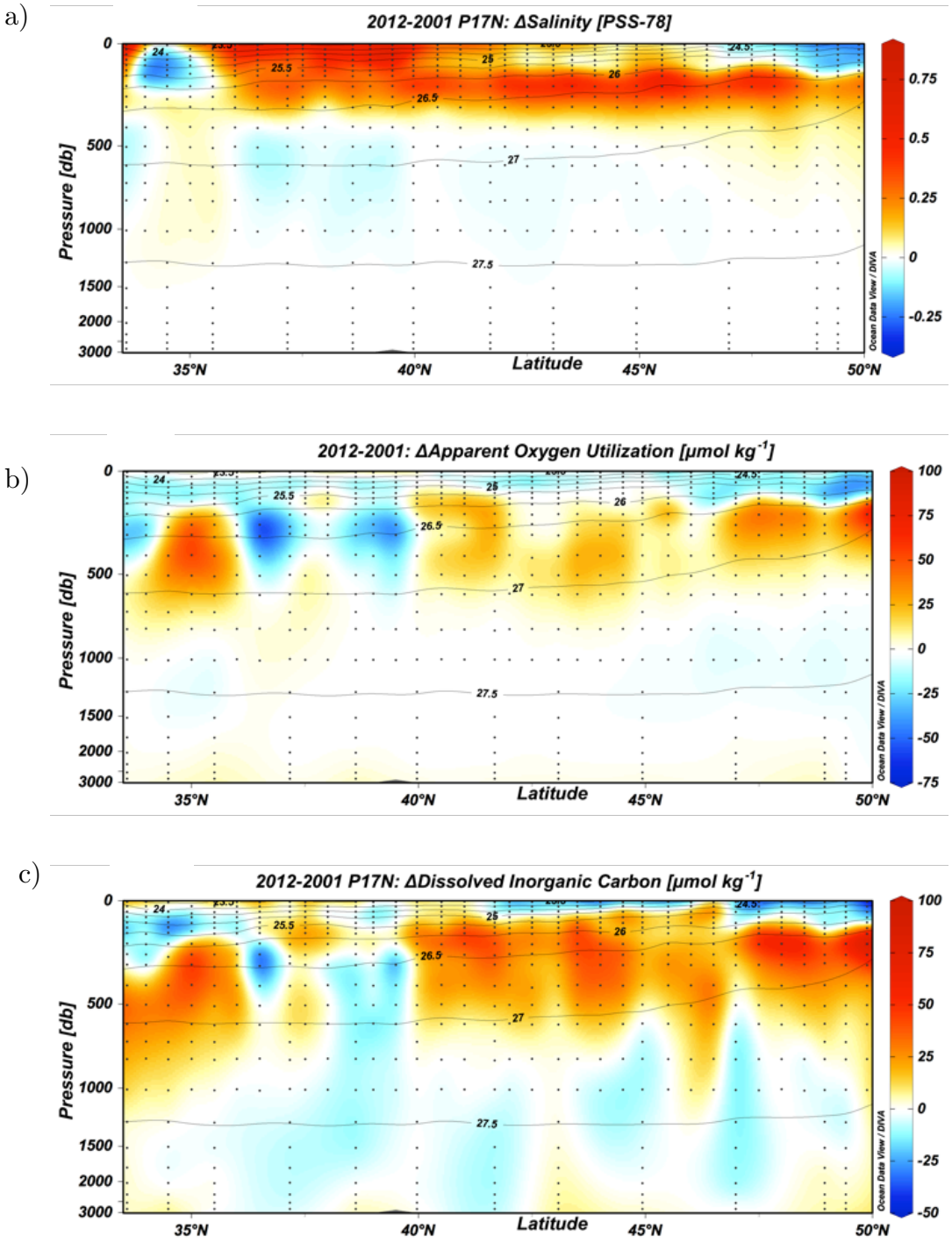

**Figure 4**. a) Cross-sectional plot of eMLR calculated change in anthropogenic $CO_2$ from 2001 to 2012 along P17N with potential density contour lines. Negative $\Delta C_{anthro}$ are displayed as zero. b) Cross-sectional plot of WOCE 1993 CFC-11 concentrations across P17.

a)

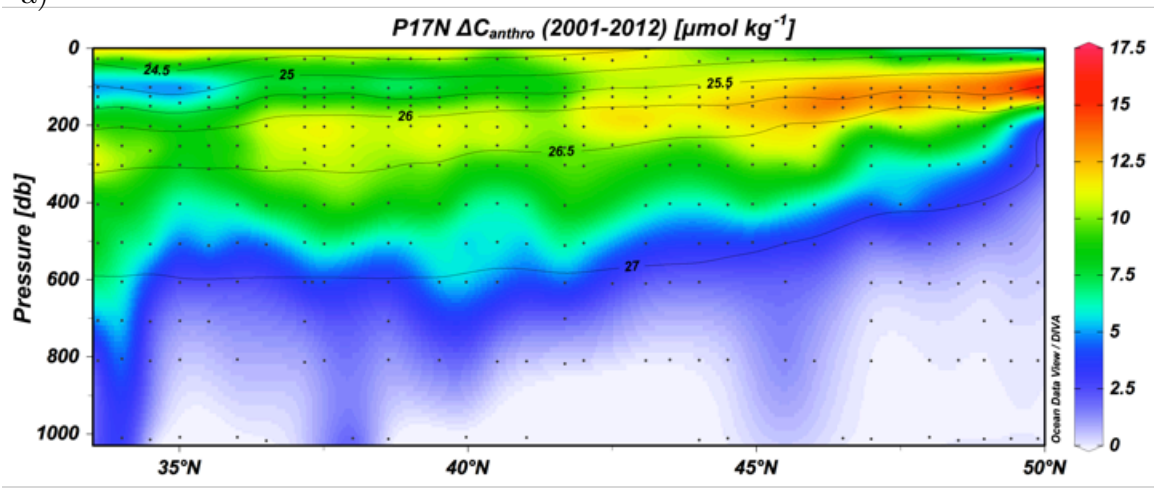


b)

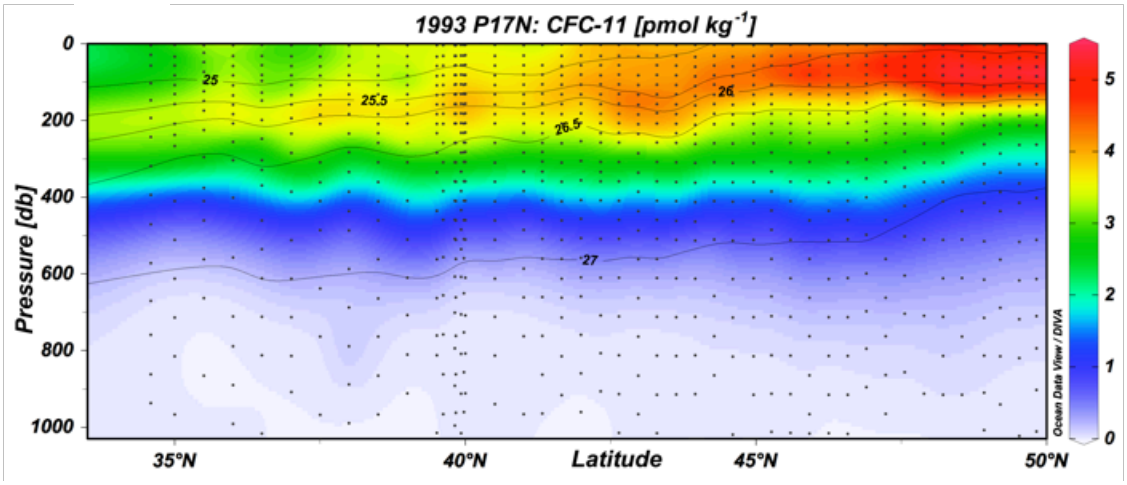

**Figure 5**. Change in column inventory of $C_{anthro}$ between 2001 and 2012 binned to 1° latitude resolution. The eMLR results (blue) are compared to those estimated using a community ecosystem model (CESM) (red) (Doney et al., 2009a, 2009b). The residual between the two models is plotted in yellow.

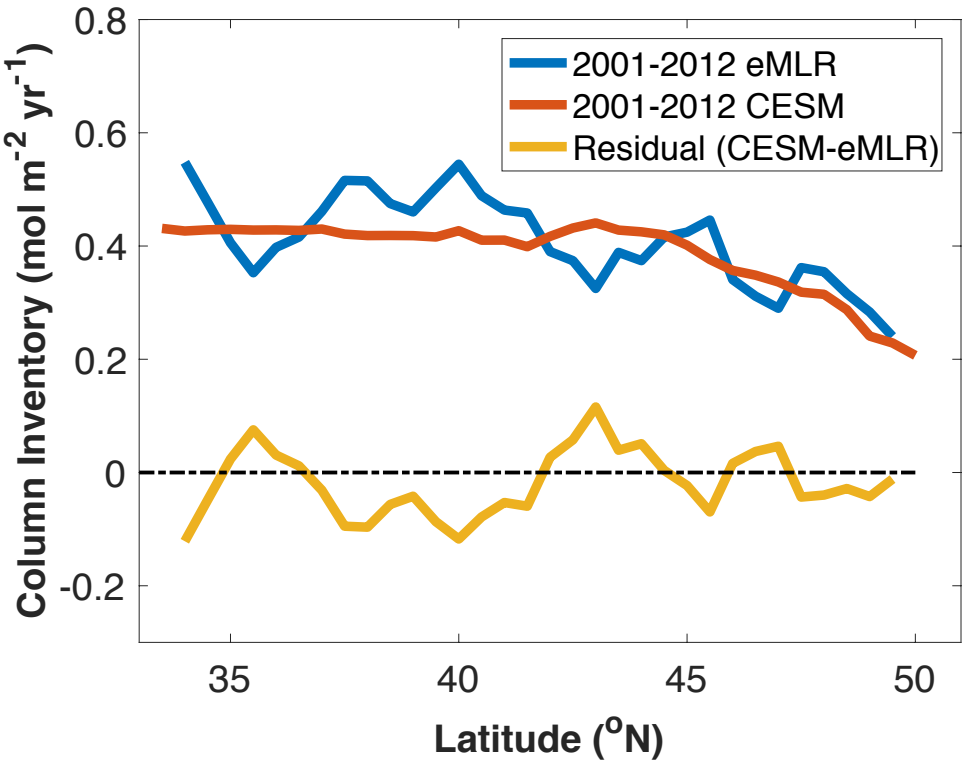

**Figure 6**. Comparison of the $\Delta C_{anthro}$ storage rates between the P17N transect (2001 – 2012) and the P16 transect (1991/1992 – 2006) (Sabine et al., 2008).

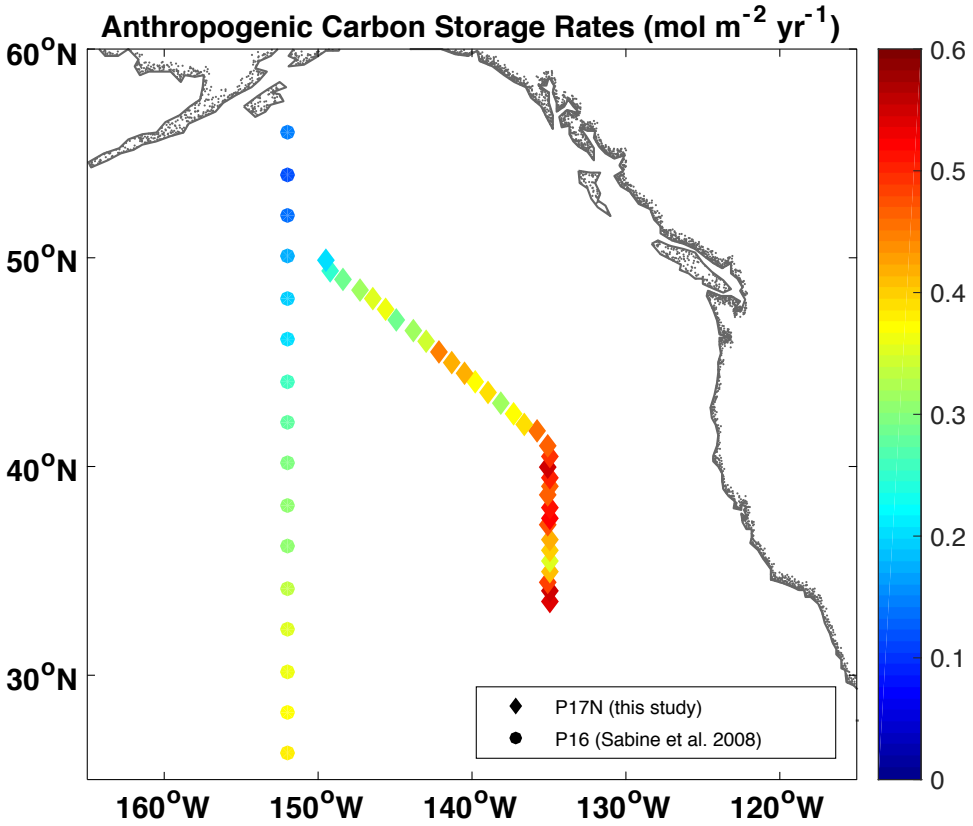

**Figure 7**. Latitudinal distribution of change in a) pH and b) aragonite saturation state due to $\Delta C_{anthro}$ along the P17 transect between 2001 and 2012 with potential density contour lines.

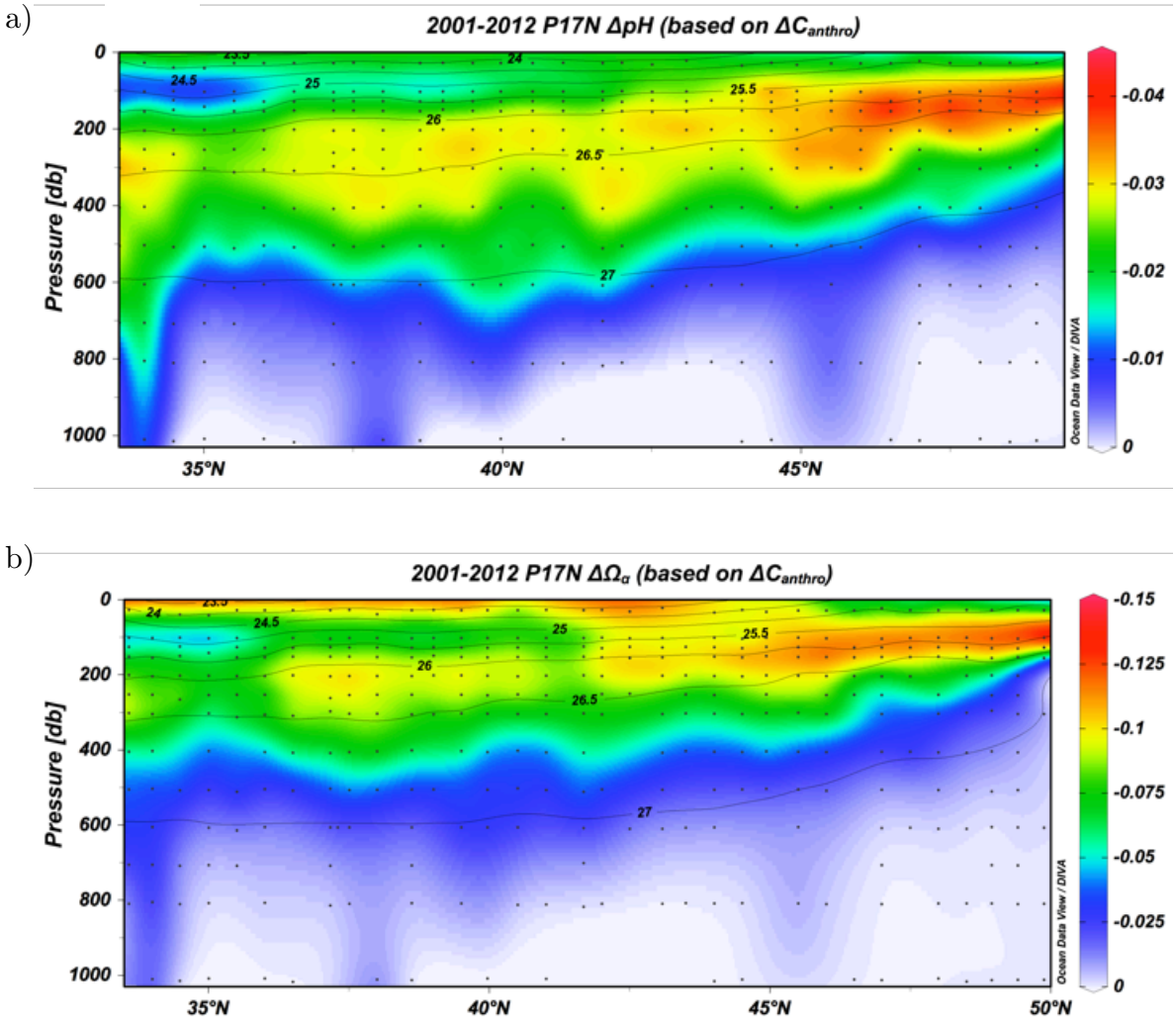

**Table 1**. PACIFICA Recommended adjustments for CLIVAR P17N 2001 are shown here along with deep isopycnal crossover results for NH1208 2012 cruise adjusted to the CLIVAR 2001 PACIFICA-corrected data.[a]

| | Salinity | Oxygen | Nitrate | Silicate | Phosphate | DIC | TA |
|---|---|---|---|---|---|---|---|
| CLIVAR 2001 | 0 | 1 | 1 | 1.048 | 1 | -4 | 8 |
| NH1208 2012 | 0 | 0.955 | 1 | 1.032 | 1.021 | 11 | 10 |

[a]Salinity, DIC, and TA factors are additive, while oxygen, nitrate, phosphate, and silicate factors are multiplicative. Units for all parameters are in μmol $kg^{-1}$ except for salinity, which is measured on the practical salinity scale.

**Table 2**. Coefficients used for the DIC (μmol $kg^{-1}$) eMLR analysis of 2001 CLIVAR and 2012 NH1208 cruises.

| | INTERCEPT | AOU (μmol $kg^{-1}$) | S (PSS-78) | ϑ (°C) | Si (μmol $kg^{-1}$) | N | RMSE | $R^2$ |
|---|---|---|---|---|---|---|---|---|
| 2001 | 892.8 ± 28.6 | 0.67 ± 0.01 | 36.25 ± 0.78 | -7.58 ± 0.18 | 0.36 ± 0.02 | 278 | 2.9 | 0.99 |
| 2012 | 797.6 ± 102.5 | 0.64 ± 0.02 | 39.96 ± 3.15 | -9.22 ± 0.46 | 0.23 ± 0.04 | 315 | 10.0 | 0.99 |

## 2.7 Supplemental information for Chapter 2

**Text S1.** Sample analysis procedures for dissolved oxygen and salinity

Dissolved oxygen (DO) samples were collected from CTD Niskin bottles into 150 mL brown glass tincture bottles. Sodium iodide-sodium hydroxide mixture and manganese chloride were added sequentially to the sample immediately after collection and mixed thoroughly. One mL of sulfuric acid was added and mixed into the sample prior to measurement. DO samples were measured after temperature equilibration, within 3 days, on an automated dissolved oxygen titrator developed at Woods Hole Oceanographic Institution. The system is based on the Winkler technique. This method has an accuracy of 1.0 μmol $kg^{-1}$ and precision of 0.2 μmol $kg^{-1}$. The titrator was standardized with sodium thiosulfate for each group of analyses, usually about 30 samples. A custom procedure was developed and implemented to detect concentrations of dissolved oxygen $< 90$ μmol $kg^{-1}$. *In situ* temperature was used to calculate potential density in order to convert from mL $L^{-1}$ to μmol $kg^{-1}$ for bottle samples. Ideally, the conversion temperature should be the temperature measured at the time of sample drawing, but those were not measured. Bottle values were used to calibrate CTD values.

Salinity samples were collected into 250 mL square cross-sectioned, borosilicate glass bottles and measured on an Autosal Salinometer (Guildline 8400B). PSS-78 salinity was calculated from measured conductivity ratios. Measurements were performed after samples had equilibrated to laboratory temperature, within 3 days after collection. The machine was standardized for each group of analyses, approximately 50 samples.

International Association for the Physical Sciences of the Oceans (IAPSO) Standard Seawater Batch P-152 was used for standardization. This method has an accuracy of ±0.003 and precision of ± 0.0002. Bottle analyses were used to calibrate CTD salinity values.

**Figure S1**. Deep isopycnal crossover analyses were used to correct systematic offsets between different cruise occupations of similar locations. Results from the analysis are shown in Table 1 in the main paper. Data from >2000 m for CLIVAR 2001 (red) and NH1208 2012 (blue) was plotted against potential density referenced to 3000 dbar ($\sigma_3$) and fit by a second-order polynomial. If an offset was found, NH1208 2012 cruise data was corrected to the CLIVAR 2001 data. The corrected data is plotted in green. (a) salinity vs. $\sigma_3$ (b) phosphate vs. $\sigma_3$ (c) nitrate vs. $\sigma_3$ (d) silicate vs. $\sigma_3$ (e) dissolved oxygen vs. $\sigma_3$ (f) dissolved inorganic carbon vs. $\sigma_3$ (g) total alkalinity vs. $\sigma_3$.

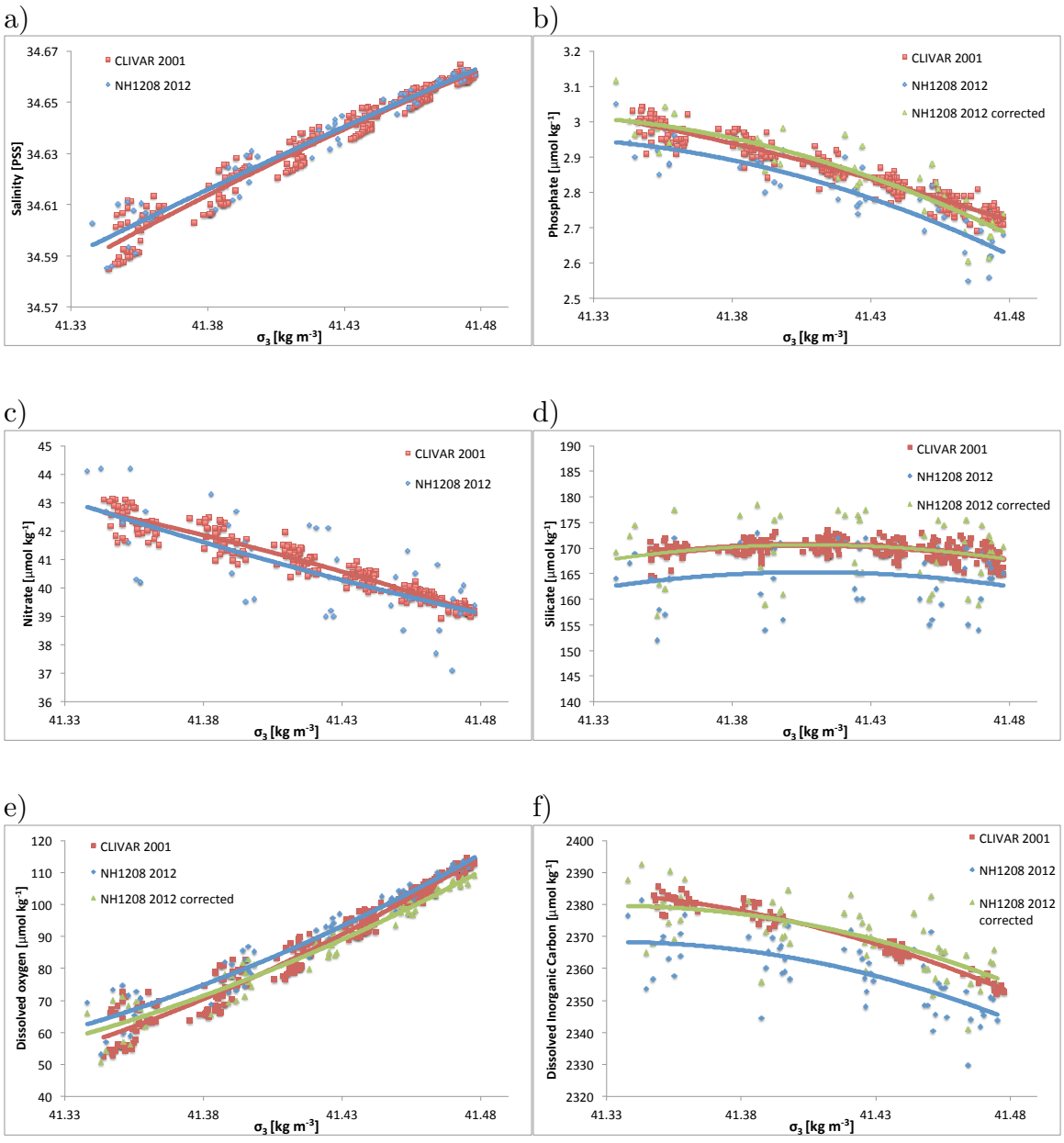

g)

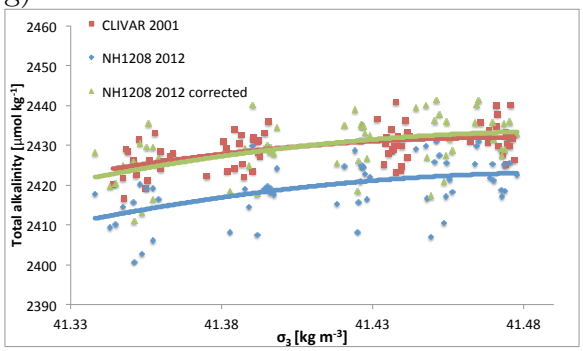
CLIVAR 2001
NH1208 2012
NH1208 2012 corrected
Total alkalinity [µmol kg-1]
2460
2450
2440
2430
2420
2410
2400
2390
41.33
41.38
41.43
41.48
σ3 [kg m-3]

**Figure S2.** Residuals between the DIC MLR model and measured values from the 2012 NH1208 cruise plotted against potential density, latitude, and depth show no significant trends, confirming that binning the dataset by potential density or latitude would not affect MLR results.

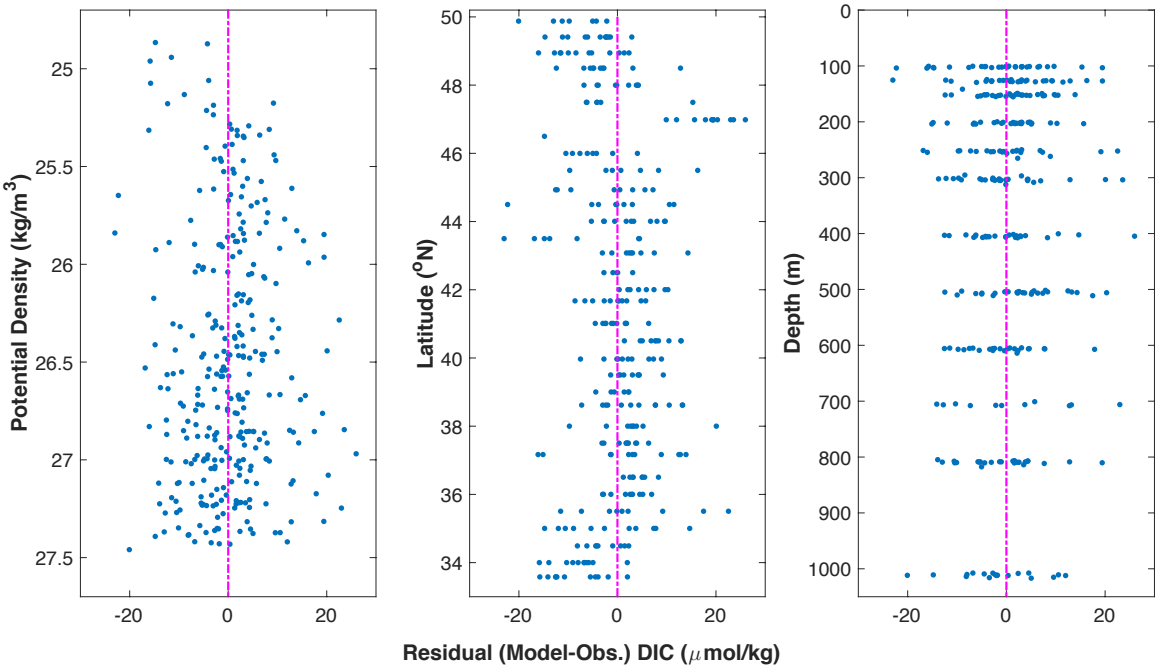

# Chapter 3

Intertidal salt marshes as an important total alkalinity source to the coastal ocean

## 3.1 Abstract

Intertidal salt marshes are potentially important to the global alkalinity budget, yet due to the extreme variability in local processes, it has been difficult to collect sufficient data to quantify tidal export of total alkalinity (TA) from marshes. In this study, high-frequency, in situ measurements of biogeochemical parameters and bottle samples are used in a multiple linear regression (MLR) empirical model to quantify the total alkalinity flux from an intertidal salt marsh – Sage Lot Pond (SLP), Waquoit Bay, MA. Discrete bottle samples showed how TA and dissolved inorganic carbon (DIC) concentrations varied greatly over tidal and seasonal cycles. After tidal exchange, ebb tides containing input from salt marsh porewaters often carried elevated concentrations of TA and DIC, the degree to which varied across seasons. Export occurred primarily during the summer, concurrent with greater rates of aerobic and anaerobic respiration. A similar empirical model was used to estimate DIC and there was reasonable agreement with directly measured DIC suggesting that the MLR method is realistic. Annual TA export from intertidal salt marshes was -12 ± 1 mol $m^{-2}$ $yr^{-1}$. Additionally, lateral export of DIC was -28 ± 3 mol $m^{-2}$ $yr^{-1}$. Scaling up these fluxes to the East Coast gives 0.15 and 0.34 Tmol $yr^{-1}$ for TA and DIC, respectively. This DIC flux is similar to 0.18-0.43 Tmol $yr^{-1}$ previously reported for U.S. East Coast tidal wetlands.

## 3.2 Introduction

Intertidal salt marshes are highly productive coastal ecosystems that export carbon and other biogeochemical species to the coastal ocean. Recent studies suggest

dissolved inorganic carbon (DIC) and total alkalinity (TA) exports from salt marshes may be important terms in coastal ocean carbon budgets (Wang and Cai 2004; Cai 2011; Bauer et al., 2013; Krumins et al., 2013). However, the published literature on salt marshes contains few studies with sufficient spatial and temporal resolution to accurately quantify these fluxes (Morris and Whiting 1986; Cai and Wang 1998; Raymond et al., 2000; Raymond and Hopkinson 2003; Wang and Cai 2004). The salt marsh TA export flux and its effects on carbon cycling of adjacent coastal systems is particularly poorly known. While it has been recognized that marshes generate alkalinity (Howarth and Giblin 1983), the export has never been quantified based on direct alkalinity measurements. Quantifying alkalinity fluxes from salt marshes is important for coastal and overall ocean alkalinity budgets in understanding the future role of alkalinity in buffering the effects of coastal ocean acidification.

Anaerobic respiration in sediments is important to generation of alkalinity in salt marshes. While aerobic respiration processes produce DIC and slightly decrease TA (if nitrate is released), anaerobic respiration processes produce both DIC and TA (Brewer and Goldman 1976; Goldman and Brewer 1980). Sediments underlying Spartina alterniflora, the major primary producer in salt marshes on the Atlantic coast of North America, are oxygen depleted 1 cm below sediment surface (Teal and Kanwisher 1961; Howes et al., 1981). Below 1 cm, anaerobic remineralization processes can lead to net generation of alkalinity. Denitrification is often coupled to nitrification, which leads to no net generation of alkalinity, and methanogenesis account for small portion of total

sediment respiration (Howarth and Teal 1979; Kaplan et al., 1979; King and Wiebe 1980) while sulfate reduction has often been identified as the dominant anaerobic remineralization pathway of organic matter in salt marshes (Skyring et al., 1979; Howarth and Teal 1979; Howarth and Giblin 1983; Howarth and Merkel 1984; Giblin 1988). Iron and sulfate reduction coupled to burial of iron sulfide minerals such as iron monosulfide and pyrite can generate a net alkalinity gain (Berner et al., 1970; Stumm and Morgan 1996; Giblin and Howarth 1984; Hu and Cai 2011). Tidal exchange transports these enriched porewater signals to overlying waters where they can be exported to the coastal ocean.

Recent studies have suggested alkalinity export from coastal sediments can be significant to the coastal alkalinity budget with anaerobic alkalinity generation facilitating as much as 10 to 60% of the $CO_2$ uptake in continental shelves and marginal seas. (Thomas et al., 2009; Hu and Cai 2011). Salt marshes are also sites of considerable anaerobic generation of alkalinity as mentioned previously and through tidal exchange, could have the potential to affect coastal buffering capacity. However, the magnitude of this alkalinity export has not yet been measured. The major objective of this study was to investigate and quantify the variability of lateral export alkalinity fluxes over tidal to annual cycles from an intertidal salt marsh. Biogeochemically-relevant parameters and water fluxes were measured using high-frequency in situ sensors. Empirical models were developed using this data along with measured bottle sample concentrations to estimate

TA and DIC fluxes. This study is the first to provide a high-resolution estimate of lateral alkalinity export from an intertidal salt marsh using high frequency data.

## 3.3 Methods

### 3.3.1 Study site description

Sage Lot Pond (SLP) is an intertidal salt marsh located in Waquoit Bay estuary on Cape Cod, Massachusetts, USA (Figure 1a). It receives relatively low nutrient loading from the watershed, at ~12 kg N $ha^{-1}$ of estuary $yr^{-1}$ (Kroeger et al., 2006) with relatively insignificant groundwater input, which will be discussed in detail later. SLP is a representative U.S. salt marsh with floral and faunal communities, relative sea level rise (2.81 ± 0.18 mm $yr^{-1}$, NOAA Tide Station ID 8447930) and mean annual temperature (9.88°C) similar to other U.S. East Coast marshes (Chmura et al., 2003). A time-series sampling site was established at the mouth of a tidal creek that drains a portion of the marsh to capture tidal exchange between the marsh and neighboring estuary (Figure 1b). Both discrete sampling and high-frequency, in situ sensor measurements were obtained at this site. A drainage area was defined using a 1-m bare-earth LiDAR-derived digital elevation model (DEM) of Massachusetts based on the North American Vertical Datum of 1988 (NAVD88) and a water drop analysis routine (Wang et al., 2016). The tidal creek drained a watershed area of 4132 $m^2$.

### 3.3.2 Discrete bottle sample collection and analysis

Discrete bottle samples were collected on 1-2 hour intervals at the tidal creek sampling site using a peristaltic or diaphragm pump for periods of a few hours up to a full tidal cycle (~12-14 hr) in June, July, August, October 2013; July, December 2014; and April, July, October, November, December 2015. There were 21 total sampling days with 30, 56, and 88 TA bottle samples and 32, 57, and 89 DIC bottle samples in spring, summer, and fall, respectively. Here, we define spring as April to June, summer as July to September, and fall as October to December. TA and DIC sample collection and analysis followed standard best practice procedures outlined by Dickson et al. (2007). Briefly, samples were collected through capsule filters with 0.45 μm pore size (Farrwest Environmental Supply, Texas, USA) into 250 mL borosilicate bottles, poisoned with 100 μL saturated mercuric chloride, sealed with a glass stopper coated with APIEZON® – L grease and secured with a rubber band.

Discrete samples of DIC were measured with an Apollo SciTech DIC auto-analyzer (Model AS-C3) by acidifying the sample with 10% phosphoric acid. The acidified $CO_2$ sample was purged with high purity nitrogen gas and total $CO_2$ gas was detected with a LICOR-7000 infrared analyzer (LI-COR Environmental, Nebraska, USA). Certified Reference Material (CRM) from Dr. A.G. Dickson at the Scripps Institution of Oceanography was used to calibrate the DIC auto-analyzer. DIC values were reported in μmol $kg^{-1}$ after being corrected for water density and mercuric chloride addition. The average difference in duplicates was 1.7 ± 12.1 μmol $kg^{-1}$ (n=8) compared

to the precision and accuracy of ± 2.0 μmol $kg^{-1}$ (1σ) of the instrument. The larger standard deviation in duplicates could be a result of the time and possible concentration difference incurred while filling the duplicate bottles one after the other over a few minutes or due to storage errors.

Discrete TA samples were measured with an Apollo SciTech alkalinity auto-titrator (AS-ALK2, Delaware, USA) using a modified Gran titration (Wang and Cai 2004; Wang et al. 2013) in an open-cell configuration with a ROSS combination electrode at 22.0 ± 0.1°C. The electrode was calibrated using pH buffers and the concentration of hydrochloric acid used in the titration was calibrated using CRM. The average difference in duplicates was 0.1 ± 2.4 μmol $kg^{-1}$ (n=8) which is similar to the precision and accuracy of the instrument, ± 2.0 μmol $kg^{-1}$. It is important to note that total alkalinity measurements may include contributions from non-carbonate sources, such as nutrient or organic acids. Based on nutrient data from this site, phosphate and silicate alkalinity are negligible (<4 μmol $kg^{-1}$). Organic alkalinity has been associated with dissolved organic matter such as fulvic acids, often referred to as humic substances (Cantrell et al., 1990; Hemond 1990; Cai et al., 1998; Lozovik et al., 2005). Direct titrations of non-carbonate alkalinity (Cai et al., 1998) from selected tidal cycle samples indicate concentrations of organic alkalinity range from negligible to 100 μmol $kg^{-1}$, in flooding and ebbing water, respectively, accounting for up to 8% of total alkalinity.

### 3.3.3 High-frequency data collection and analysis

High-frequency, time-series *in situ* sensors were deployed from April 2013 – December 2015 at the Sage Lot Pond tidal creek study site to continuously monitor and record parameters in the creek water column. An EXO2 Multiparameter Sonde (YSI Inc., Yellow Springs, OH) measured temperature (T), salinity (S), dissolved oxygen (DO), fluorescent dissolved organic matter (FDOM), oxidation/reduction potential (ORP), and probe pH. A SonTek IQ Plus acoustic Doppler velocity meter (ADVM) (Sontek/YSI, San Diego, CA) measured water flux and surface elevation. The YSI EXO2 recorded at intervals ranging from 2 min to 8 min and the Sontek IQ recorded time-averaged data every 15 min. The relative elevation of the SonTek IQ was referenced to NAVD88, which is based on repeated long-term GPS base station occupations and associated with negligible error. Sensors were cleaned and calibrated according to manufacturer recommendations. After a deployment period of 2-4 weeks, YSI EXO2 data was evaluated for fouling and calibration drift. A correction factor based on calibration standards and the assumption of linear drift was applied to the data as needed. When correction was greater than 30% of the calibration value for ORP or salinity, or greater than 2 pH units for pH, data was discarded (Wagner et al., 2006). YSI EXO2 pH measurements (NBS scale) have a measurement uncertainty of up to 0.20 pH units and other YSI EXO2 parameters have uncertainties up to 1% for salinity, 0.05 °C for temperature, 1% for dissolved oxygen, and 20 mV for ORP.

The SonTek IQ ADVM includes a vertical beam and integrated pressure sensor to measure water level in addition to four transducers with two along-axis beams and two skew beams to measure velocity. SonTek IQ ADVM proprietary software internally calculates cross-sectional area with user-provided creek geometry and SonTek IQ measured water depth. Cross-sectional area is then multiplied by mean channel velocity to provide flow in and out of the creek. The uncertainty in water flux arising from cross-sectional area and velocity measurement as well as internal algorithms is less than 5%. Data from YSI EXO2 and SonTek IQ in situ sensors were averaged over 5 min intervals.

A high-frequency, in situ, carbon sensor, CHANnelized Optical Sensor (CHANOS) (Wang et al., 2015), was also deployed at the tidal creek sampling site from April-December 2015. CHANOS has two separate channels to measure pH and DIC, where the pH channel uses a flow-through, spectrophotometric method (Wang et al., 2007) and the DIC channel uses an improved spectrophotometric method described in detail in Wang et al. (2013). For this study, only CHANOS DIC measurements were used. They were compared to calculated DIC from a multiple linear regression model that will be discussed in the section 3.4.4. Discussion regarding generation of CHANOS DIC fluxes can be found in Chapter 4 of this thesis.

### 3.3.4 Buffer capacity

Buffer capacity was evaluated using the buffer factor, $\beta_{H,}$ where $\beta_H = -\left(\frac{\partial pH}{\partial [H^+]}\right)^{-1}$ (Morel and Hering 1993; Egleston et al., 2010). $\beta_H$ was calculated using discrete bottle measurements of TA and DIC as well as in situ sensor measurements of

salinity and temperature (Egleston et al., 2010). A larger $\beta_H$ indicates a larger resistance to change of pH in the system due to addition of an acid or base. When alkalinity concentrations are greater than DIC concentrations, the buffering is predominantly related to the carbonate ion concentration. Buffering capacity is at a minimum where TA≈DIC and seawater pH˜7.5, which is halfway between the first and second acidity constants for carbonic acid. This is similar to the way the buffering capacity of a weak acid is greatest when pH is close to acidity constant of the weak acid (Morel and Hering, 1983; Egleston et al., 2010; Wang et al., 2016). When there is an addition of $CO_2$, DIC increases and pH decreases, but there is no effect on TA. If the DIC increase is large enough, buffering capacity in the tidal water could be pushed beyond the minimum buffering point (where TA≈DIC) to where buffering capacity increases with increasing DIC concentration. Unknown non-carbonate alkalinity may affect buffering capacity calculations. In the calculation for $\beta_H$, organic alkalinity was treated as part of carbonate alkalinity. In the summer, when organic alkalinity can reach 100 μmol $kg^{-1}$ in ebbing tide when DIC=2600 μmol $kg^{-1}$, TA=2100 μmol $kg^{-1}$, S=28, t=25 °C (mean condition of summer ebb tide), and if the organic acid has a pK of 5.4 (Cai et al., 1998), the calculation underestimates $\beta_H$ by $< 10\%$.

### 3.3.5 Multiple linear regression models to estimate total alkalinity and dissolved inorganic carbon

Multiple linear regression (MLR) models were created using discrete TA and DIC bottle measurements and in situ sensor parameters to estimate high-frequency TA and

DIC concentrations. Data used for the MLRs covered the time period from June 2013 to December 2015 when bottle and sensor measurements were taken. The best set of parameters to characterize TA concentration was Day', T, S, and DO. Here, Day' = $\sin\left(\frac{2\pi Jday}{365}\right)$, where Jday is Julian Day, a value between 1-365. The Day' term accounts for seasonal cycling, where January is treated similarly to December and February (Lefevre et al., 2005; Friedrich and Oschlies 2009, Signorini et al., 2013). For DIC concentration, parameters were also Day', S, and DO, but ORP instead of T as in the TA MLR. Model parameters for either TA or DIC were not strongly co-varied. Coefficients for the TA and DIC MLRs for this study are shown in Table 1. Parameters were chosen based on data availability, data quality, and goodness of fit. The MLR was selected for a higher correlation coefficient ($R^2$) and lower root mean square error (RMSE). Salinity characterizes mixing effects of the estuary and marsh water on TA and DIC. DO and ORP both represent the effects of respiration processes that occur in the marsh waters as well as sediments. MLRs were able to capture TA and DIC variability at 79% and 77% with an RMSE of 73 and 92 μmol $kg^{-1}$, respectively. These model errors do not have strong effects on the flux calculations due to random errors being partially canceled out when incoming and outgoing (positive and negative) fluxes are integrated as will be discussed later and was also shown in Wang et al. (2016). No significant systematic trends were found when plotting the residuals (model-observation) against parameters used in the MLRs (Supporting information Figure S1).

### 3.3.6 Water fluxes

The water fluxes from the SonTek IQ measurements in the tidal creek were used to derive the base water fluxes used for calculation of high-resolution DIC fluxes as in Wang et al. (2016) and Chapter 4 of this thesis. Corrections were made to the base SonTek IQ fluxes to account for overland flow and groundwater contributions to the marsh. Overland flow occurs if flooding or ebbing tidal water inundates or drains the marsh without going through the creek channel when tidal height is above the marsh surface. The SonTek IQ did not capture the water that flowed over the marsh and not through the creek channel. To correct for overland flow, a hydrodynamic model was created for the drainage basin of the tidal creek using the 1-m DEM with the Coupled Ocean-Atmosphere-Wave-Sediment Transport (COAWST) model (Warner et al., 2010). A ratio of within-channel water to total water over the drainage area was used to develop flood and ebb correction equations. These correction equations were applied to the measured SonTek IQ water fluxes in the creek to derive total fluxes as a function of water level and flow direction (supplemental Figure S2 for overland correction function from Wang et al., 2016). We have treated creek and overland water flow the same based on limited preliminary data that suggests water in the creek is chemically similar to sheet flow over the marsh.

The second correction to the water fluxes was to account for groundwater input. Groundwater affects DIC and TA in two ways. The first way is that groundwater is treated as a net seaward flow of water to flush out marsh DIC and TA without

considering the concentration of DIC and TA in the groundwater. The second way is that groundwater can act as a pathway to directly export DIC and TA. The first correction is applied as a correction to the water fluxes. The mean flow over the study period was shifted by a correction to match to the net groundwater flow estimate. The net groundwater estimate over the study period was -0.00024 $m^3$ $s^{-1}$ or -7570 $m^3$ $yr^{-1}$ calculated using the isohaline method from MacCready (2011) and the salt balance application from Ganju (2011). Adapted from Wang et al. (2016), the groundwater correction shift that was applied was 0.00007 $m^3$ $s^{-1}$, which is only 0.1% of the mean tidal flow magnitude (0.075 $m^3$ $s^{-1}$). The second correction is applied as a concentration correction to the net annual TA and DIC flux estimate. This will be discussed further in section 3.4.3.

### 3.3.7 Error analysis for TA and DIC fluxes

Uncertainty was assessed by error propagation using the maximum uncertainties for parameters used to calculate TA and DIC fluxes. For TA and DIC concentration, there are two methods of error propagation that were investigated. One method involved taking the RMSE from each MLR and applying the RMSE to the lowest TA and DIC concentrations. This allows the uncertainty to be the largest percentage of the concentration. This method yielded a maximum uncertainty of 5% and 8% for TA and DIC concentrations, respectively. The other method involved taking the uncertainty for each parameter in the MLR and propagating the error (square root of the sum of squares of individual errors). A 5% error was assumed for Day, and other uncertainties were

from YSI EXO2 manual, 1% for S, 1% for T, 1% for DO, and 5% for ORP. This led to an error of 5% and 7% for TA and DIC concentrations, respectively. To maximize the error, the first method was used for concentrations.

For water fluxes, uncertainty was assessed for base measurements and corrections. Water flow measurement uncertainty from the ADVM was 5%. Uncertainty for overland and groundwater corrections to water fluxes was assessed two different ways by adjusting flood and ebb equations from the overland correction. First, we applied a factor of ±25% error on the flood and ebb equations to find a range of the error effects. This resulted in ± 6% error on net concentration fluxes. This is representative of how changes in channel geometry would cause changes in the overland correction by affecting the ratio of within channel to total water flow over the drainage area. A widening of the channel would cause shallower water levels and therefore less flooding of the marsh. In contrast, deepening of the channel would cause higher water levels and therefore more flooding of the marsh. Both processes, widening and deepening of the channel, occurring together might have a different effect. Further exploration of these effects will be explored in the future using the 3D hydrodynamic model.

The second way uncertainty due to overland correction was assessed was by applying 100 realizations of random amplifications of errors for flood and ebb equations centered at 25%. The effect on corrected net concentration fluxes was 6% for overland correction, similar to the range of errors calculated in the previous method, and 1% for groundwater correction. Using propagation of error as the square root of the sum of the

squares of individual errors, total error for the instantaneous TA and DIC fluxes was 9% and 11%, respectively.

### 3.4. Results and Discussion

#### 3.4.1 Carbonate chemistry changes over tidal and seasonal cycles

TA and DIC concentrations are strongly affected by seasonal marsh productivity as well as tidal exchange and mixing. In the following discussion, results are presented from 3 sampling days during each season, excluding winter, from 2013 and 2015. In total, there were 21 sampling days over the three years with 12 days of samples covering a full tidal cycle. In spring, the range of concentrations over a tidal cycle for TA was <100 μmol $kg^{-1}$ on 6/12/13 and 4/30/15 and ~400 μmol $kg^{-1}$ in 4/17/15 (Figure 2a). For DIC, the range was ~200-300 μmol $kg^{-1}$ in 2013 and 2015. pH (total scale) and $pCO_2$ were calculated based on TA and DIC bottle sample values using CO2SYS (Lewis and Wallace 1998; Pierrot et al., 2006) with constants from Mehrbach et al. (1973) refit by Dickson and Millero (1987). Calculated pH varied from 7.3-7.7 at low tide to 8-8.3 at high tide with $pCO_2$ following the opposite trend and values <2000 μatm. The highest buffer factor $\beta_H$ of ~0.6 mmol $kg^{-1}$ in the spring occurs on 6/12/13 following high tide, where TA > DIC, which indicated a buffering capacity based mostly on carbonate ion buffering. This will be explained in more detail in the next section. There is not a clear trend from these three spring sampling days due to heavy rain for two days prior to but not on the day of sampling on 6/12/13 and rain occurred for the first half of the day on 4/17/15 (NOAA NERRS). The rain was likely driving the lower concentration ranges of

TA and DIC due to dilution because at high tide, the estuarine endmember should be ~1800-1900 DIC based on bottle samples. Particularly, on 4/17/15, there was low pH and high $pCO_2$ at low tide, which is expected but also low concentrations of TA and DIC, which was unexpected. Taking 4/30/15 to be a typical day without the influence of rain, there was small variation of alkalinity over tidal cycle indicating that marsh inputs do not strongly affect alkalinity and therefore pointing to the lack of anaerobic respiration. This indicated high rates of plant growth in the spring and low export rate of respiration (Raymond et al., 2000; Neubauer and Anderson 2003; Wang and Cai, 2004; Wang et al., 2016).

In the summer, TA and DIC concentrations were higher than spring or fall and have the greatest tidal difference in concentration of up to ~200 μmol $kg^{-1}$ from 2000-2200 μmol $kg^{-1}$ for TA and up to ~650 μmol $kg^{-1}$ from 1750-2400 μmol $kg^{-1}$ for DIC (Figure 2b). Unlike the spring, DIC concentrations in the summer were often greater than alkalinity concentrations especially during ebb tide. Even though TA concentrations at low tide were greater than high tide suggesting anaerobic generation of TA, aerobic and anaerobic processes both contributed to DIC generation (Howarth and Giblin 1983; Cai and Wang 1998). Buffer capacity $\beta_H$ in the summer often had higher values at ebbing tide than flooding tide. For the first two July days, there were two peaks of $\beta_H$, one at first low tide when DIC concentrations exceed TA concentrations where $pCO_2$ values reach >8000 μatm and relatively low pH (<7) and the second during incoming tide, when TA concentrations exceed DIC concentrations. The buffering

capacity at low tide, was due in large part to bicarbonate ($HCO_3^-$) buffering produced from anaerobic respiration such as sulfate reduction, while at high tide, buffering was through the more traditional buffering species, the carbonate ($CO_3^{2-}$) ion. Similar results were reported for summer conditions in Wang et al. (2016).

In the fall, TA and DIC concentrations fell to 1800-2100 μmol $kg^{-1}$ with variation over the tidal cycle mostly in DIC and relatively constant TA at <100 μmol $kg^{-1}$ change over the tidal cycle (Figure 2c). Similar to spring, alkalinity concentrations were generally greater than DIC concentrations over the tidal cycle. There was no clear signal of alkalinity generation, though there was still respiration occurring that produces DIC but not as much as in the summer. Buffer capacity ranged from ~0.25-0.4 with maximum values during flooding tide when TA concentrations were greater than DIC. pH ranged from 7.25 to 8 with lower values at low tide and $pCO_2$ behaved inversely, with values up to 2000 μatm at low tide.

To look closer at the seasonal changes in buffering capacity, $\beta_H$ was calculated for all available bottle samples (Figure 3). On the left side, where DIC:TA<1, is typical seawater buffering with the carbonate ($CO_3^{2-}$) ion (Figure 3a). After tidal exchange and addition of marsh porewaters containing high concentrations of DIC, the DIC:TA ratio is pushed towards the right, where bicarbonate ($HCO_3^-$) buffering dominates. In extreme cases, especially in the summer, this can lead to higher buffering capacity at ebbing tide than flooding tide. Interestingly, these special cases are also low pH (≤7.1) (Figure 3b), suggesting that salt marshes may be exporting waters with high buffering capacity and

low pH simultaneously buffering and acidifying the coastal ocean. These results are in agreement with Wang et al. (2016).

### 3.4.2 Biogeochemical drivers of tidal and seasonal variation of TA and DIC

To delve deeper into the mechanisms that produce the tidal and seasonal variation seen in TA and DIC concentrations, salinity normalized DIC ($DIC_n$) and TA ($TA_n$) (Friis et al., 2003 using mean salinity over each day instead of 35 as reference salinity) were plotted against each other for the same sampling days in 2013 and 2015 discussed in the previous section (Figure 4). The slopes from these plots can be compared TA:DIC ratios that arise from organic matter remineralization reactions where aerobic respiration = -0.15, sulfate reduction = 1.0, denitrification = 0.8, calcium carbonate dissolution = 2.0, manganese reduction = 4.4, and iron reduction = 8.0 (Canfield et al., 1993; Chen and Wang 1999; Borges et al., 2003; Sippo et al., 2016). Denitrification and methanogenesis were likely not significant due to the abundance of dissolved sulfate in seawater and relatively higher energy yield for bacteria to get from sulfate reduction (Howarth and Giblin 1983; Johnson et al., 1994). We assume that the two major remineralization processes were aerobic respiration and sulfate reduction, which is in agreement with other studies from coastal regions such as mangroves, fresh and salt water marshes (Raymond et al., 2000; Neubauer and Anderson 2003; Borges et al., 2003; Wang and Cai 2004; Alongi et al., 2005; Sippo et al., 2016; Wang et al., 2016). Slopes from the spring vary from 0.29 to 1.2, indicating that there was both aerobic respiration and sulfate reduction occurring. As previously mentioned, there was rain

influence on the first two days of spring sampling, which likely affects these results. Summer slopes ranged from 0.33 to 0.48 on days where $DIC_n$ and $TA_n$ were strongly correlated consistent with a combination of aerobic respiration and sulfate reduction. Fall slopes were on average lower than the summer. The slope on 4/30/15, the spring day not affected by rain, was likely a result of a higher rate of aerobic respiration compared to sulfate reduction, which caused the slope to have lower values. The spring and fall slopes are comparable, excluding the rainy day in the spring, suggesting that similar degradation processes were occurring during both seasons. Summer values have higher slopes indicating the occurrence of higher rates of sulfate reduction relative to aerobic respiration.

### 3.4.3 Monthly and annual fluxes of modeled TA and DIC

Using the MLR described in section 3.3.5, high frequency TA and DIC concentrations were calculated and combined with density and water fluxes to yield TA and DIC instantaneous fluxes. A portion of the MLR estimated TA concentration and corresponding water level, water flux, and chemical flux from July 2015 show the relationship between fluxes and water level (Figure 5). Over a tidal cycle, the largest water fluxes occur right before and after high tide and subsequently drive the largest chemical fluxes at the same time.

Averaging TA and DIC instantaneous fluxes calculated from June 2013 to December 2015 over each month show that the marsh exports TA and DIC from April to December (Table 2). January to March are not included due to the marsh being

frozen over most of this time period and therefore a lack of bottle samples and low data coverage from *in situ* sensors. Overland corrections reduced fluxes by a significant amount up to 100% in April, while the groundwater corrections were minimal (~1 mol $m^{-2}$ $yr^{-1}$). Data coverage refers to the percentage of time during a given month where TA or DIC data was available. Annual fluxes were estimated by subtracting the average annual groundwater flux (2.7 ± 0.7 mol $m^{-2}$ $yr^{-1}$ for TA, 3.2 ± 0.8 mol $m^{-2}$ $yr^{-1}$ for DIC, Meagan Gonneea, unpublished data) from the average flux over the nine months. Groundwater DIC and TA concentrations were not measured or modeled at high-frequency. In order to correct instantaneous DIC and TA fluxes, the seasonally measured DIC and TA in groundwater were averaged to give annual estimates. The annual flux for TA was -12 ± 1 mol $m^{-2}$ $yr^{-1}$ and DIC was -28 ± 3 mol $m^{-2}$ $yr^{-1}$ (last row of Table 2). Mean annual DIC flux from this study is similar to -35 ± 3 mol $m^{-2}$ $yr^{-1}$ from Wang et al. (2016) calculated using a similar MLR method for the same location from 2012-2014. The annual fluxes reported here are minimum values, as they do not cover January-March when water is still exchanged with the marsh underneath the surface ice sheet, however it is likely that not much biologically mediated production of TA and DIC occur in the freezing temperatures during this period of time. For alkalinity fluxes, 10% of the annual flux is exported in the spring (Apr-Jun), 70% in the summer (Jul-Sep), and 20% in the fall (Oct-Dec). For DIC fluxes, 20% is exported in the spring, 70% in the summer, and 10% in the fall.

Average corrected monthly fluxes of TA and DIC vary greatly from April to December (Figure 6). TA export in April was statistically no different from zero and reached a maximum export in August and dropped back down in the fall. A minor contribution, a few percent, of total alkalinity exported is likely organic alkalinity, due to dissolved organic carbon in the form of organic acids, however carbonate alkalinity export is the majority of total alkalinity export. Monthly DIC followed a similar pattern with higher magnitude fluxes than TA. Average monthly fluxes from 2013, 2014, and 2015 show the interannual variability over this time period (Figure 7a). Some months showed positive fluxes or net import but those periods of time did not contribute greatly to the overall 2013-2015 averages due to data coverage (Figure 7b). For example, in July 2014, >50 mol $m^{-2}$ $yr^{-1}$ of TA was imported into the marsh. The total TA flux for July over the entire study period of 2013-2015 (Figure 6, Table 2) was an export -27 mol $m^{-2}$ $yr^{-1}$. Only 6% of the July flux was from 2014, while 2013 and 2015 made up the majority and resulted in negative fluxes indicating export. Interannual changes can result from differences in concentrations as a result of changes in primary production or microbial metabolic pathways, as well as differences in hydrological fluxes among other factors.

### 3.4.4 Measured and modeled high frequency DIC fluxes

To check the validity of the MLR model, DIC MLR results are compared to directly measured DIC fluxes from CHANOS (discussion here will focus only on comparison with the MLR method, further details regarding CHANOS DIC fluxes are presented in Chapter 4). For this evaluation, the MLR method was calculated over the

same dates as available CHANOS DIC fluxes, however missing periods of data within the time periods in the CHANOS measurements were not removed from the MLR model results. DIC concentrations compared well within the model uncertainty (Figure 8). DIC concentrations were within an average of 5 μmol $kg^{-1}$ in July-Aug and DIC instantaneous fluxes were very similar in the July 7 – August 11 time period. The average residual between model and CHANOS DIC flux was -0.005 ± 0.006 mol $s^{-1}$ (1σ) or 0.4 ± 4 % of total CHANOS flux. Concentrations in November and December were positively biased by 37 and 45 μmol $kg^{-1}$, respectively, where the model overestimated DIC compared to CHANOS. The overall pattern in Nov and December DIC fluxes matched but there were larger residuals of up to 0.05 in November and up to 0.1 in December. The overestimation occured primarily around high tide, when water fluxes were largest, causing larger residuals. Average net residual were 6 ± 60% for November and 21 ± 48% for December compared to CHANOS DIC fluxes. While there may have been large residuals, the residuals in the DIC fluxes occurred in opposite directions and often cancelled out in the net fluxes. These results demonstrated that the MLR modeling method was relatively robust and revealed the importance of acquiring accurate concentrations before and after high tide, when water flux is largest and most of DIC flux occurs.

### 3.4.5 3D hydrodynamic water model and hypsographic method

In cases where there may not be a readily available ADVM to measure water fluxes but elevation of the drainage basin and water levels are known, another method

has been used in the past to estimate water fluxes. A hypsographic method uses the topography of the drainage area and a time series of water levels to estimate change in water volume over time, thereby providing a water flux. Results showed that the hypsographic method underestimated alkalinity flux at -2 mol $m^{-2}$ $yr^{-1}$ compared to -12 mol $m^{-2}$ $yr^{-1}$ in our model (Figure 9). Unlike the 3D hydrodynamic model used in this study, the hypsographic method does not route water, thus it is not realistic. This method allows water to fill in upland where elevation is low, but before water has even filled the channel. Maximum water fluxes in the hypsographic method are no longer centered at high tide. Instead they are skewed slightly earlier, such that the maximum incoming water flux still occurs at the estuarine endmember but outgoing water flux occurs before tidal water contains much input from the marsh. Differences in timing of the water flux maximums between the water models using the hypsographic method and 3D model cause differences total TA export. While it is not certain which method is correct, the 3D model is more realistic in its ability to route water properly and it also contains overland flow and groundwater corrections.

### 3.4.6 Alkalinity budget estimates

If we assume that sulfate reduction is the major source of alkalinity generated at Sage Lot Pond, an alkalinity export of 12 mol $m^{-2}$ $yr^{-1}$ translates to sulfate reduction rate of 6 mol $m^{-2}$ $yr^{-1}$, assuming two mol of alkalinity are generated per mol of $SO_4^{2-}$ reduced. This is a third of the sulfate reduction rate reported for nearby Great Sippewissett marsh of 18 mol $m^{-2}$ $yr^{-1}$ (Howes et al., 1984). Great Sippewissett has a nitrogen loading of

almost a factor of 3 greater than Sage Lot Pond at 280 kg $ha^{-1}$ $yr^{-1}$ (Valiela et al., 1978) and likely has a greater rate of primary production (Callaway et al., 1995; D'Avanzo et al., 1996).

Areal fluxes reported here were scaled up to compare to published estimated TA and DIC fluxes where available. Using Atlantic coast marsh area for brackish and salt water marshes of 9700 $km^2$ and 2600 $km^2$ for freshwater marshes (U.S. Fish and Wildlife Service National Wetlands Inventory), TA lateral export was 0.15 Tmol $yr^{-1}$. DIC export was 0.34 Tmol $yr^{-1}$ (4.1 Tg C $yr^{-1}$). This agrees with 0.18-0.43 Tmol $yr^{-1}$ (2.2-5.1 Tg C $yr^{-1}$) previously reported for U.S. East coast tidal wetlands (Najjar et al., 2012; Wang et al., 2016).

If results are extrapolated even further to all salt marshes using the area of 0.24 x $10^6$ $km^2$ (Woodwell et al., 1973; Duarte et al., 2005; Bouillon et al., 2008; Cai 2011), total fluxes are 3.0 and 6.7 Tmol $yr^{-1}$ for TA and DIC, respectively (Table 3). The alkalinity flux from this study is similar to 4.2 Tmol $yr^{-1}$ exported from mangroves (Sippo et al., 2016), while the DIC export almost 2 times greater than mangrove DIC export of 3.6 Tmol $yr^{-1}$. Mangroves and salt marshes are similar in that anaerobic respiration in sediments is a primary driver of DIC production that is subsequently exported through tidal pumping. Slight differences in export may be due to higher organic carbon in mangroves than in salt marshes, which could lead to differences in anaerobic respiration processes (Chmura et al., 2003) or it is also possible that differences are due to methodology. Sippo et al. (2016) measured alkalinity and DIC at various sites along the

Australian coast, however sampling periods were only for 25 hrs. In contrast, while this study was limited to only one site, the data coverage was multiple days of bottle sampling and high frequency in situ data for intermittent periods over 2.5 years. TA fluxes from salt marshes were 8-11% of riverine annual discharge and 10-75% of the alkalinity produced from continental shelves. In areal weighted alkalinity export, salt marshes are 10-80 times greater than continental shelves suggesting that salt marshes are key players in the delivery of TA and DIC to the coastal ocean.

### 3.5 Conclusions

This study is the first to estimate lateral alkalinity export from an intertidal salt marsh using high-frequency data. Salt marsh contribution to coastal and global alkalinity budgets is particularly important to quantify as marshes continue to be threatened by land development and sea level rise (Woodroffe 1995; Duarte et al., 2005; Silliman et al., 2009; Hopkinson et al., 2012). Results presented here are from only one intertidal salt marsh sampling site so there are limitations to extrapolating results to all other salt marshes. However, these results use 2.5 years of seasonal bottle samples and in situ, high-frequency data to estimate fluxes, which is a significant improvement over previous studies that have used a few days of bottle samples to extrapolate to annual rates. We were also able to calculate DIC fluxes to compare with the TA fluxes and investigate the change in marsh processes over tidal, monthly, and seasonal scales. The MLR method was tested and validated with high frequency direct measurements of DIC. The annual DIC flux calculated here confirms the export calculated in Wang et al. (2016), suggesting

DIC lateral export is a significant portion of the ultimate fate of $CO_2$ uptake by plants in salt marshes. The annual TA flux is also important for the marsh carbon budget and coastal carbon cycling. Quantifying the effect of TA and DIC marsh export on the carbonate chemistry in coastal ocean is a goal for future studies. Studies involving high-frequency, in situ data at additional salt marshes to cover spatial and temporal variability are required to further examine the robustness of the MLR method in estimating DIC and TA fluxes and improve evaluations of the coastal carbon budget.

**Acknowledgements**

Thank you to contributions to this work by Zhaohui Aleck Wang, Kevin D. Kroeger, and Meagan Eagle Gonneea. Thanks to Neil K. Ganju for his help with the water fluxes and corrections. Thank you to Harry Hemond and Dan McCorkle for their helpful comments. To everyone who helped to collect and analyze samples, thank you to Lloyd Anderson, Katie Carter, Tom Kraemer, Linda Kraemer, Zoe Sandwith, and Kate Morkeski. Jennifer O'Keefe Suttles, Adrian Mann, and Sandy Brosnahan helped in collecting and processing YSI and water flux data. Thank you to Waquoit Bay National Estuarine Research Reserve for providing the infrastructure to conduct this work. This work was funded by USGS, NSF NOAA Science Collaborative (NA09NOS4190153).

**References**


Alongi, D. M. 2005. Mangrove-microbe-soil relations, in Interactions Between Macro- and Microorganisms in Marine Sediments, Coastal Estuarine Stud., vol. 60, edited by E. Kristensen, J. E. Kostka, and R. H. Haese, pp. 85–103, AGU, Washington, D. C.

Amiotte Suchet, P., J.-L. Probst, and W. Ludwig 2003. Worldwide distribution of continental rock lithology: Implications for the atmospheric/soil CO2 uptake by continental weathering and alkalinity river transport to the oceans, Global Biogeochem. Cycles, 17(2), 1038, doi:10.1029/2002GB001891.

Bauer, J. E., W. J. Cai, P. A. Raymond, T. S. Bianchi, C. S. Hopkinson, and P. A. G. Regnier. 2013. The changing carbon cycle of the coastal ocean. Nature 504: 61-70.

Berner, R. A. 1970. Sedimentary pyrite formation. American journal of science, 268(1), 1-23.

Borges, A. V., S. Djenidi, G. Lacroix, J. Théate, B. Delille, and M. Frankignoulle 2003. Atmospheric CO2 flux from mangrove surrounding waters, Geophys. Res. Lett., 30(11), 1558, doi:10.1029/2003GL017143.

Bouillon, S. and others 2008. Mangrove production and carbon sinks: A revision of global budget estimates. Global Biogeochem. Cy. 22. doi: GB2013, doi:10.1029/2007GB003052.

Brewer Peter G. , Goldman Joel C. 1976. Alkalinity changes generated by phytoplankton growth, Limnology and Oceanography, 1, doi: 10.4319/lo.1976.21.1.0108.

Cai, W. J. 2011. Estuarine and coastal ocean carbon paradox: CO2 sinks or sites of terrestrial carbon incineration? Annu. Rev. Mar. Sci. 3: 123-145.

Cai, W. J., and Y. Wang. 1998. The chemistry, fluxes, and sources of carbon dioxide in the estuarine waters of the Satilla and Altamaha Rivers, Georgia. Limnol Oceanogr 43: 657-668.

Cai W-J, Guo X, Chen C-TA, Dai M, Zhang L, et al. 2008. A comparative overview of weathering intensity and HCO3 − flux in the world's major rivers with emphasis on the Changjiang, Huanghe, Zhujiang (Pearl) and Mississippi Rivers. Cont. Shelf Res. 28:1538–49

Callaway, D.W., Valiela, I., Foreman, K. and Soucy, L.A., 1995. Effects of nitrogen loading and salt marsh habitat on gross primary production and chlorophyll a in estuaries of Waquoit Bay. The Biological Bulletin, 189(2), pp.254-255.

Canfield, D. E. 1993. Organic matter oxidation in marine sediments. In Interactions of C, N, P and S biogeochemical Cycles and Global Change (pp. 333-363). Springer Berlin Heidelberg.

Cantrell, K. J., Serkiz, S. M., & Perdue, E. M. 1990. Evaluation of acid neutralizing capacity data for solutions containing natural organic acids. Geochimica et Cosmochimica Acta, 54(5), 1247-1254.

Chen, C. T. A., & Wang, S. L. 1999. Carbon, alkalinity and nutrient budgets on the East China Sea continental shelf. Journal of Geophysical Research: Oceans, 104(C9), 20675-20686.

Chmura, G. L., S. C. Anisfeld, D. R. Cahoon, and J. C. Lynch. 2003. Global carbon sequestration in tidal, saline wetland soils. Global Biogeochem. Cy. 17. doi: 1029/2002GB00191.

D'Avanzo, C., K. JN, and Wainright S C (1996), Ecosystem production and respiration in response to eutrophication in shallow temperate estuaries , Mar. Ecol. Prog. Ser., 141, 263–274.

Dickson, A. G., and F. J. Millero (1987), A comparison of the equilibrium constants for the dissociation of carbonic acid in seawater media, Deep Sea Res. Part A, 34(10), 1733–1743, doi:10.1016/0198-0149(87)90021-5.

Dickson, A. G., C. L. Sabine, and J. R. Christian. 2007. Guide to best practices for ocean CO2 measurements. PICES Special Publication.

Duarte, C. M., J. J. Middelburg, and N. Caraco. 2005. Major role of marine vegetation on the oceanic carbon cycle. Biogeosciences 2: 1-8.

Egleston, E. S., C. L. Sabine, and F. M. M. Morel. 2010. Revelle revisited: Buffer factors that quantify the response of ocean chemistry to changes in DIC and alkalinity. Global Biogeochem. Cy. 24. doi: 10.1029/2008GB003407.

Friedrich, T., and A. Oschlies. 2009. Neural network-based estimates of North Atlantic surface pCO(2) from satellite data: A methodological study. J. Geophys. Res. Oceans 114. doi: 10.1029/2007JC004646.

Friis, K., Körtzinger, A. and Wallace, D.W., 2003. The salinity normalization of marine inorganic carbon chemistry data. Geophysical Research Letters, 30(2).

Ganju, N. K. 2011. A novel approach for direct estimation of fresh groundwater discharge to an estuary. Geophys. Res. Lett. 38. doi: 10.1029/2011GL047718.

Gedan, K. B., B. R. Silliman, and M. D. Bertness. 2009. Centuries of Human-Driven Change in Salt Marsh Ecosystems. Annu. Rev. Mar. Sci. 1: 117-141.

Giblin, A. E. 1988. Pyrite Formation in Marshes during Early Diagenesis. Geomicrobiol. J. 6: 77-97.

Giblin, A. E., and R. W. Howarth. 1984. Porewater Evidence for a Dynamic Sedimentary Iron Cycle in Salt Marshes. Limnol. Oceanogr. 29: 47-63.

Giri, C., E. Ochieng, L. L. Tieszen, Z. Zhu, A. Singh, T. Loveland, J. Masek, and N. Duke (2011), Status and distribution of mangrove forests of the world using Earth observation satellite data, Global Ecol. Biogeogr., 20(1), 154–159, doi:10.1111/j.1466-8238.2010.00584.x.

Goldman Joel C. , Brewer Peter G. 1980, Effect of nitrogen source and growth rate on phytoplankton-mediated changes in alkalinity, Limnology and Oceanography, 25, doi: 10.4319/lo.1980.25.2.0352.

Hemond, H. F. 1990. Acid neutralizing capacity, alkalinity, and acid-base status of natural waters containing organic acids. Environmental Science & Technology, 24(10), 1486-1489.

Hopkinson, C. S., W. J. Cai, and X. P. Hu. 2012. Carbon sequestration in wetland dominated coastal systems - a global sink of rapidly diminishing magnitude. Curr Opin Env Sust 4: 186-194.

Howarth, R. W., and J. M. Teal 1979. Sulfate reduction in a New England Salt Marsh, Lim, 24(6), 999–1013.

Howarth, R., and A. Giblin 1983. Sulfate reduction in the salt marshes at Sapelo Island, Georgia, Limnol. Ocean., 28(l), 70–82.

Howarth, R. W., and S. Merkel. 1984. Pyrite Formation and the Measurement of Sulfate Reduction in Salt-Marsh Sediments. Limnol. Oceanogr. 29: 598-608.

Howes, B. L., Howarth, R. W., Teal, J. M., & Valiela, I. 1981. Oxidation-reduction potentials in a salt marsh: Spatial patterns and interactions with primary production. Limnology and Oceanography, 26(2), 350-360.

Hu, X. P., and W. J. Cai. 2011. An assessment of ocean margin anaerobic processes on oceanic alkalinity budget. Global Biogeochem. Cy. 25. doi: doi:10.1029/2010GB003859.

Johnson, R., LaMontagne, M., & Valiela, I. 1994. Rate of denitrification in submerged salt marsh sediments. The Biological Bulletin, 187(2), 289-291.Kroeger, K. D., M. L. Cole, and I. Valiela. 2006. Groundwater-transported dissolved organic nitrogen exports from coastal watersheds. Limnol. Oceanogr. 51: 2248-2261.

Jørgensen, B. B. 1977. The sulfur cycle of a coastal marine sediment (Limfjorden, Denmark). Limnology and Oceanography, 22(5), 814-832.

Kaplan, W., Valiela, I., & Teal, J. M. 1979. Denitrification in a salt marsh ecosystem. Limnol. Oceanogr, 24(4), 726-734.

King, G. M., & Wiebe, W. J. 1980. Regulation of sulfate concentrations and methanogenesis in salt marsh soils. Estuarine and Coastal Marine Science, 10(2), 215-223.

Krumins, V., M. Gehlen, S. Arndt, P. Van Cappellen, and P. Regnier 2013. Dissolved inorganic carbon and alkalinity fluxes from coastal marine sediments: Model estimates for different shelf environments and sensitivity to global change, Biogeosciences, 10(1), 371–398, doi:10.5194/ bg-10-371-2013.

Lefevre, N., A. J. Watson, and A. R. Watson. 2005. A comparison of multiple regression and neural network techniques for mapping in situ pCO(2) data. Tellus B 57: 375-384.

Lozovik, P. A. (2005). Contribution of organic acid anions to the alkalinity of natural humic water. Journal of Analytical Chemistry, 60(11), 1000-1004.

Ludwig, W., Amiotte-Suchet, P., Munhoven, G., & Probst, J. L. 1998. Atmospheric CO 2 consumption by continental erosion: present-day controls and implications for the last glacial maximum. Global and Planetary Change, 16, 107-120.

MacCready, P. 2011. Calculating Estuarine Exchange Flow Using Isohaline Coordinates. J. Phys. Oceanogr. 41: 1116-1124.

Mehrbach, C., C. H. Culberson, J. E. Hawley, and R. M. Pytkowicz. 1973. Measurement of the apparent dissociation constants of carbonic acid in seawater at atmospheric pressure, Limnol. Oceanogr., 18(6), 897–907, doi:10.4319/lo.1973.18.6.0897.

Morel, F. M. M., and J. G. Hering. 1993. Principles and Applications of Aquatic Chemistry. John Wiley.

Morris, J. T., and G. J. Whiting. 1986. Emission of Gaseous Carbon-Dioxide from Salt-Marsh Sediments and Its Relation to Other Carbon Losses. Estuaries 9: 9-19.

Najjar, R. G., M. Friedrichs, and W.-J. Cai. 2012. Report of the U.S. East Coast Carbon Cycle Synthesis Workshop, p. 34.

Neubauer, S. C., and I. C. Anderson. 2003. Transport of dissolved inorganic carbon from a tidal freshwater marsh to the York River estuary. Limnol. Oceanogr. 48: 299-307.

Pierrot, D., E. Lewis, and D. W. R. Wallace. 2006. MS Excel pro- gram developed for CO2 system calculations. Carbon Dioxide Information Analysis Center, Oak Ridge National Laboratory.

Raymond, P. A., J. E. Bauer, and J. J. Cole. 2000. Atmospheric CO2 evasion, dissolved inorganic carbon production, and net heterotrophy in the York River estuary. Limnol. Oceanogr. 45: 1707-1717.

Raymond, P. A., and C. S. Hopkinson. 2003. Ecosystem modulation of dissolved carbon age in a temperate marsh-dominated estuary. Ecosystems 6: 694-705.

Raymond, P. A., Hartmann, J., Lauerwald, R., Sobek, S., McDonald, C., Hoover, M., ... & Kortelainen, P. 2013. Global carbon dioxide emissions from inland waters. Nature, 503(7476), 355-359.

Signorini, S. R., Mannino, A., Najjar, R. G., Friedrichs, M. A., Cai, W. J., Salisbury, J., ... & Shadwick, E. 2013. Surface ocean pCO2 seasonality and sea-air CO2 flux estimates for the North American east coast. Journal of Geophysical Research: Oceans, 118(10), 5439-5460.

Silliman, Brian R., Edwin Grosholz, and Mark D. Bertness. 2009. Human impacts on salt marshes: a global perspective. Univ of California Press.

Sippo, J. Z., D. T. Maher, D. R. Tait, C. Holloway, and I. R. Santos 2016. Are mangroves drivers or buffers of coastal acidification? Insights from alkalinity and dissolved inorganic carbon export estimates across a latitudinal transect, Global Biogeochem. Cycles, 30, 753–766, doi:10.1002/2015GB005324.

Skyring, G. W., Oshrain, R. L., & Wiebe, W. J. 1979. Sulfate reduction rates in Georgia marshland soils. Geomicrobiology Journal, 1(4), 389-400.

Smith, S. V., and J. T. Hollibaugh. 1993. Coastal Metabolism and the oceanic organic-carbon balance. Rev. Geophys. 31: 75-89.

Stumm, W. and Morgan, J.J., 1996. Aquatic Chemistry. John Wiley & Sons, Inc., 1022 pp.

Teal, J. M., Kanwisher, J. 1961. Gas exchange in a Georgia salt marsh. Limnology and Oceanography, 6, doi: 10.4319/lo.1961.6.4.0388.

Thomas, H., Schiettecatte, L.S., Suykens, K., M Kone, Y.J., Shadwick, E.H., F Prowe, A.E., Bozec, Y., W de Baar, H.J. and Borges, A.V., 2008. Enhanced ocean carbon storage from anaerobic alkalinity generation in coastal sediments. Biogeosciences Discussions.

Valiela, I., Teal, J.M., Volkmann, S., Shafer, D. and Carpenter, E.J., 1978. Nutrient and particulate fluxes in a salt marsh ecosystem: tidal exchanges and inputs by precipitation and groundwater. Limnology and Oceanography, 23(4), pp.798-812.

Wagner, R. J., Boulger, R. W. J., Oblinger, C. J. & Smith, B. A. 2006. Guidelines and standard procedures for continuous water-quality monitors: station operation, record computation, and data reporting. United States Geological Survey Tech. Meth. 1-D3, 51 pp.

Walsh JJ. 1988. On the Nature of Continental Shelves. San Diego: Academic. 520 pp.

Wang, Z. A., and W. J. Cai. 2004. Carbon dioxide degassing and inorganic carbon export from a marsh-dominated estuary (the Duplin River): A marsh CO2 pump. Limnol. Oceanogr. 49: 341-354.

Wang, Z. A., Kroeger, K. D., Ganju, N. K., Gonneea, M. E. and Chu, S. N. 2016. Intertidal salt marshes as an important source of inorganic carbon to the coastal ocean. Limnol. Oceanogr., 61: 1916–1931. doi:10.1002/lno.10347

Woodwell GM, Rich PH, Hall CAS. 1973. Carbon in estuaries. In Carbon and the Biosphere, ed. GM Woodwell, EV Pecan. U.S. Atomic Comm., Springfield, Virg.

**Figure 1.** The Sage Lot Pond field sampling site and drainage basin in Waquoit Bay National Estuarine Research Reserve (WBNERR) on Cape Cod, Massachusetts.

a)

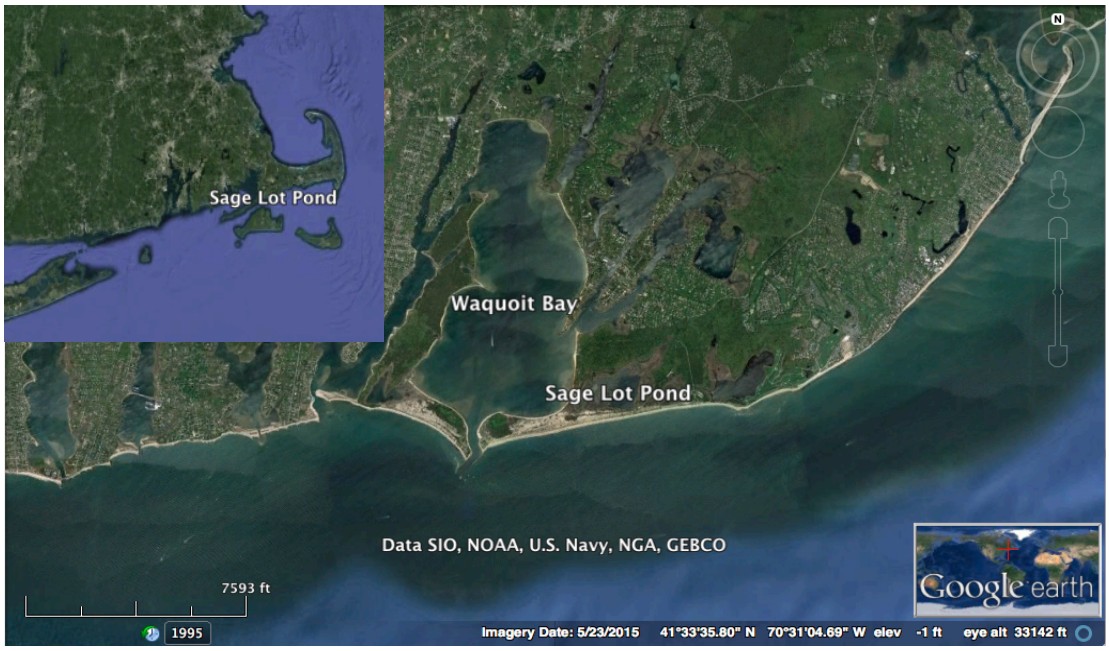


b)

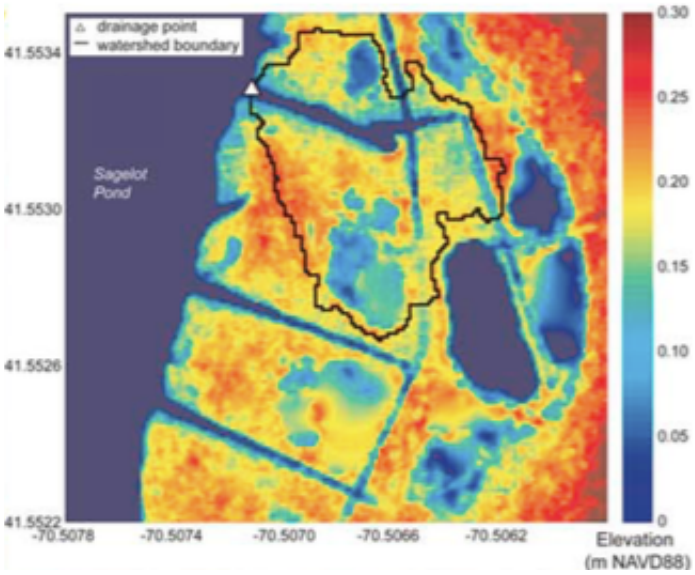

**Figure 2.** TA and DIC concentrations from bottle samples are plotted for full tidal cycle sampling days from 2013 to 2015 in a) spring, b) summer, and c) fall. Calculated pH, $pCO_2$, and $\beta_H$ as well as water level are also plotted to show the tidal phase and auxiliary data corresponding to the TA and DIC bottle samples. Dashed lines mark high tide.

a)

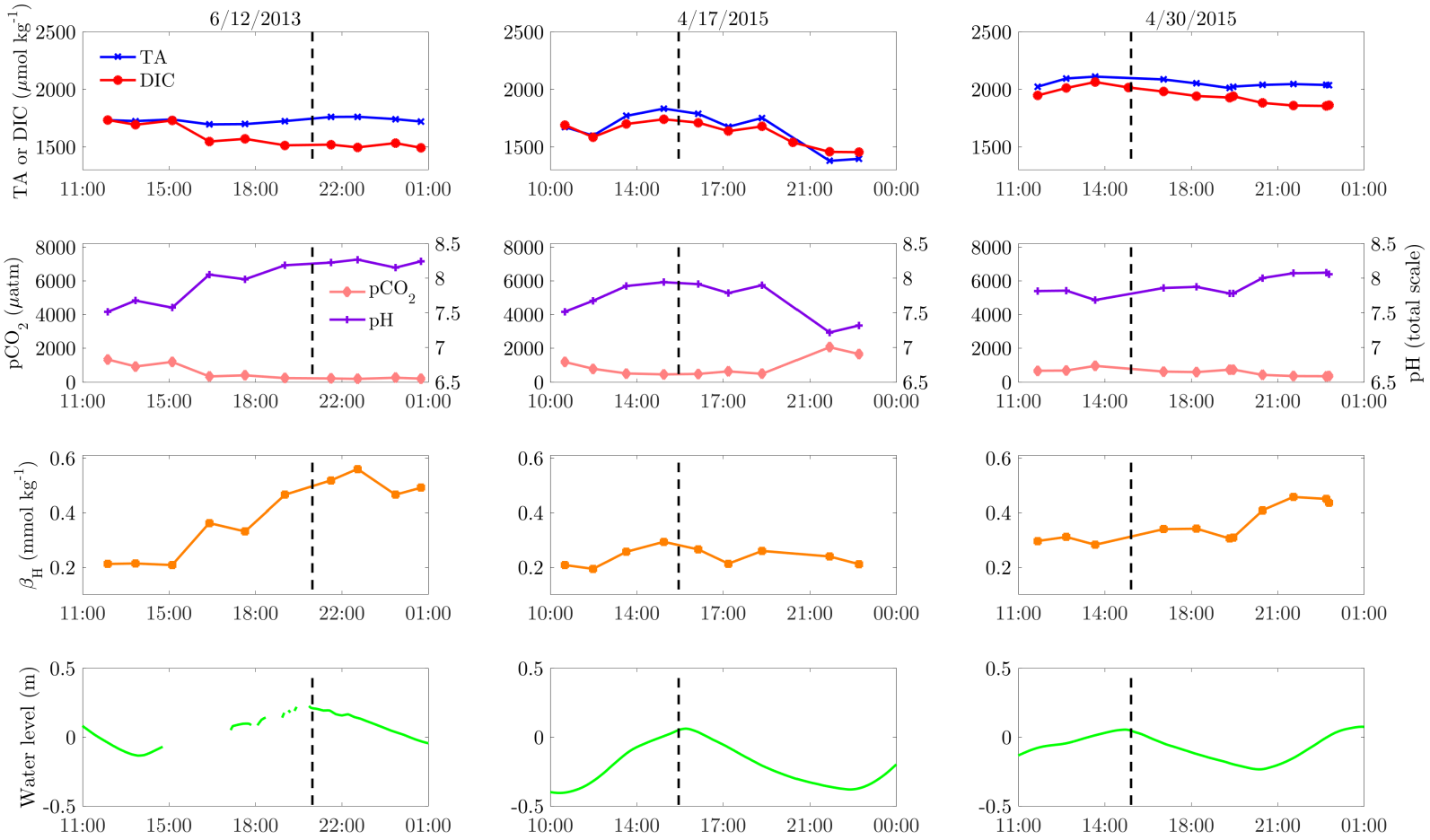

**Figure 2** (continued).

b)

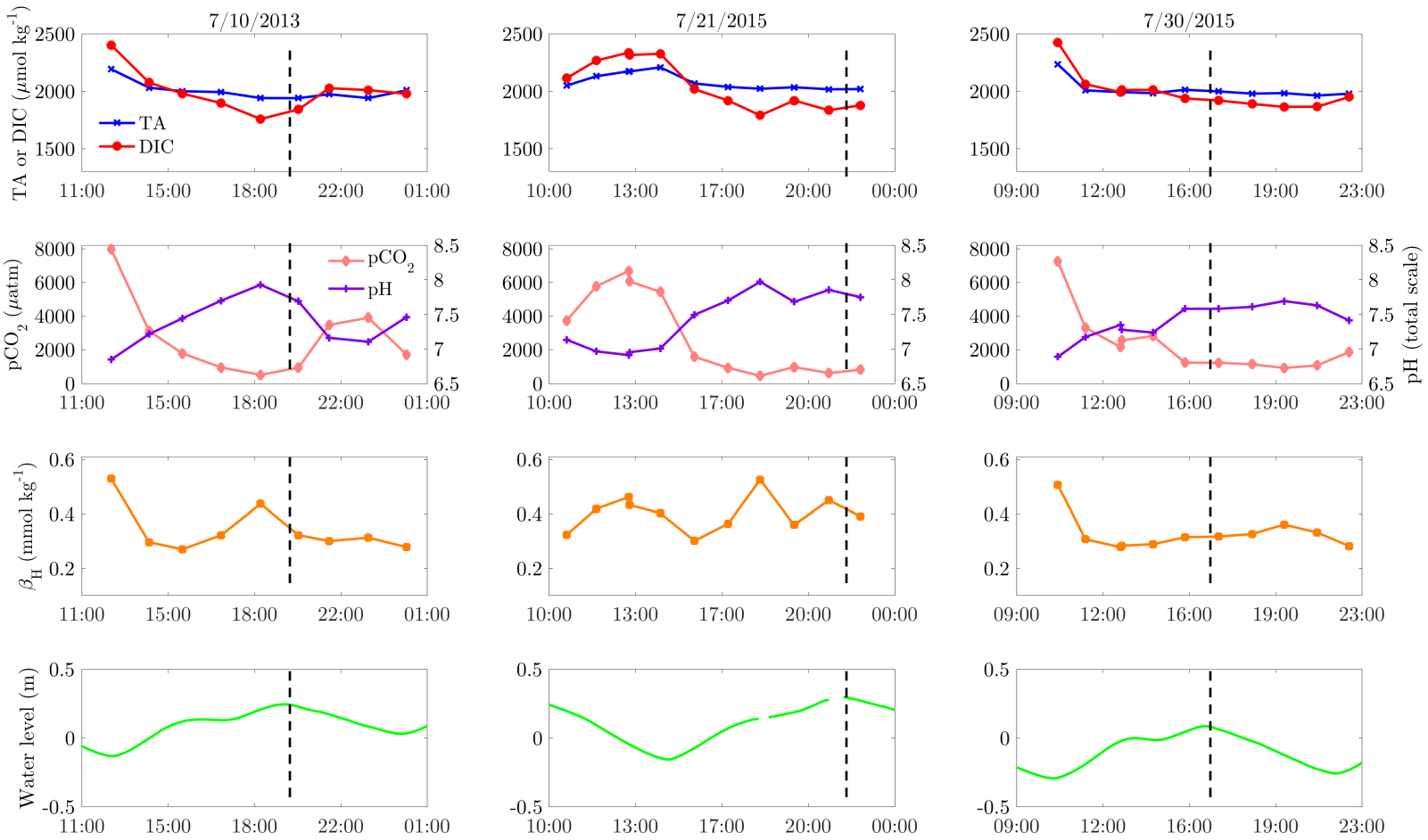

**Figure 2** (continued).

c)

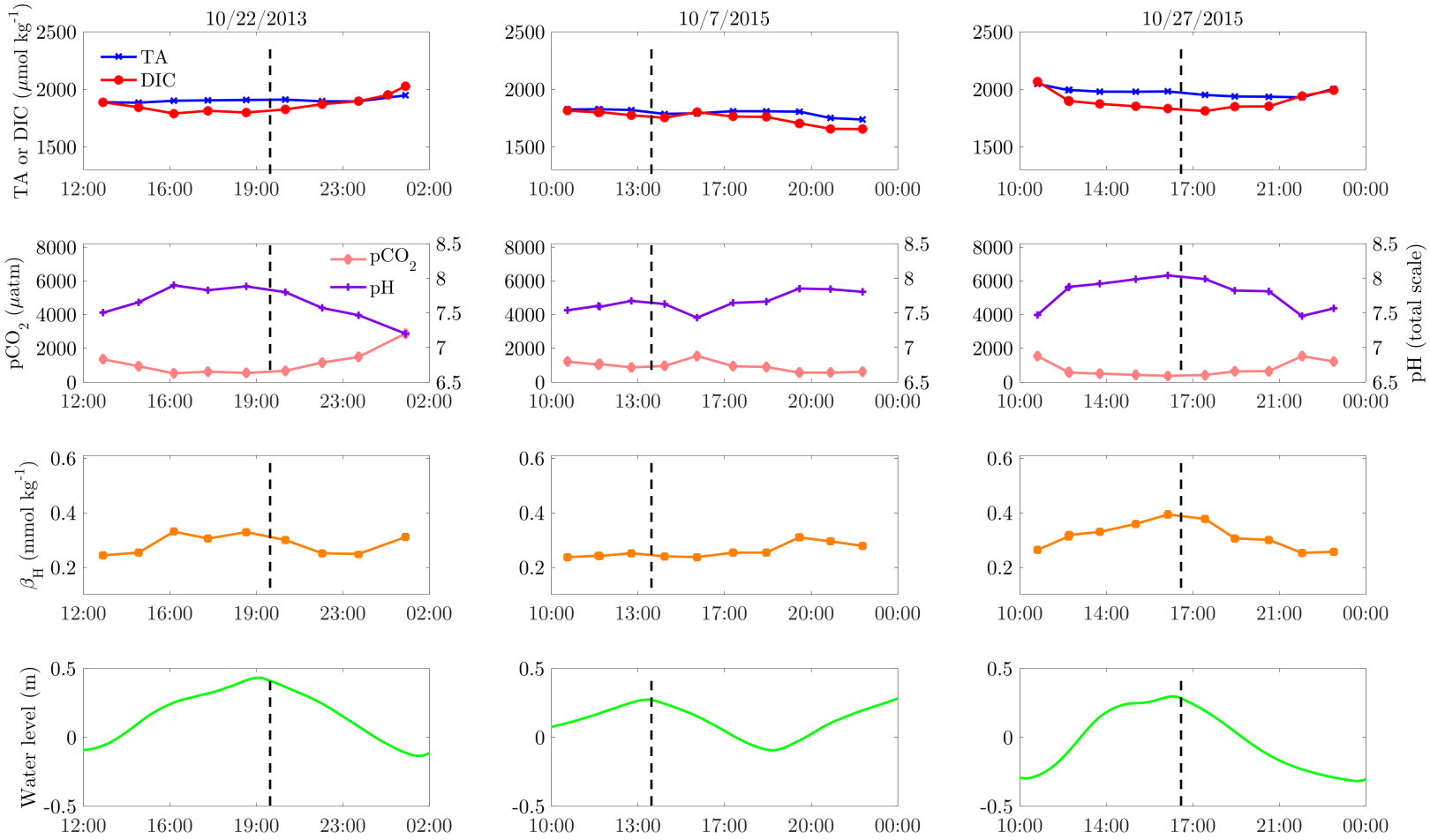

**Figure 3.** Buffer factor $\beta_H$ plotted against DIC:TA to show seasonal signals as well as pH patterns.

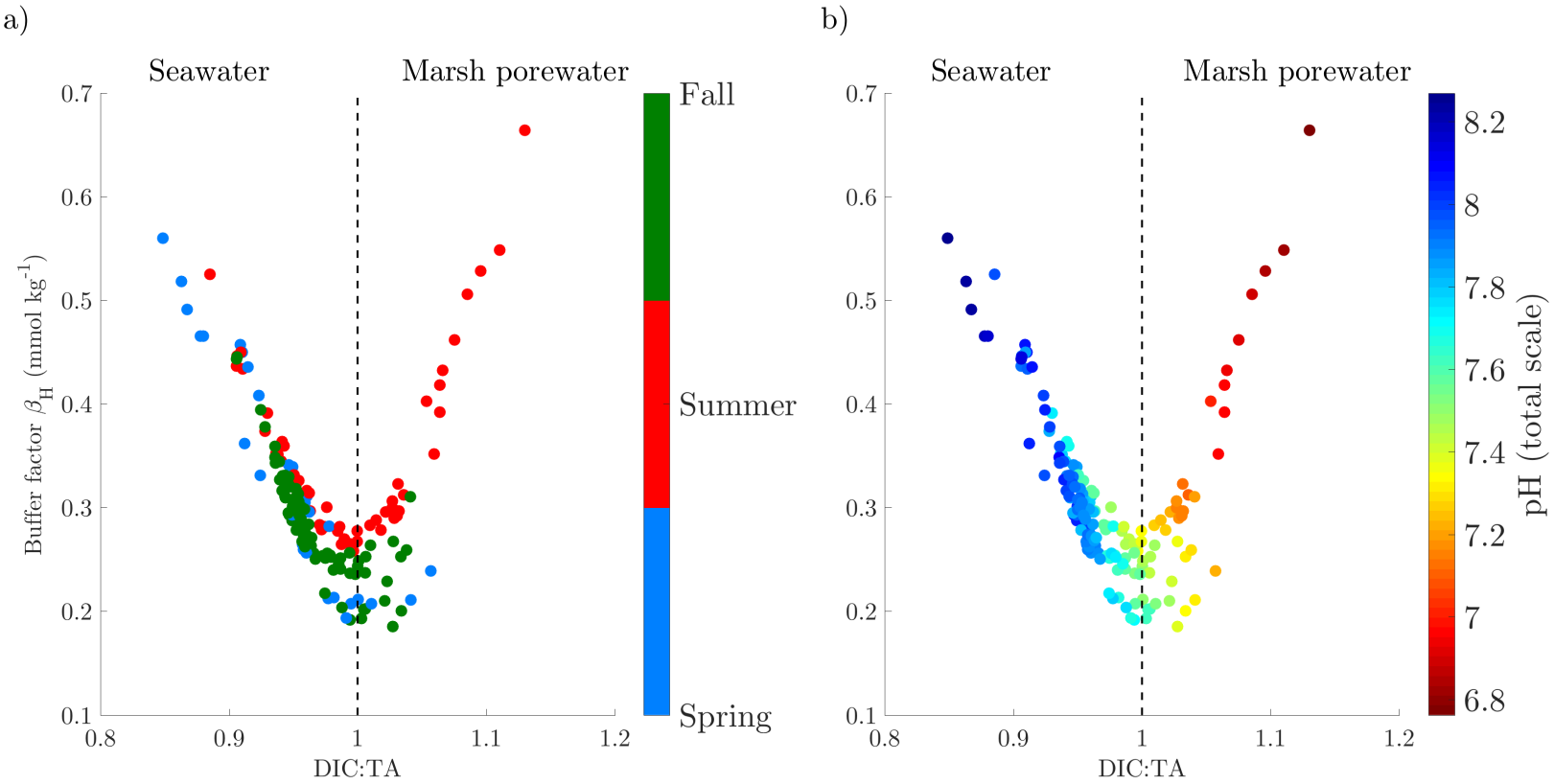

**Figure 4.** Salinity normalized DIC (μmol kg$^{-1}$) plotted against normalized TA (μmol kg$^{-1}$) to look at slope of the line of best fit (red line) in order to compare to different respiration processes such as aerobic respiration (slope =-0.15, green line) and sulfate reduction (slope =1, blue line).

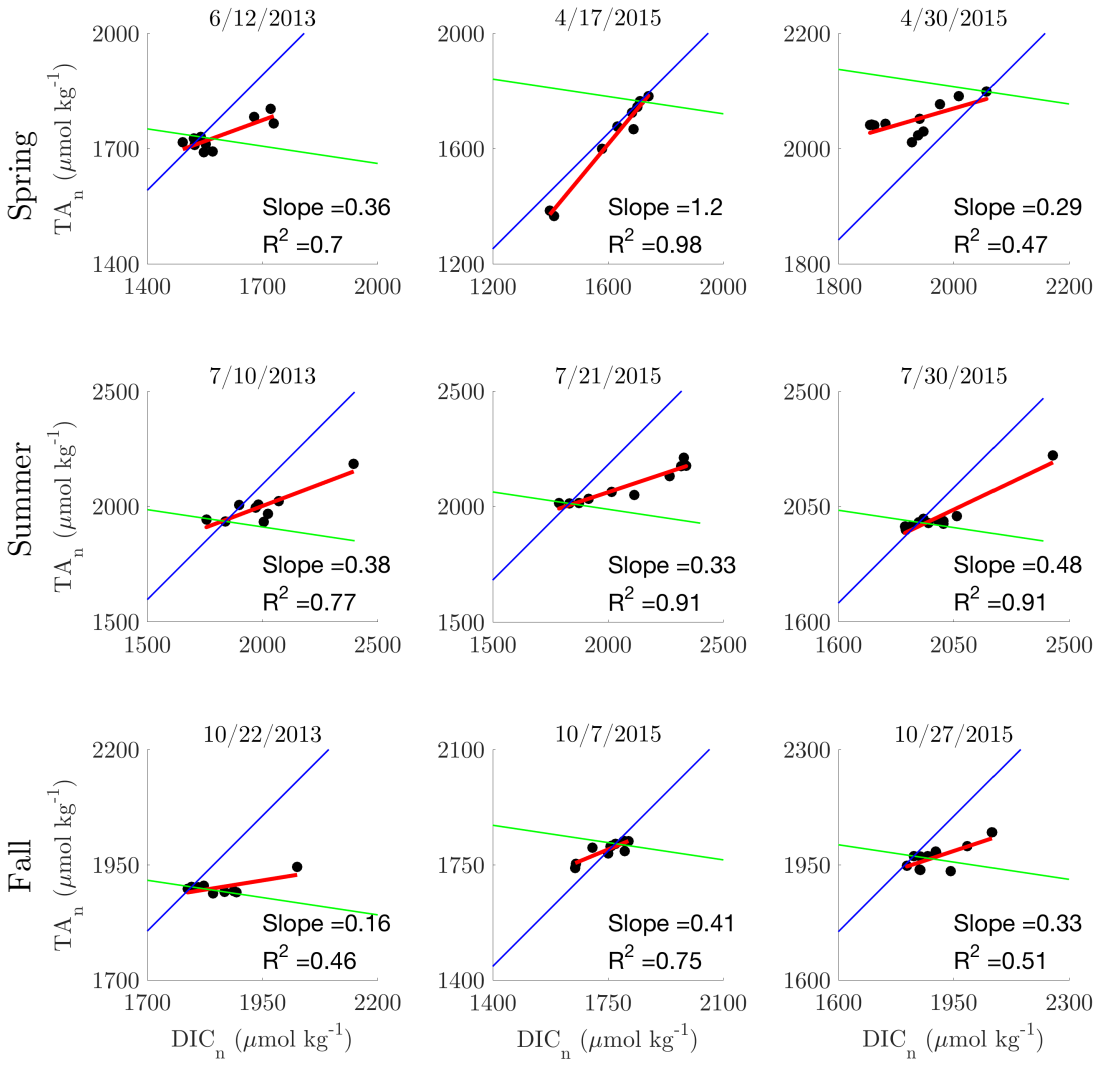

**Figure 5.** TA concentration estimated from MLR, water level (m), water flux, and TA flux from July 2015. High tide is marked to show how water fluxes are greatest immediately preceding and following high tide.

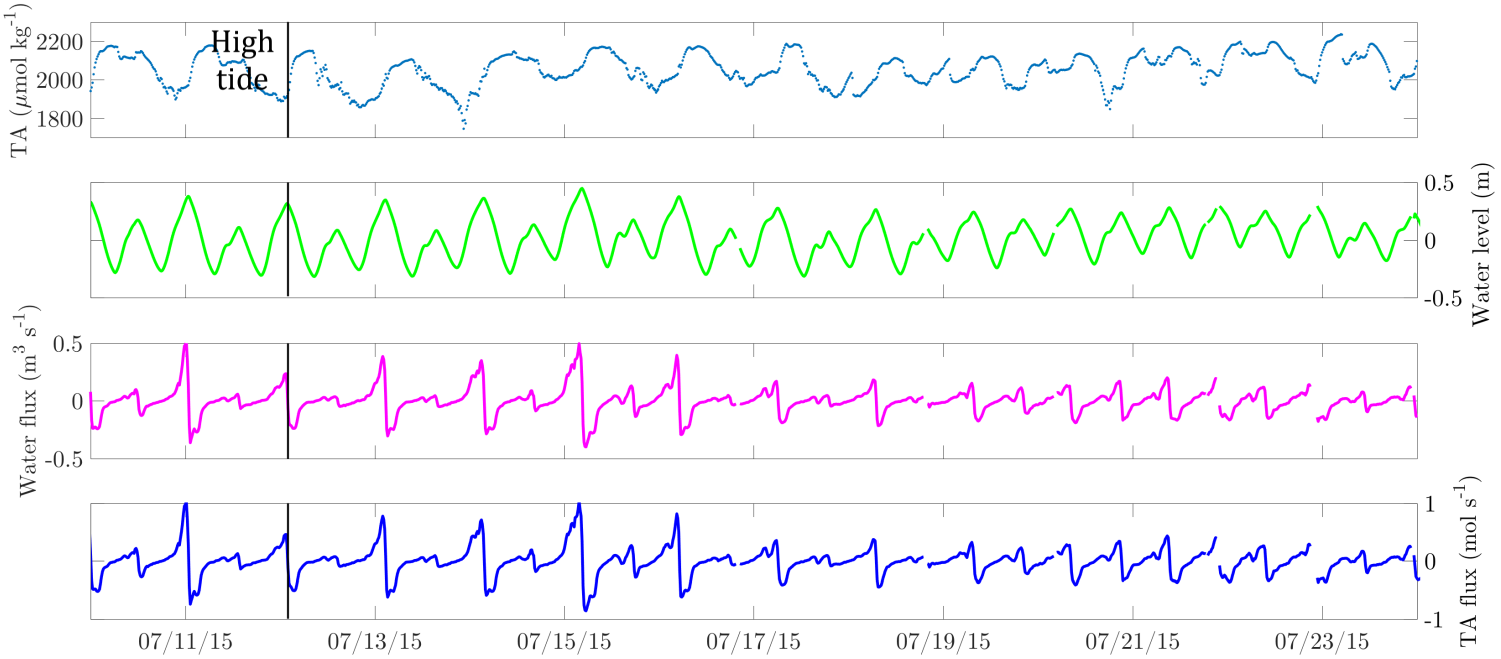

**Figure 6.** a) Average monthly TA and DIC (mol $m^{-2}$ $yr^{-1}$) fluxes from this study at Sage Lot Pond, MA over the period from 2013-2015 and b) corresponding data coverage per month. Values reported in Table 2.

a)

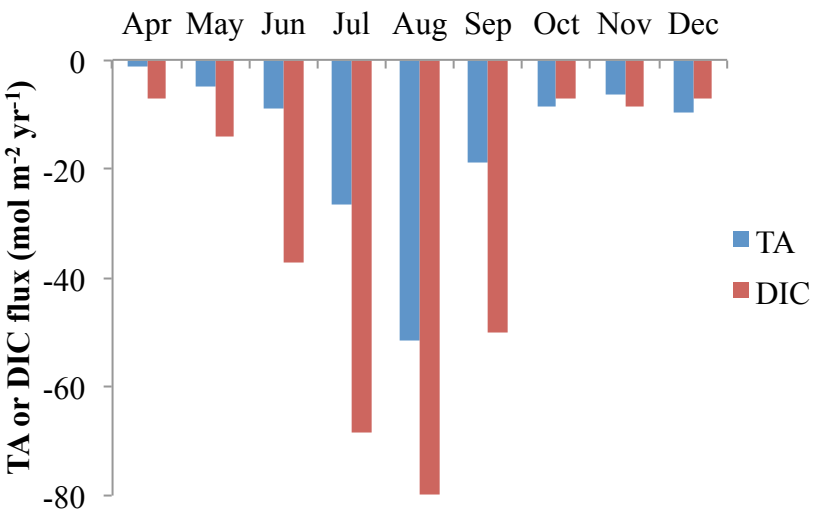


b)

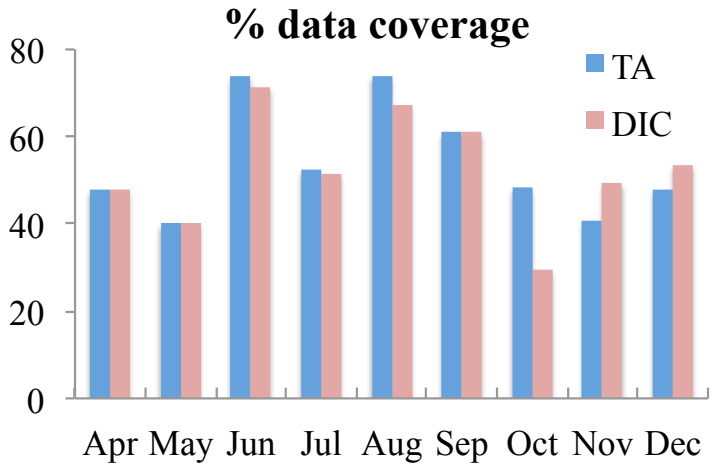

**Figure 7.** a) Interannual variability of monthly TA fluxes from this study at Sage Lot Pond, MA. b) The contribution of each year to the calculation of the total flux.

a)

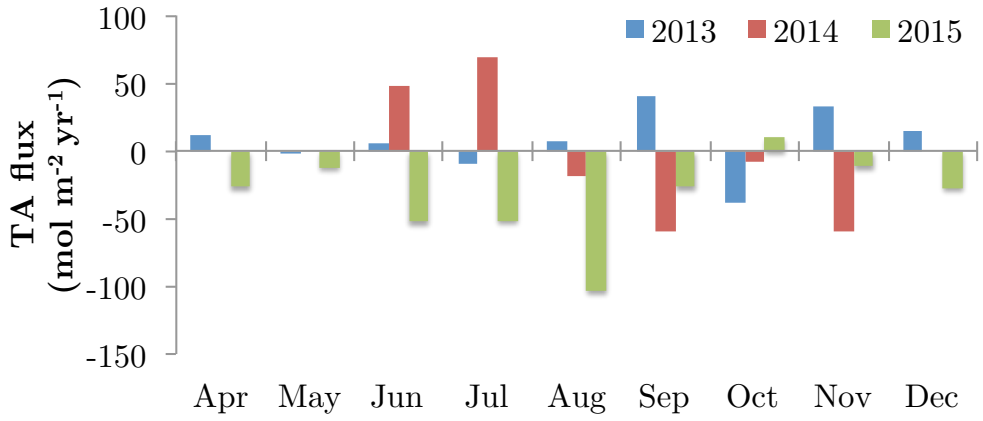


b)

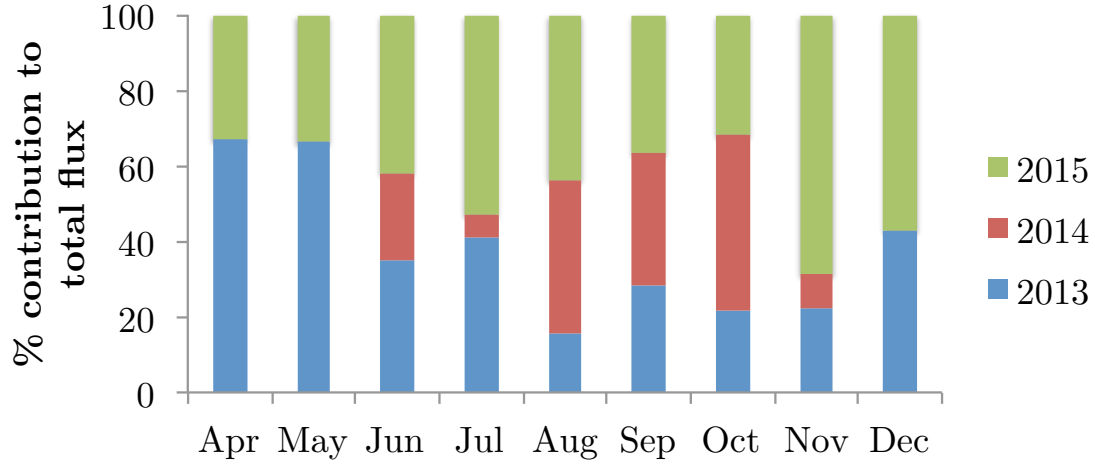

**Figure 8.** Comparing average tide for summer (July 7- August 11) and fall (November 5 – 24, November 30 – December 18) periods of continuous data using MLR modeled data and CHANOS data for DIC concentration (top row) and instantaneous flux (bottom row). Residuals are plotted in the right hand side y-axes for each plot. Shaded area represents error in model values and vertical lines mark average high tide.

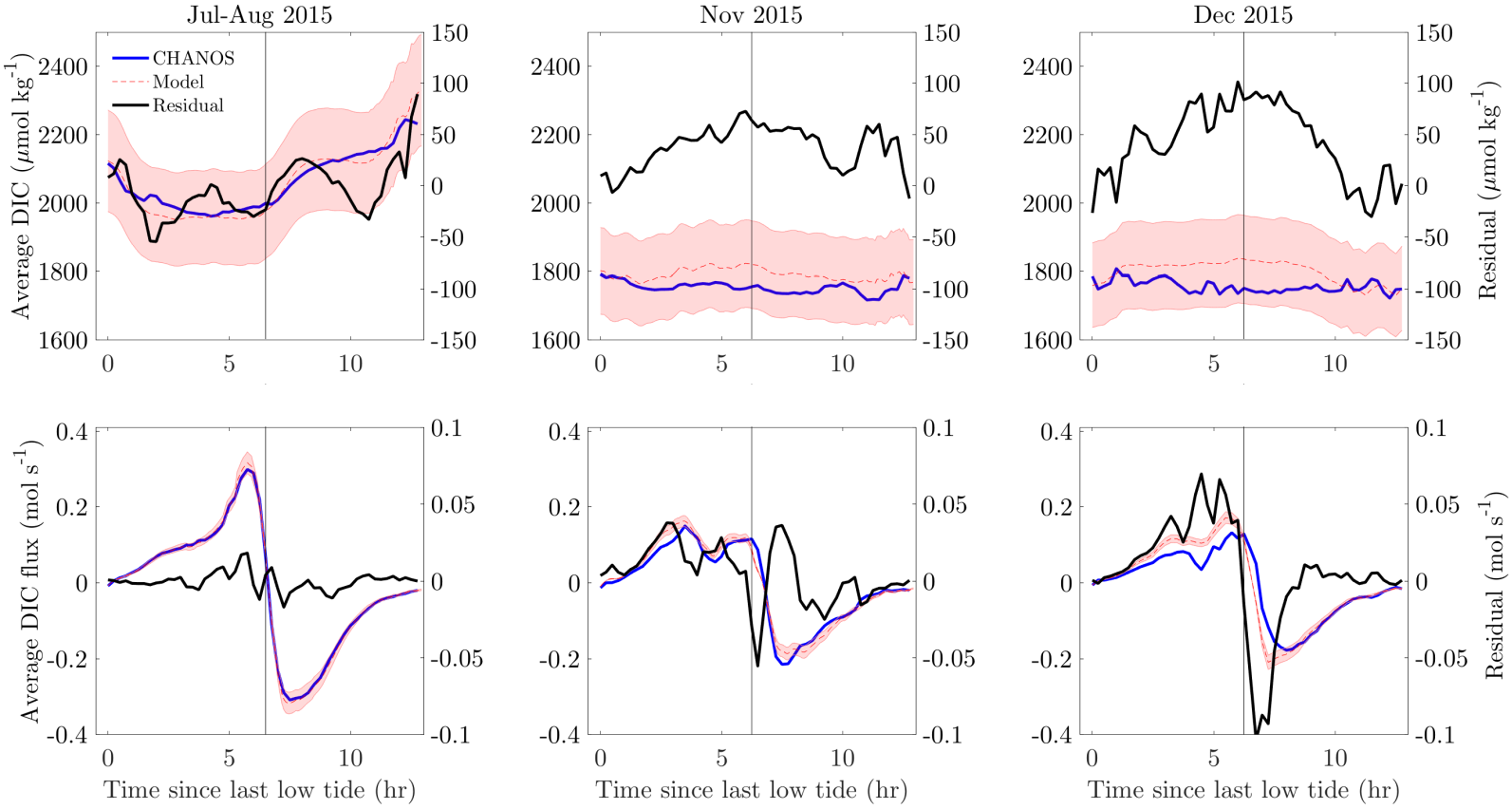

**Figure 9.** Comparison of TA fluxes from hypsographic water model vs 3D hydrodynamic water model used in this study.

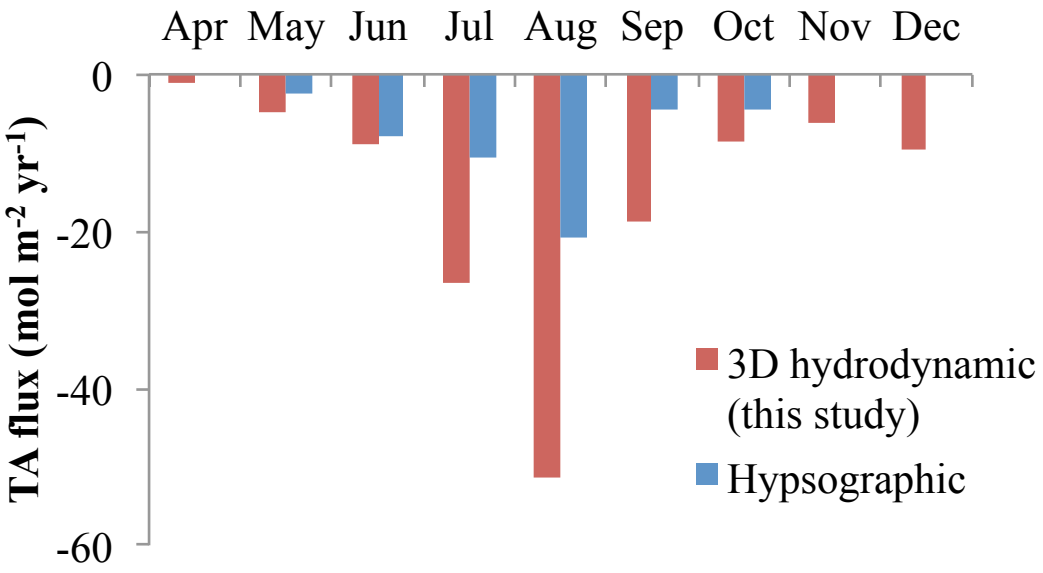

**Table 1.** Coefficients used for the TA and DIC multiple linear regressions.

| | Int. | Day' | Temp. (°C) | Sal. (PSS) | DO (%) | ORP (mV) | n | $R^2$ | RMSE |
|---|---|---|---|---|---|---|---|---|---|
| TA (µmol $kg^{-1}$) | 530 ± 48 | 77.9 ± 12.5 | 2.9 ± 1.0 | 52.4 ± 2.8 | -1.7 ± 0.2 | NA | 174 | 0.79 | 75 |
| DIC (µmol $kg^{-1}$) | 748 ± 77 | 44.1 ± 15.6 | NA | 52.7 ± 3.4 | -4.2 ± 0.3 | -0.2 ± 0.1 | 178 | 0.77 | 96 |

**Table 2.** Monthly and annual TA and DIC fluxes from June 2013-December 2015 (mol $m^{-2}$ $yr^{-1}$). Negative fluxes indicate export. Area of the drainage basin was used to convert from mol $s^{-1}$ to mol $m^{-2}$ $yr^{-1}$. Monthly fluxes were estimated by averaging all of the instantaneous fluxes in a given month from June 2013 to December 2015. January-March are not reported (details in text). Corrections to the base fluxes were made according to the overland and groundwater correction described in section 3.3.6.

| | Base flux (mol $m^{-2}$ $yr^{-1}$) | | Overland corrected flux (mol $m^{-2}$ $yr^{-1}$) | | Overland and groundwater corrected flux (mol $m^{-2}$ $yr^{-1}$) | | % Data coverage | |
|---|---|---|---|---|---|---|---|---|
| | TA | DIC | TA | DIC | TA | DIC | TA | DIC |
| April | -28 | -33 | 0 | -6 | -1 | -7 | 48 | 48 |
| May | -28 | -35 | -4 | -13 | -5 | -14 | 40 | 40 |
| June | -74 | -96 | -8 | -36 | -9 | -37 | 74 | 71 |
| July | -89 | -120 | -25 | -67 | -27 | -68 | 52 | 52 |
| August | -116 | -144 | -50 | -79 | -51 | -80 | 74 | 67 |
| September | -77 | -102 | -18 | -49 | -19 | -50 | 61 | 61 |
| October | -60 | -72 | -8 | -6 | -9 | -7 | 48 | 30 |
| November | -59 | -61 | -5 | -8 | -6 | -9 | 41 | 49 |
| December | -54 | -52 | -8 | -6 | -9 | -7 | 48 | 53 |
| Mean | | | | | -15 | -31 | | |
| Annual | | | | | -12 | -28 | | |

Table 3. Alkalinity export fluxes (Tmol $yr^{-1}$ and Tmol $m^{-2}$ $yr^{-1}$) from coastal marine environments.

| | TA export (Tmol $yr^{-1}$) | Area-weighted TA export (Tmol $m^{-2}$ $yr^{-1}$) | Study |
|---|---|---|---|
| Salt marsh | 3.0 | 12 | This study |
| Mangrove | 4.2 | 30 | Sippo et al. 2016 |
| Rivers | 26-37 | | Ludwig et al. 1998, Amiotte Suchet et al. 2003, Cai et al. 2008 |
| Global continental shelf | 4-29 | 0.2-1.1 | Hu and Cai 2011, Krumins et al. 2013 |

Total salt marsh and mangrove area: 0.38 x $10^{12}$ $m^2$ (Woodwell et al. 1973)
Mangrove area: 0.14 x $10^{12}$ $m^2$ (Giri et al. 2011)
Salt marsh area: 0.24 x $10^{12}$ $m^2$ (difference of Woodwell et al. 1973 and Giri et al. 2011)
River: 0.624 x $10^{12}$ $m^2$ (Raymond et al. 2013)
Shelves: 26 x $10^{12}$ $m^2$ (Walsh et al. 1988)

## 3.6 Supporting information for Chapter 3

**Figure S1.** Residual plots for TA MLR

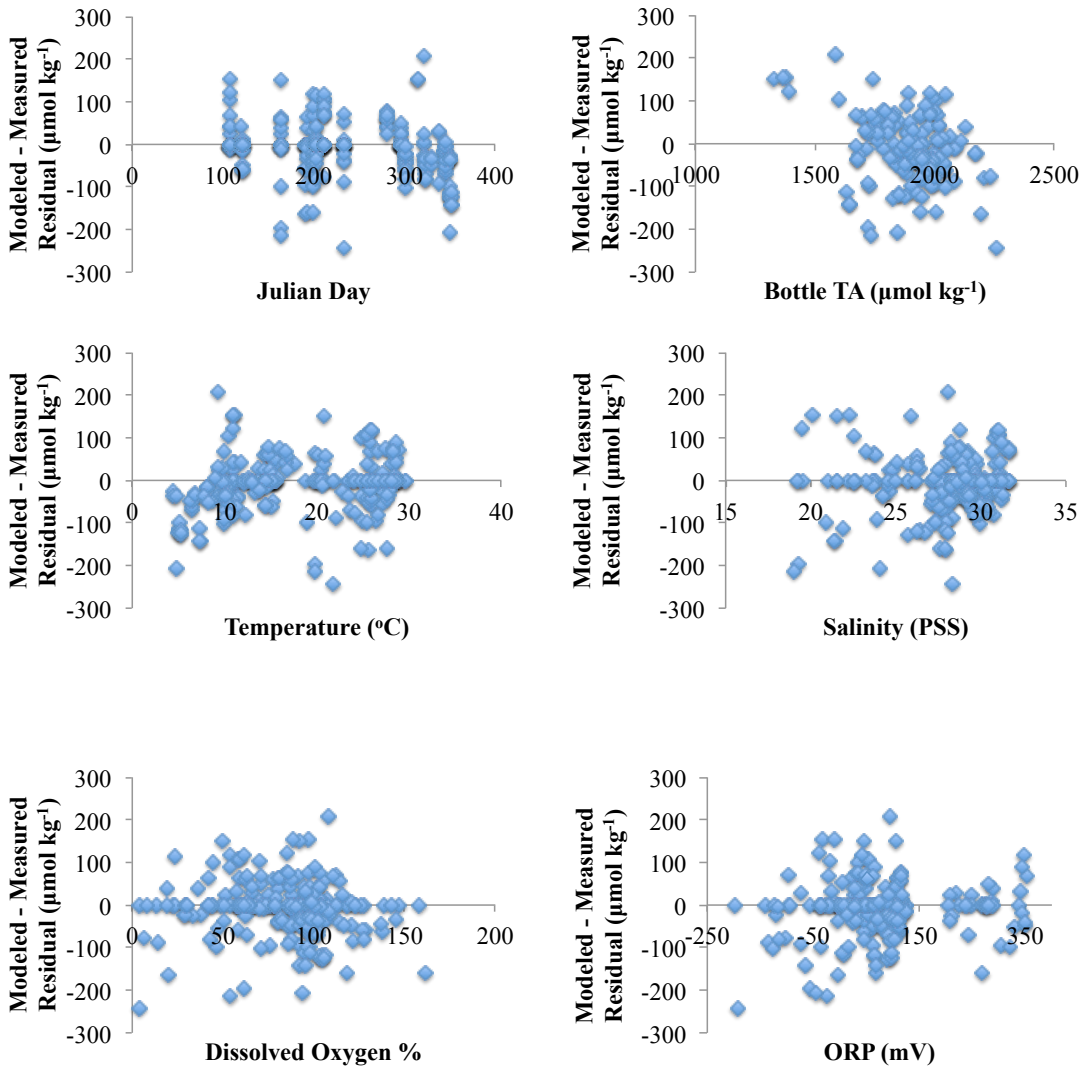

**Figure S2.** Model-derived ratio of total (to and from the drainage area) to within-channel water fluxes as a function of tide level in Sage Lot Pond. (Wang et al. 2016 Supplemental information). This function is used for the overland correction in the water fluxes.

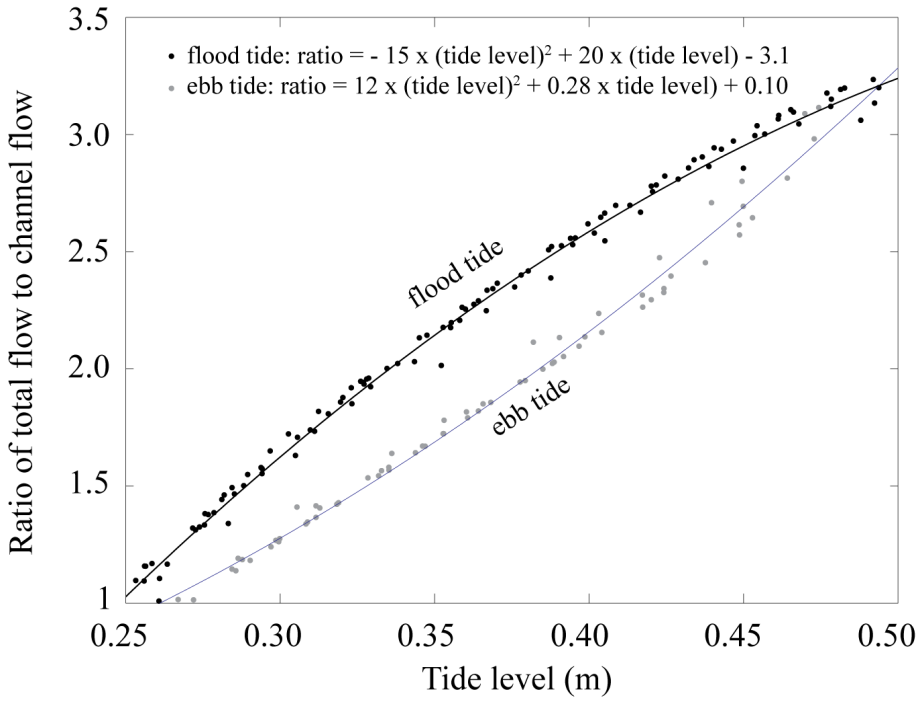

# Chapter 4

Revealing the intricacies of inorganic carbon export from intertidal salt marshes using high frequency direct measurements

## 4.1 Abstract

Intertidal salt marshes are productive coastal ecosystems that play a major role in the coastal carbon cycle. Here, results are presented from the first study to measure high-resolution dissolved inorganic carbon (DIC) concentrations in a tidal creek of an intertidal salt marsh – Sage Lot Pond (SLP), in Waquoit Bay, MA. The directly measured high frequency DIC data were combined with high frequency water fluxes to yield instantaneous DIC fluxes. These fluxes were summed over periods of time in the summer and fall to calculate tidal exchange between the marsh and adjacent estuary during periods of the summer and fall. DIC export fluxes were also calculated over different time intervals including tidal, spring-neap, and seasonal cycles. On tidal scales, most of DIC export occurred close to high tide. The net DIC export from the SLP salt marsh was greater in summer than fall, and largest export occurred at when tidal range was lowest, at neap tides. DIC generated in salt marshes was highly variable over daily, spring-neap, and seasonal timescales as a result of changes in concentration and water fluxes. High frequency, direct measurements allowed us to fully characterize timescales over which DIC export fluxes occurred in order to inform best sampling strategies to capture the true dynamics of carbon exports from tidal wetlands.

## 4.2 Introduction

Intertidal salt marshes are highly productive, vegetated coastal ecosystems located at the interface between the land and the ocean. Considering their small areal coverage, salt marshes act as significant $CO_2$ sinks, sequestering 4.8 ± 0.5 – 87.2 ± 9.6

Tg C $yr^{-1}$ with an average carbon burial rate 218 ± 24 g C $m^{-2}$ $yr^{-1}$ (Chmura et al., 2003; Duarte et al., 2005; Mcleod et al., 2011). The importance of the ability of salt marshes to outwell organic carbon (OC) and nutrients to the coastal ocean has been suggested for decades (Teal 1962; Odum 1968). More recently, studies have suggested that wetlands are also important sources of dissolved inorganic carbon (DIC) to adjacent waters by tidal exchange (Morris and Whiting 1986; Cai and Wang 1998; Raymond et al., 2000; Raymond and Hopkinson 2003; Neubauer and Anderson 2003; Wang and Cai 2004). However, published literature contains few studies with sufficient resolution to fully resolve the effects of the marsh export of DIC on carbonate chemistry and carbon cycling in adjacent coastal systems, and to accurately quantify the marsh DIC export flux under tidal and seasonal variability (Duarte et al., 2005; Bouillon et al., 2008; Cai 2011). This leads to high uncertainties in coastal carbon budgets regarding the coastal wetlands contribution (Cai 2011; Bauer et al., 2013; Herrmann et al., 2015). As salt marshes continue to be rapidly destroyed by land development and threatened by sea level rise (Woodroffe 1995; Duarte et al., 2005; Silliman et al., 2009; Hopkinson et al., 2012), it is important to be able to accurately quantify inorganic carbon flux to understand baseline DIC export from the marsh to the coastal ocean. DIC fluxes are affected by simultaneous contributions of marsh-derived materials carried by porewater and surface water exchange as well as terrestrial inputs carried by groundwater discharge. Measurements over timescales appropriate to processes being studied are crucial to obtaining accurate estimates of chemical fluxes. High-resolution fluxes can also help to determine suitable

sampling schemes and evaluate whether infrequent bottle sampling is adequate to capture the large variability seen in coastal systems.

Traditionally, salt marsh studies have estimated inorganic carbon export using sampling plans that include taking at most hourly bottle samples on a monthly or seasonal interval (Morris and Whiting 1986; Neubauer and Anderson 2003; Wang and Cai 2004). Water fluxes were not directly measured but were estimated using tidal prisms in addition to large extrapolations between sampling events generated estimates of export associated with large uncertainties (Downing et al., 2009; Ganju et al., 2012). A recently published study by Wang et al. (2016) used data from seasonal bottle samples and *in situ* biogeochemical sensors in a multiple linear regression to estimate high frequency DIC concentrations. DIC and measured water fluxes were used to calculate high frequency annual DIC fluxes. Wang et al. (2016) estimated -414 g C $m^{-2}$ $yr^{-1}$, which was twice the previous DIC export rate. This was likely due to being able to capture more variability in concentrations and water fluxes. Here, we use a recently developed instrument to measure high-frequency DIC concentrations over specific periods during summer and fall of 2015 in an intertidal salt marsh. This is the first time there have been simultaneous, high-frequency direct measurements of DIC and water fluxes over significant periods of time in a salt marsh. We investigated DIC export at tidal, spring-neap, and seasonal timescales. Over these timescales, export primarily occurred around high tide, at neap tides, and during the summer. We were also able to assess

uncertainties associated with different sampling protocols and suggest the best times to capture DIC export fluxes from an intertidal salt marsh.

## 4.3 Methods

### 4.3.1 Study site

Sage Lot Pond (SLP) is an intertidal salt marsh located near the eastern inlet of Waquoit Bay, on Cape Cod, Massachusetts (Figure 1). Staff from Waquoit Bay National Estuarine Research Reserve (WBNERR) monitor the estuary and manage infrastructure to facilitate the study of biogeochemical cycles in the wetlands system. Sage Lot Pond is ideal for a baseline study because it is comparable to other Atlantic salt marshes with respect to faunal and floral communities, where the low marsh is dominated by *Spartina alterniflora* and the high marsh is dominated by *Distichlis spicata* and *Juncus gerardii*. This site is also similar in its relative sea level rise (2.83 ± 0.18 mm $yr^{-1}$, NOAA Tide Station ID 8447930) and its mean annual temperature (9.88°C) (Chmura et al., 2003). It has a small, forested watershed that delivers a relatively low level of nutrient loading, estimated at ~12 kg N $ha^{-1}$ of estuary $yr^{-1}$ (Kroeger et al., 2006). A drainage area was defined using a 1-m bare-earth LiDAR-derived digital elevation model (DEM) of Massachusetts based on the North American Vertical Datum of 1988 (NAVD88) and a water drop analysis routine (Wang et al., 2016). The drainage basin associated with the chosen tidal creek site has an area of 4132 $m^2$ with relatively insignificant groundwater input, which will be discussed in detail later. To measure tidal exchange within the SLP marsh, a time-series sampling site was established at the mouth of a tidal creek that

drains a portion of the marsh. Both discrete sampling and high-frequency *in situ* sensor measurements were obtained at this site.

### 4.3.2 Discrete sampling and analysis

Discrete bottle samples were collected every 1-2 hours at the tidal creek sampling site using a peristaltic or diaphragm pump for periods up to a full tidal cycle (~12-14 hr) in April, July, October, November, and December in 2015. Dissolved inorganic carbon (DIC) collection and analysis followed standard best practice procedures outlined by Dickson et al. (2007). Samples were collected through capsule filters with 0.45 μm pore size (Farrwest Environmental Supply, Texas, USA) into 250 mL borosilicate bottles, poisoned with 100 uL saturated mercuric chloride, sealed with a glass stopper coated with APIEZON® – L grease and secured with a rubber band.

Discrete samples of DIC were measured with an Apollo SciTech DIC auto-analyzer (Model AS-C3) by acidifying the sample with 10% phosphoric acid. The acidified $CO_2$ sample was purged with high purity nitrogen gas and total $CO_2$ gas was detected with a LICOR-7000 infrared analyzer (LI-COR Environmental, Nebraska, USA). Certified Reference Material (CRM) from Dr. A.G. Dickson at the Scripps Institution of Oceanography was used to calibrate the DIC auto-analyzer. DIC values were reported in μmol $kg^{-1}$ after being corrected for water density and mercuric chloride addition. The average difference in duplicates was 1.7 ± 12.1 μmol $kg^{-1}$ (n=8) compared to the precision and accuracy of ± 2.0 μmol $kg^{-1}$ (1σ) of the instrument. The larger standard deviation in duplicates could be a result of differences in time and

concentration incurred while filling the duplicate bottles over a few minutes or due to storage errors.

### 4.3.3 High-frequency sensor measurements

High frequency, time-series *in situ* sensors were deployed at the Sage Lot Pond tidal creek to monitor and record water column features. An EXO2 Multiparameter Sonde (YSI Inc., Yellow Springs, OH) measured temperature, salinity, water depth, dissolved oxygen (DO), fluorescent dissolved organic matter (fDOM), chlorophyll, oxidation/reduction potential, probe pH, and a SonTek IQ Plus acoustic Doppler velocity meter (ADVM) (Sontek/YSI, San Diego, CA) measured water flux and surface elevation. The YSI EXO2 recorded at intervals ranging from 2 min to 8 min and the Sontek IQ recorded time-averaged data every 15 min. The relative elevation of the deployed Sontek IQ was referenced to North American Vertical Datum of 1988 (NAVD88), which is based on repeated long-term GPS base station occupations using a Trimble receiver (63 cm) and is associated with negligible error. All sensors were cleaned and calibrated regularly according to manufacturer recommended methods to maintain performance. After a deployment period of 2-4 weeks, YSI EXO2 data was evaluated for fouling and calibration drift. A correction factor based on calibration standards and the assumption of linear drift was applied to the data as needed. When correction was greater than, 30% of the calibration value for ORP or salinity, or greater than 2 pH units for pH, data was discarded (Wagner et al., 2006). YSI EXO2 pH measurements (NBS scale) have a measurement uncertainty of up to 0.20 pH units and other YSI

EXO2 parameters have uncertainties up to 1% for salinity, 0.05 ºC for temperature, 1% for dissolved oxygen, and 20 mV for ORP.

The Sontek IQ ADVM includes a vertical beam and integrated pressure sensor to measure water level in addition to four transducers with two along-axis beams and two skew beams to measure velocity. Sontek IQ ADVM proprietary software internally calculates cross-sectional area with user-provided creek geometry and Sontek IQ measured water depth. Cross-sectional area is then multiplied by mean channel velocity to provide flow in and out of the creek. The uncertainty in water flux arising from cross-sectional area and velocity measurement as well as internal algorithms is less than 5%. Data from YSI EXO2 and Sontek IQ sensors were averaged over 15 min intervals.

In addition to the Sontek IQ and YSI EXO2, a recently developed high-resolution, *in situ* carbon sensor, CHANnelized Optical Sensor (CHANOS) (Wang et al., 2015), was also deployed at the tidal creek sampling site. CHANOS uses spectrophotometric principles to measure DIC and pH, which can define the $CO_2$ system through thermodynamic calculations with relatively small calculation errors. CHANOS has two separate channels to measure pH and DIC. The pH channel uses a flow-through, spectrophotometric method (Wang et al., 2007). For this study, only DIC measurements were used. The DIC channel uses an improved spectrophotometric method described in detail in Wang et al. (2013). Briefly, it uses a countercurrent flow configuration between acidified seawater and a pH-sensitive indicator solution in a tube-in-tube design. This design allows the indicator to flow inside a highly $CO_2$-permeable membrane (Teflon AF

2400) that is placed inside a sample tubing where acidified seawater flows surrounding the Teflon tubing. After $CO_2$ exchange in the countercurrent flow cell, the indicator solution is directed into an optical z-cell for absorbance detection. The improved DIC method can achieve a response time of ~1.5 mins for full equilibration. The CHANOS consists of syringe drivers, electronics housing, Teflon tube sample loop, spectrophotometer, and z-cell. Each measurement cycle is ~15 min, which includes a reference in addition to sample measurement, flushing time and syringe filling and discharging. The system achieved a precision of ~±2.5 μmol $kg^{-1}$ and an accuracy of ~±5.0 μmol $kg^{-1}$ during coastal deployment. Temperature measured by the CHANOS and salinity from the YSI EXO2 were incorporated into the final DIC calculation.

For deployment in the marsh, CHANOS was adapted to run off batteries, which were charged with two 250 W solar panels (Renogy, Ontario, CA). Even though CHANOS was designed to be *in situ*, it was placed on a platform atop the marsh due to size constraints prohibiting the sensor to be deployed in the tidal creek. This led to a discrepancy between measurement temperature and *in situ* temperature, which will be discussed in further detail shortly. In order to keep the internal pump working well without clogging, water was thoroughly filtered. The inlet to the CHANOS was initially filtered to remove large debris and additionally filtered with a 100 μm plastic disc filter (Keller Products, Acton, MA) and a copper mesh filter.

CHANOS received calibration with Certified Reference Material (CRM) over the range of temperatures at which measurements were conducted. Automated *in situ*

calibration is possible with CHANOS, however, in order to avoid discharging CRM, which contains a small percentage of mercuric chloride, into the marsh, calibration was conducted during site visits so waste could be collected and disposed of properly. Additional laboratory CRM calibrations were also conducted. CHANOS DIC measurements were calibrated first using CRM and then corrected with discrete bottle samples that were analyzed using a traditional method described in the previous section. 14-17 discrete bottle samples were collected over 2-3 days during each CHANOS deployment, in July, November, and December. Bottle samples were matched to CHANOS measurements taken at most 8 minutes apart. These bottle samples were used to correct CHANOS data on a monthly basis (Figure 2). After correction, the mean residual between CHANOS and bottle measurements was 0 ± 56 μmol $kg^{-1}$ with $n = 47$ and $R^2$=0.8 for all points.

Possible sources of larger uncertainty (± 56 μmol $kg^{-1}$) between the corrected CHANOS and bottle measurements compared to the coastal deployment a few years ago (± 5.0 μmol $kg^{-1}$, Wang et al., 2015) could be the following: 1) Temperature discrepancies - Because the CHANOS instrument could not be deployed in the water, sample temperature was measured by a thermistor in air near the measurement cell and could be higher or lower than the actual *in situ* water temperature. Sample temperature was likely between *in situ* temperature and air temperature and the difference was affected by many factors, such as time of day, season, or weather conditions. If sample temperature measured was a degree Celsius higher than actual *in situ* temperature, it

would result in a DIC concentration of 7-9 μmol $kg^{-1}$ less than what it should be (details will be discussed shortly). 2) Due to the dynamic nature of the marsh, matching up the salinity data from the YSI EXO2 deployed in the tidal creek to calculate CHANOS DIC and the difference in time in matching CHANOS measurements with a discrete bottle sample could also affect the uncertainty. 3) Indicator solutions were prepared in large batches of ~13L and bagged into 2L aluminum gas-impermeable bags (Calibrated Instruments, Inc). Changes in indicator solution composition either between bags or in the same bag over time could affect DIC concentration. This is likely a minor source of error compared to temperature discrepancy.

CHANOS measurements were calibrated with discrete bottle samples collected in each month of deployment (Figure 2), similar to how CTD salinity is often post-calibrated using discrete bottle salinity samples in addition to pre-calibration of the conductivity sensor. The offset between CHANOS and bottle samples is likely a combination of the previously mentioned sources of error. Residual (CHANOS DIC – bottle DIC) plots before bottle calibration confirm the slight dependence of concentration differences on temperature and salinity (Supporting information Figure S1). The effect of temperature and salinity on DIC concentrations was assessed using the range of 1700-2200 μmol kg-1 for alkalinity discrete samples and the range of 6.7-8.3 for calculated pH reported in Wang et al. (2016). CO2SYS (Lewis and Wallace 1998; Pierrot et al., 2006) with constants from Mehrbach et al. (1973) refit by Dickson and Millero (1987) was used to calculate a decrease in DIC concentration of 7-9 μmol $kg^{-1}$ for each degree celsius

temperature increase. A unit of salinity increase resulted in a decrease in DIC concentration of 3-10 μmol $kg^{-1}$. It is likely that in July, the measured sample temperature (in air) was higher than the *in situ* temperature (in water), which could have skewed the CHANOS DIC calculation to be lower than it should have been and necessitate the correction seen here. Cooler temperatures in the fall could result in lower air temperatures than water, and the opposite slope relationship as seen in November and December. A calculation for DIC based on a temperature higher than actual temperature, would result in a lower value of DIC. The lack of significant patterns in the residual plots (Supporting information Figure S1) after correction gives us confidence that this issue has been corrected.

#### 4.3.4 Water fluxes

The water fluxes from the SonTek IQ ADVM measurements in the tidal creek were used to derive the base water fluxes used for calculation of high-resolution DIC fluxes as in Wang et al. (2016) as well as Chapter 3 of this thesis. Corrections were made to the base SonTek IQ fluxes to account for overland flow and groundwater contributions to the marsh. Overland flow occurs if flooding or ebbing tidal water inundates or drains the marsh without going through the creek channel when tidal height is above the marsh surface. Water that flows over the marsh without going through the creek channel is not measured by the ADVM. To correct for overland flow, a hydrodynamic model was created for the drainage basin of the tidal creek using the 1-m DEM with the Coupled Ocean-Atmosphere-Wave-Sediment Transport (COAWST)

model (Warner et al., 2010). The ratio of the tidal creek water fluxes to total water fluxes over the drainage area was used to develop a flood and ebb corrections to apply to the measured ADVM water fluxes in the creek channel to derive total fluxes as a function of water level and flow direction.

The second correction to the water fluxes was to account for groundwater input. Groundwater affects DIC in two ways. The first way is that groundwater is treated as a net seaward flow of water to flush out marsh DIC without considering the concentration of DIC in the groundwater. The second way is that groundwater can act as a pathway to directly export DIC. The first correction is applied as a correction to the water fluxes. The mean flow over the study period was shifted by a correction to match to the net groundwater flow estimate. The net groundwater estimate over the study period was -0.00024 $m^3$ $s^{-1}$ or -7570 $m^3$ $yr^{-1}$ calculated using the isohaline method from MacCready (2011) and the salt balance application from Ganju (2011). The groundwater correction shift was 0.00007 $m^3$ $s^{-1}$, adapted from Wang et al. (2016). This is only 0.1% of the mean tidal flow magnitude (0.075 $m^3$ $s^{-1}$), suggesting that groundwater input is not significant at this site. The second correction is applied as a concentration correction to the net annual DIC flux estimate. Groundwater was measured seasonally and was not able to be modeled at high frequency to correct the DIC flux. An average annual groundwater flux of 39 ± 10 g C $m^{-2}$ $yr^{-1}$ (Gonneea, unpublished data) could be applied to the average DIC flux, however, our results only cover monthly scales and therefore, the second portion of this groundwater correction was not applied.

### 4.3.5 Error analysis for flux estimates

Uncertainty was assessed by error propagation using the maximum uncertainty possible. For DIC concentration, the standard deviation from the bottle sample correction was 55 μmol $kg^{-1}$. 55 μmol $kg^{-1}$ was applied the lowest DIC value of 1185 μmol $kg^{-1}$ measured during CHANOS deployment in order to assess the maximum effect of this uncertainty, which gave an uncertainty of 5%. Water flow measurement uncertainty from the ADVM was 5%. Uncertainty for overland and groundwater corrections to water fluxes was assessed by random amplification of flood and ebb equations from the overland correction. 100 realizations were applied assuming random errors for flood and ebb equations centered at 25%, where the effect on corrected net concentration fluxes was 6% for overland correction and 1% for groundwater correction. Using propagation of error as the square root of the sum of the squares of individual errors, the total uncertainty for final calculated DIC fluxes is 9%.

## 4.4. Results

### 4.4.1 High frequency time series data from summer and fall

DIC concentrations in the tidal creek are affected by seasonal biogeochemical activity in the creek water and marsh sediments as well as water mixing between the estuary and marsh. CHANOS DIC measurements capture the overall effect of these contributing factors. CHANOS deployment occurred in the summer and late fall during the months of July, August, November, and December (Figure 3). In the summer

(Figure 3a-b), CHANOS DIC is driven by a clear tidal signal for most of the period. At high tide, DIC is closer to the estuary end member around ~1800-1900 μmol $kg^{-1}$ and at low tide, DIC represents the marsh end member reaching values of ~2200-2400 μmol $kg^{-1}$. These concentrations are similar to the ranges of discrete DIC bottle samples reported for July and August in Wang et al. (2016), where high tide DIC is ~1800 μmol $kg^{-1}$ and low tide DIC is ~2400-2600 μmol $kg^{-1}$. Marsh respiration processes add $CO_2$ to the water and increase DIC concentrations (Neubauer and Anderson 2003; Wang and Cai, 2004). Temperatures during this time period followed a diurnal variation ranging from 20-30°C. Salinity stayed relatively constant between 29-31 ppt with most of the variability due to mixing of estuary and marsh end members because of the lack of rainfall over this period (NOAA NERRS). Water level ranged from -0.4 to +0.4 m at spring tides and -0.1 to +0.25 m at neap tides when the tidal range is smallest. Discrete DIC bottle samples agree well with the corrected CHANOS measurements with an average offset of 57 μmol $kg^{-1}$ for July, less than 15% of the average tidal variability of DIC.

In contrast to the summer, DIC concentrations in the fall (Figure 3c-d) do not show a clear tidal signal over the majority of the time sampled. Where DIC concentrations follow a tidal signal, the range was much smaller at ~100 μmol $kg^{-1}$ over a tidal cycle compared to the ~400 μmol $kg^{-1}$ seen during the summer. The larger range in DIC in the summer are a result of higher rates of biological productivity and respiration in the water column and sediments in the summer. Higher evapotranspiration in the summer can increase salinity thereby decreasing DIC concentration faster at low tide.

However, the overall range of concentrations seen in the fall is quite large from ~1200-2100 μmol $kg^{-1}$. There a few periods of extremely low DIC concentrations (~1200-1400 μmol $kg^{-1}$) such as November 15-17 and December 5-9. The period from December 5-9 also corresponds to a drop in salinity and lower water levels.

In general, there is much more variability in the salinity in the fall than in the summer with several drops below 20 ppt. Some of these drops in salinity coincide with drops in water level as well, indicating that fresher water, either groundwater or rain, or both, may be a larger proportion of the water flow and therefore cause the salinity to decrease. Low sea level increases the hydraulic gradient and allows for seaward movement of the interface between the groundwater head and sea level, which can cause lower salinity (Gonneea et al., 2013). There were substantially more rain events in the fall compared to the summer (NOAA NERRS, Figure 3). Rain corresponded to drops in barometric pressure (not shown), which was also related to higher water level, especially during the event from November 10-13.

### 4.4.2 Instantaneous DIC fluxes from salt marshes

To calculate instantaneous DIC flux, CHANOS DIC concentration was multiplied by the water flux measured by the Sontek IQ ADVM. As discussed in the methods section, instantaneous DIC base fluxes were corrected for flow that occurred outside of the creek (overland flow), and for net water export due to terrestrial (freshwater) groundwater discharge. Because of our ~monthly timescales, we did not correct for inputs of terrestrial DIC from discharge of fresh groundwater. Table 1 reports the

average DIC and the water fluxes through each step. These values were estimated by averaging the instantaneous fluxes over the given time period. Average DIC was higher in July-August at 2056 μmol $kg^{-1}$ compared to November and December values of 1757-1764 μmol $kg^{-1}$. Water fluxes were also greatest water in July and August with overland and corrected water fluxes of -2.85 x $10^{-3}$ $m^3$ $s^{-1}$.

Calculated DIC fluxes were negative indicating lateral export from the salt marsh over the entire study period. The overland flow correction reduced estimated DIC base fluxes significantly by 0.07 g C $s^{-1}$ or 560 g C $m^{-2}$ $yr^{-1}$ or ~28% for July, 0.06 g C $s^{-1}$ or 480 g C $m^{-2}$ $yr^{-1}$ or ~90% for November, and 0.05 g C $s^{-1}$ or 330 g C $m^{-2}$ $yr^{-1}$ or ~31% for December. Values are reported in g $s^{-1}$ and the rate for each period of time is normalized to an annual areal rate in g C $m^{-2}$ $yr^{-1}$ in order to compare to other studies. The groundwater correction increased export by 12-14 g C $m^{-2}$ $yr^{-1}$.

Final corrected DIC fluxes (overland and groundwater corrected fluxes) showed high export occurring in the summer period of -1430 g C $m^{-2}$ $yr^{-1}$ and lower export occurred in the fall with only -68 g C $m^{-2}$ $yr^{-1}$ in November and -759 g C $m^{-2}$ $yr^{-1}$ in December. It is important to note that applying the July rate to the entire year would likely overestimate the annual flux. November export was less than annual published literature values from more traditional sampling plans (e.g., – 156 to – 197 g C $m^{-2}$ $yr^{-1}$ for DIC export from salt and freshwater marshes from along the US East Coast (Morris and Whiting 1986; Neubauer and Anderson 2003; Wang and Cai 2004). December export of -759 g C $m^{-2}$ $yr^{-1}$ was significantly larger and twice the December rate of – 376 g C $m^{-2}$

$yr^{-1}$ found at this location using a modeled DIC flux from previous years 2012-2014 from Wang et al. (2016) (Supplement information Table S1). This study's summer export of – 1430 g C $m^{-2}$ $yr^{-1}$ was much greater than – 500 to – 650 g C $m^{-2}$ $yr^{-1}$ in Wang et al. (2016). November is showing a small negative DIC flux indicating small export of DIC from the marsh. November experienced discontinuous data segments, due to lack of CHANOS or water flux measurements. In addition, CHANOS only measured the first half of the >40 mm rain event from November 10-12 (NOAA NERRS), which if integrated over this period, resulted in a positive flux. Because November data collection periods were intermittent, this rainstorm event had a greater influence on the overall flux for November. If only part of a day or storm event was measured, the calculated total export flux could be skewed depending on whether only the incoming or outgoing tide was measured or if only part of a storm was measured. Quantifying the effect of storm events on DIC export will be explored in the future when a larger data set is available.

To further discuss the effect of data availability, number of days is included in the last column of Table 2. Here, we have quantified the number of days or the percentage of time that the CHANOS measured data. For example, in the July-August period, there was 25.7 days covered out of 36 days for a data coverage percentage of 71%. Because CHANOS data was averaged at 15-minute intervals, 71% of the 15-minute intervals from July 7 to August 11 had CHANOS DIC measurements. This is not scaled

up to 100% because it is not a valid to assume that the time period measured is representative of the missing data, especially if there were rain or storm events.

## 4.5 Discussion

### 4.5.1 Average seasonal DIC signals

To more easily compare seasonal data, average tides from summer and fall can show typical differences between the two seasons without as much influence from brief weather events. Tidal cycles were separated into ~12.5 hour cycles using the time when the water level was lowest (low tide) as the starting point of each tidal cycle. Measured parameters were binned into 15-minute intervals over a tidal cycle and averaged across each bin for summer (July-August) and fall (December). For example, a bin that contained data from 1 hour after low tide was averaged across all tidal cycles that contained data in the bin for 1 hour after low tide. November data was not used due to its lack of continuous data coverage and storm influence.

Calculated average tides from each season were plotted together to show the differences between seasons (Figure 4). In the top panel, average DIC from the summer (blue) was higher than in the fall (red). DIC concentration in summer varies from 2200 μmol $kg^{-1}$ at low tide to 2000 μmol $kg^{-1}$ at high tide while fall showed almost no difference in DIC concentration staying around 1750-1800 μmol $kg^{-1}$ between high and low tide. Lower DIC concentration in the fall may be a combination of processes such as colder temperatures, lower rates of biological activity in the marsh, and reduced sediment respiration (Wang and Cai 2004; Wang et al., 2016).

Average DIC and overland and groundwater corrected water fluxes discussed in the previous section (Table 1) were 2054 μmol $kg^{-1}$ and -0.0029 $m^3$ $s^{-1}$ in the summer, respectively. Fall values were much lower in both average DIC and average water flow at 1756 μmol $kg^{-1}$ and -0.0008 $m^3$ $s^{-1}$, respectively. Instantaneous DIC flux in summer ranged from -4 to 4 g C $s^{-1}$ compared to the -2 to 2 g C $s^{-1}$ in fall and average fluxes reflected those differences in magnitude as -0.19 and -0.10 g C $s^{-1}$ for summer and fall (Table 2). These average fluxes allowed for exploration of different strategies for sampling total flux from a tidal cycle without taking 15 min bottle samples or sensor measurements over the entire tidal cycle.

### 4.5.2 Sampling strategies based on average tides

To investigate whether it is possible to capture most or all of the flux over a tidal cycle without having to take bottle samples over the entire tidal cycle, average tides were tested with different sampling strategies. A caveat is that these results may not be applicable to other sites, however, these sampling strategies, if tested and confirmed to work well, would reduce the overall effort required to measure fluxes from salt marshes and reduce uncertainties in the coastal marsh-estuary budget. The data consistently showed the greatest water flux and DIC flux a few hours before and after the high tide. Most of the flux occurred when the water level was high, even though concentrations were high when the water level was low. With this in mind, different sampling windows around high tide were calculated to test how much total flux could be captured during a shorter amount of time than a full tidal cycle. We found that for the summer, a window

of time ~2 hours before and after high tide for a total of 4 hours represents the period of time needed to capture approximately 100% of the total flux from the entire tidal cycle (Figure 5). Starting at high tide DIC flux and moving away from high tide in both directions in half hour increments allowed us to find the amount of sample time to capture 100% of total flux from the entire tidal cycle. Instead of sampling for 12 hours to cover an entire tidal cycle, sampling in summer could be less than half the time, at 4 hours total, ± 2 hours centered at high tide. For fall, the amount of time was 3.25 hours before and after high tide - sampling must occur for 6.5 hours to capture the total flux in the late fall, compared to 4 hours in the summer. Water fluxes were higher in the summer so summer export occurred faster. It is important to note here that these calculations only apply to high-resolution 15-minute data. If 15-minute sample intervals are not possible and the 4-hour sampling window around high tide is used, samples taken at half hour intervals would result in an overestimation of the DIC flux by 30%. If hourly samples were taken such that there were 5 samples times, 2 hours and 1 hour before and after high tide as well as at high tide, the DIC flux would be an overestimation of 89%. This shows the importance of high frequency data, especially during high water levels, when water fluxes are largest.

High frequency measured DIC fluxes were compared to more traditional methods of sampling. Here, fluxes from mean tides were averaged for summer and fall to estimate uncertainties involved in strategies for sampling at every hour or two hours, and at high and low tide (Table 3). The beginning of each sampling strategy started at low tide. For

the summer period, the closest sampling scheme to estimating total flux was hourly sampling that captured ~86% of the total flux. For December, sampling every hour overestimates the flux by 9% and every 2 hours samples estimates 87% of the total December flux. Sampling every 2 hours can give almost the same estimate of the total flux as an estimate using 15-minute data. The protocol for sampling only at high and low tide does a much poorer job, by estimating large magnitudes of DIC import by more than 100 times the real total flux for these two periods in the summer and fall. A caveat is that these are averaged tides with the signal has been smoothed out.

To test the applicability of these sampling strategies based on average tides, individual tidal cycle data from this study was used (Table 4). The best sampling protocol for the summer was once an hour sampling starting at low tide, which captured 75-125% of the total flux 38% of the tidal cycles during the July-Aug period. The data coverage over this period was good with data for 70% of 71 tidal cycles. Sampling centered at high tide did not work well for the summer or fall, where estimated fluxes only captured ±25% net DIC flux over a tidal cycle 5-16% of the time. Missing data in an individual tide can affect the flux calculation in that if the tidal cycle flux is calculated without complete coverage, the total flux may be skewed. On the other hand, if there is missing data in the sampling protocol, that would also skew the flux calculation. For the sampling protocols centered at high tide, missing data would have a larger effect than the every hour or 2 hour sampling protocols that cover the complete tidal cycle, which would explain why those strategies did not work as well.

### 4.5.3 Tidal range influences on DIC export fluxes

Tides are caused by gravitational forces of the sun and the moon acting on Earth's waters. Spring tides occur when the sun and the moon are in alignment causing the largest tidal ranges to occur with high high tides and low low tides. Neap tides occur when there is the smallest tidal amplitude between high tide and low tide. It has been shown that spring-neap tidal cycles can drive the water content and hydraulic gradient in salt marshes (Nuttle 1988). During neap tides, the marsh surface does not flood so there is a net loss of water from the sediment. This occurs through evapotranspiration and drainage near creek banks and causes the hydraulic gradient to decrease. Up to 40% of the water loss within 10 m of the creek bank occurs during nonflooding, neap tide time periods (Nuttle and Hemond 1988). Because of the strong influence of the spring-neap cycle on water transport in salt marshes, we investigated the effects of spring and neap tides regarding DIC export.

Initially, spring and neap tides were designated based on moon phases with quarter moons as neap tides and full and new moons as spring tides. However, at SLP, due to the location of creek and morphology of the marsh in addition to meteorological events, spring-neap signals were obscured in the water level time series (Figure 6). Instead the time series was separated into equally spaced high, middle, and low tidal ranges, where each tidal cycle started at low tide. The tidal ranges were averaged over two tidal cycles to account for the unequal semidiurnal tides, where one tidal cycle often had higher water levels than the following tidal cycle. Here, the high tidal range

represents spring tide and low tidal range represents neap tide with middle tidal range transitioning between the two extremes. In the July-Aug period, water levels were separated into 6 bins of high, middle, or low tidal ranges (Figure 6a). Accumulated DIC flux along the sampling period is shown in the bottom panel as a percentage of the total flux over the sampling period. Decreases in the flux accumulation correspond to positive DIC fluxes during flooding tide when DIC is being imported into the marsh. There is steady accumulation of DIC flux in July-Aug. In contrast, December water levels are more variable and separated into 8 bins of high, middle, and low tidal range (Figure 6b). DIC export accumulates steadily for the first week and then increases considerably in a few bursts of large DIC fluxes around 12/10 and 12/18.

Total fluxes were averaged over these categories of tides (Figure 7, supplemental information Table S2). These results suggest that greatest export occurs at neap tides with less export during the spring tides. This outcome seems counter-intuitive in that it would seem that more DIC would be exported during spring tides because of increased tidal amplitude. When water during a spring tide floods the marsh, some of the water does not immediately return through the creek, but remains in the sediments and diffuses into porewaters (Nuttle 1988). This explains the lower export of DIC. Then during neap tides, when the tidal amplitude decreases and causes the hydraulic gradient to decrease, porewaters drain back into creek waters and result in the negative fluxes and export seen during neap tides. Middle tidal ranges have small export in the summer and positive import in the fall. Recently, a mangrove study on $CO_2$ and methane fluxes

over spring-neap cycles (Call et al., 2015) found more gases were released during neap tides. These results support the need to investigate chemical fluxes at spring-neap timescales.

### 4.6 Future considerations and conclusions

Here, we have directly measured high-frequency DIC fluxes from an intertidal salt marsh for the first time. Results suggest that it is important to use *in situ* sensors to monitor these environments to capture as much continuous data as possible especially during storm events including rain and wind that may affect water fluxes. Capturing part of a weather event could skew the estimated fluxes, as we see in November fluxes. Spring and neap tides are important to consider in sampling practices. Though our data do not cover the entire summer or fall season, results suggest that sampling procedures could differ for each season; sampling every hour in the summer can capture 86% of the total flux that would be captured using 15-minute resolution data, while sampling every hour or every two hours would capture 109% and 87% in the fall. Sampling before and after high tide would reduce the amount of time required to estimate total flux over a tidal cycle where summer tides could be sampled for 4 hours around high tide and fall tides could be sampled at 6.5 hours around high tide. However, in our tidal cycle testing, high tide sampling was not as reliable as every hour or two hour sampling.

In the future, we would like to consider more closely the effects of wind, rain, and light on the DIC export fluxes. We would also like to be able to apply an offset between high resolution and low-resolution sampling estimated fluxes to literature values to

update the fluxes that have been previously calculated using bottle samples taken for less frequent time intervals.

**Acknowledgements**

This chapter is made possible by contributions from Zhaohui Aleck Wang, Kevin D. Kroeger, Meagan Eagle Gonneea and especially to Neil K. Ganju for his help with the water fluxes and corrections. Thank you to Harry Hemond and Dan McCorkle for their helpful comments. Lloyd Anderson, Katie Carter, Tom Kraemer, Linda Kraemer, Zoe Sandwith, and Kate Morkeski helped with sample collection and analysis. Jennifer O'Keefe Suttles, Adrian Mann, and Sandy Brosnahan collected and processed YSI and water flux data. Thank you to WBNERR for providing the infrastructure to conduct this work. This work was funded by NSF Graduate Resarch Fellowship Program, Link Foundation Ocean Engineering and Instrumentation Fellowship, National Institute of Science and Technologies (NIST no. 60NANB10D024), USGS, NSF (OCE-1459521) and NOAA Science Collaborative (NA09NOS4190153).

**References**


Bauer, J. E., W. J. Cai, P. A. Raymond, T. S. Bianchi, C. S. Hopkinson, and P. A. G. Regnier. 2013. The changing carbon cycle of the coastal ocean. Nature **504:** 61-70.

Bouillon, S. and others 2008. Mangrove production and carbon sinks: A revision of global budget estimates. Global Biogeochem. Cy. **22**. doi: GB2013, doi:10.1029/2007GB003052.

Cai, W. J. 2011. Estuarine and coastal ocean carbon paradox: $CO_2$ sinks or sites of terrestrial carbon incineration? Annu. Rev. Mar. Sci. **3:** 123-145.

Cai, W. J., and Y. Wang. 1998. The chemistry, fluxes, and sources of carbon dioxide in the estuarine waters of the Satilla and Altamaha Rivers, Georgia. Limnol Oceanogr **43:** 657-668.

Chmura, G. L., S. C. Anisfeld, D. R. Cahoon, and J. C. Lynch. 2003. Global carbon sequestration in tidal, saline wetland soils. Global Biogeochem. Cy. **17**. doi: 1029/2002GB00191.

Dickson, A. G., and F. J. Millero. 1987. A comparison of the equilibrium constants for the dissociation of carbonic acid in seawater media, Deep Sea Res. Part A, 34(10), 1733–1743, doi:10.1016/0198-0149(87)90021-5.

Dickson, A. G., C. L. Sabine, and J. R. Christian. 2007. Guide to best practices for ocean $CO_2$ measurements. PICES Special Publication.

Downing, B. D., and others. 2009. Quantifying fluxes and characterizing compositional changes of dissolved organic matter in aquatic systems in situ using combined acoustic and optical measurements. Limnol. Oceanogr.: Methods 7: 119–131. doi:10.4319/lom.2009.7.119

Duarte, C. M., J. J. Middelburg, and N. Caraco. 2005. Major role of marine vegetation on the oceanic carbon cycle. Biogeosciences **2:** 1-8.

Ganju, N. K. 2011. A novel approach for direct estimation of fresh groundwater discharge to an estuary. Geophys. Res. Lett. 38. doi: 10.1029/2011GL047718.

Ganju, N. K., M. Hayn, S. N. Chen, R. W. Howarth, P. J. Dickhudt, A. L. Aretxabaleta, and R. Marino. 2012. Tidal and groundwater fluxes to a shallow, microtidal estuary: Constraining inputs through field observations and hydrodynamic modeling. Estuaries Coast. 35: 1285–1298. doi:10.1007/s12237-012-9515-x

Gonneea, Meagan Eagle, Ann E. Mulligan, and Matthew A. Charette. "Climate - driven sea level anomalies modulate coastal groundwater dynamics and discharge." Geophysical Research Letters 40.11 (2013): 2701-2706.

Herrmann, M. and others 2015. Net ecosystem production and organic carbon balance of U.S. East Coast estuaries: A synthesis approach. Global Biogeochem. Cy. 29: 96-111.

Hopkinson, C. S., W. J. Cai, and X. P. Hu. 2012. Carbon sequestration in wetland dominated coastal systems - a global sink of rapidly diminishing magnitude. Curr Opin Env Sust **4:** 186-194.

Kroeger, K. D., M. L. Cole, and I. Valiela. 2006. Groundwater-transported dissolved organic nitrogen exports from coastal watersheds. Limnol. Oceanogr. 51: 2248-2261.

Lewis, E., Wallace, D.W.R., 1998. Program Developed for CO2 System Calculations. ORNL/ CDIAC-105.

MacCready, P. 2011. Calculating Estuarine Exchange Flow Using Isohaline Coordinates. J. Phys. Oceanogr. 41: 1116-1124.

Mcleod, E., Chmura, G. L., Bouillon, S., Salm, R., Björk, M., Duarte, C. M., ... & Silliman, B. R. 2011. A blueprint for blue carbon: toward an improved understanding of the role of vegetated coastal habitats in sequestering CO2. Frontiers in Ecology and the Environment, 9(10), 552-560.

Mehrbach, C., C. H. Culberson, J. E. Hawley, and R. M. Pytkowicz. 1973. Measurement of the apparent dissociation constants of carbonic acid in seawater at atmospheric pressure, Limnol. Oceanogr., 18(6), 897–907, doi:10.4319/lo.1973.18.6.0897.

Morris, J. T., and G. J. Whiting. 1986. Emission of Gaseous Carbon-Dioxide from Salt-Marsh Sediments and Its Relation to Other Carbon Losses. Estuaries **9:** 9-19.

Neubauer, S. C., and I. C. Anderson. 2003. Transport of dissolved inorganic carbon from a tidal freshwater marsh to the York River estuary. Limnol. Oceanogr. 48: 299-307.

NOAA National Estuarine Research Reserve System (NERRS). System-wide Monitoring Program. Data accessed from the NOAA NERRS Centralized Data Management Office website: http://www.nerrsdata.org/; accessed 12 October 2016.

Nuttle, W. K., and H. F. Hemond. 1988. Salt marsh hydrology: Implications for biogeochemical fluxes to the atmosphere and estuaries, Global Biogeochem. Cycles, 2(2), 91–114, doi:10.1029/GB002i002p00091.

Nuttle, W.K., 1988. The extent of lateral water movement in the sediments of a New England salt marsh. Water Resources Research, 24(12), pp.2077-2085.

Odum, E. P. 1968. Energy Flow in Ecosystems - a Historical Review. Am. Zool. 8: 11-18.

Pierrot, D., Lewis, E., & Wallace, D. W. R. 2006. MS Excel program developed for CO2 system calculations. ORNL/CDIAC-105a. Carbon Dioxide Information Analysis Center, Oak Ridge National Laboratory, US Department of Energy, Oak Ridge, Tennessee.

Raymond, P. A., J. E. Bauer, and J. J. Cole. 2000. Atmospheric CO2 evasion, dissolved inorganic carbon production, and net heterotrophy in the York River estuary. Limnol. Oceanogr. 45: 1707-1717.

Raymond, P. A., and C. S. Hopkinson. 2003. Ecosystem modulation of dissolved carbon age in a temperate marsh-dominated estuary. Ecosystems **6:** 694-705.

Silliman, Brian R., Edwin Grosholz, and Mark D. Bertness. 2009. Human impacts on salt marshes: a global perspective. Univ of California Press.

Teal, J. M. 1962. Energy flow in the salt marsh ecosystem of Georgia. Ecology, 43(4), 614-624.

Wagner, R. J., Boulger, R. W. J., Oblinger, C. J. & Smith, B. A. 2006. Guidelines and standard procedures for continuous water-quality monitors: station operation, record computation, and data reporting. United States Geological Survey Tech. Meth. 1-D3, 51 pp.

Wang, Z. A., and W. J. Cai. 2004. Carbon dioxide degassing and inorganic carbon export from a marsh-dominated estuary (the Duplin River): A marsh CO2 pump. Limnol. Oceanogr. 49: 341-354.

Wang, Z. A., X. Liu, R. H. Byrne, R. Wanninkhof, R. E. Bernstein, E. a Kaltenbacher, and J. Patten. 2007. Simultaneous spectrophotometric flow-through measurements of pH, carbon dioxide fugacity, and total inorganic carbon in seawater., Anal. Chim. Acta, 596(1), 23–36, doi:10.1016/j.aca.2007.05.048.

Wang, Z. A., Chu, S. N., & Hoering, K. A. 2013. High-frequency spectrophotometric measurements of total dissolved inorganic carbon in seawater. Environmental science & technology, 47(14), 7840-7847.

Wang, Z. A., F. N. Sonnichsen, A. M. Bradley, K. A. Hoering, T. M. Lanagan, S. N. Chu, T. R. Hammar, and R. Camilli (2015), In situ sensor technology for simultaneous spectrophotometric measurements of seawater total dissolved inorganic carbon and pH, Environ. Sci. Technol., 49(7), 4441–4449, doi:10.1021/es504893n.

Wang, Z. A., Kroeger, K. D., Ganju, N. K., Gonneea, M. E. and Chu, S. N. 2016. Intertidal salt marshes as an important source of inorganic carbon to the coastal ocean. Limnol. Oceanogr., 61: 1916–1931. doi:10.1002/lno.10347

Warner, J. C., B. Armstrong, R. Y. He, and J. B. Zambon. 2010. Development of a Coupled Ocean-Atmosphere-Wave-Sediment Transport (COAWST) Modeling System. Ocean Model. Online 35: 230-244.

Woodroffe CD. 1995. Response of tide-dominated mangrove shorelines in northern Australia to anticipated sea-level rise. Earth Surf Proc Land 20: 65–85.

**Figure 1.** The Sage Lot Pond field sampling site and drainage basin in Waquoit Bay National Estuarine Research Reserve (WBNERR) in Cape Cod, Massachusetts.

a)

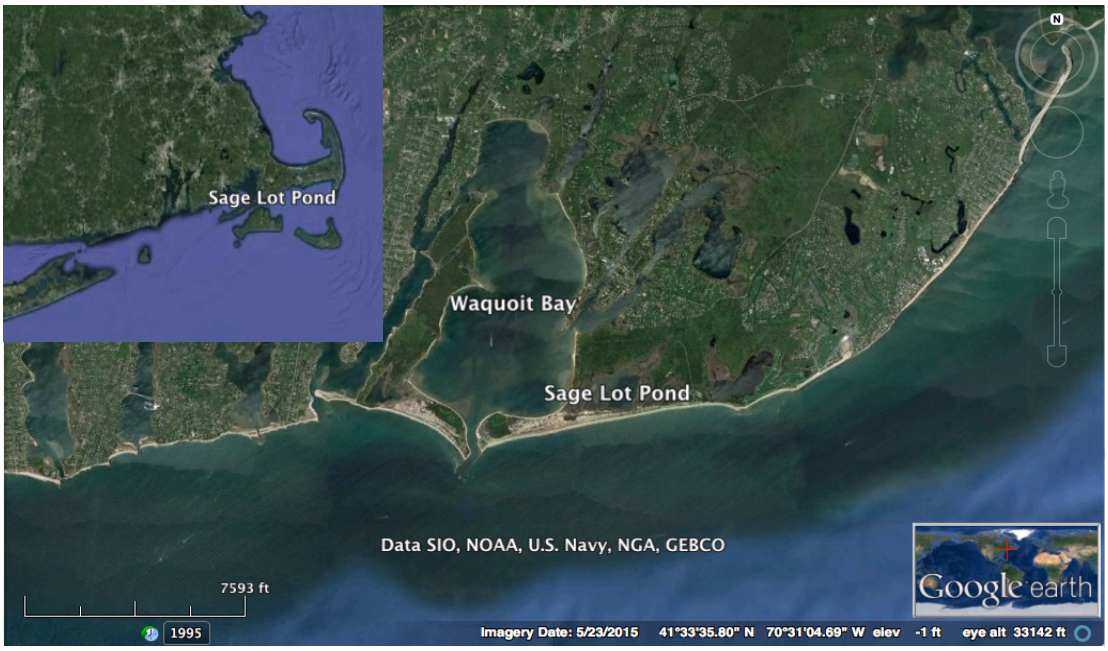


b)

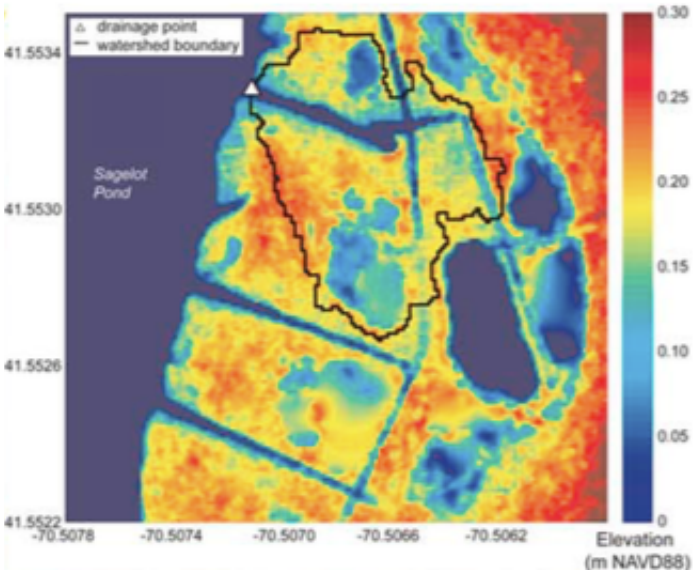

**Figure 2.** Monthly DIC calibrations of discrete bottle samples and CHANOS measurements.

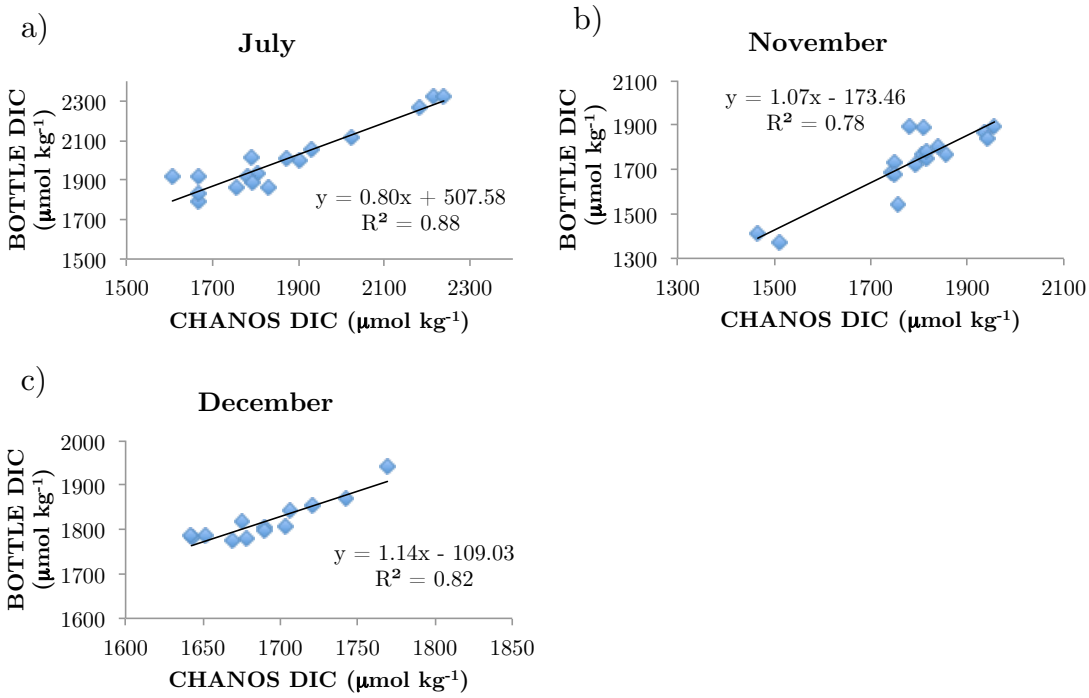

**Figure 3.** Time series of CHANOS DIC data from 2015. DIC measured by CHANOS in a) July and August c) November and December. Panels b) and d) show temperature (°C), salinity (PSS), and water level (m) referenced to NAVD88. DIC

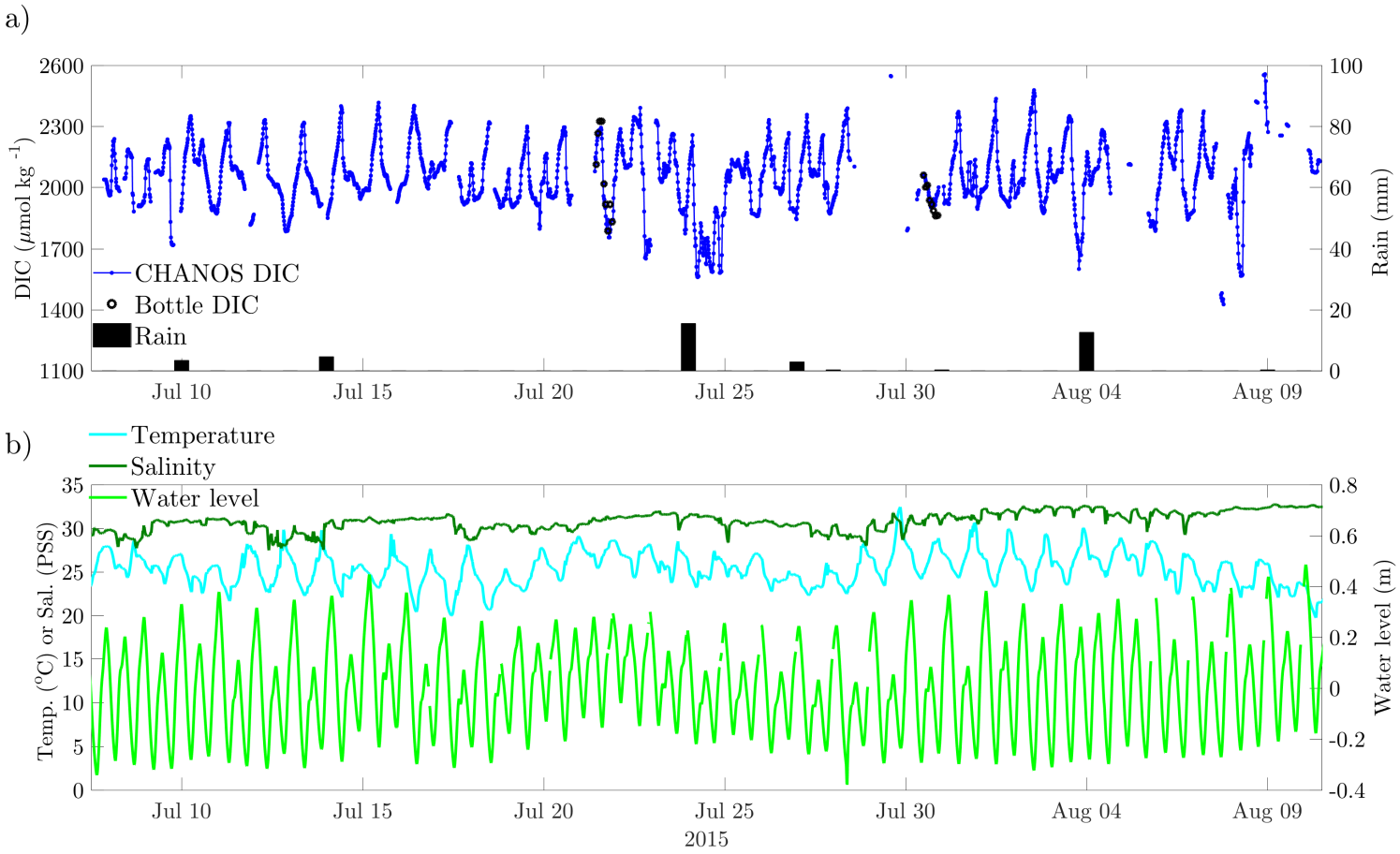

**Figure 3** (continued).

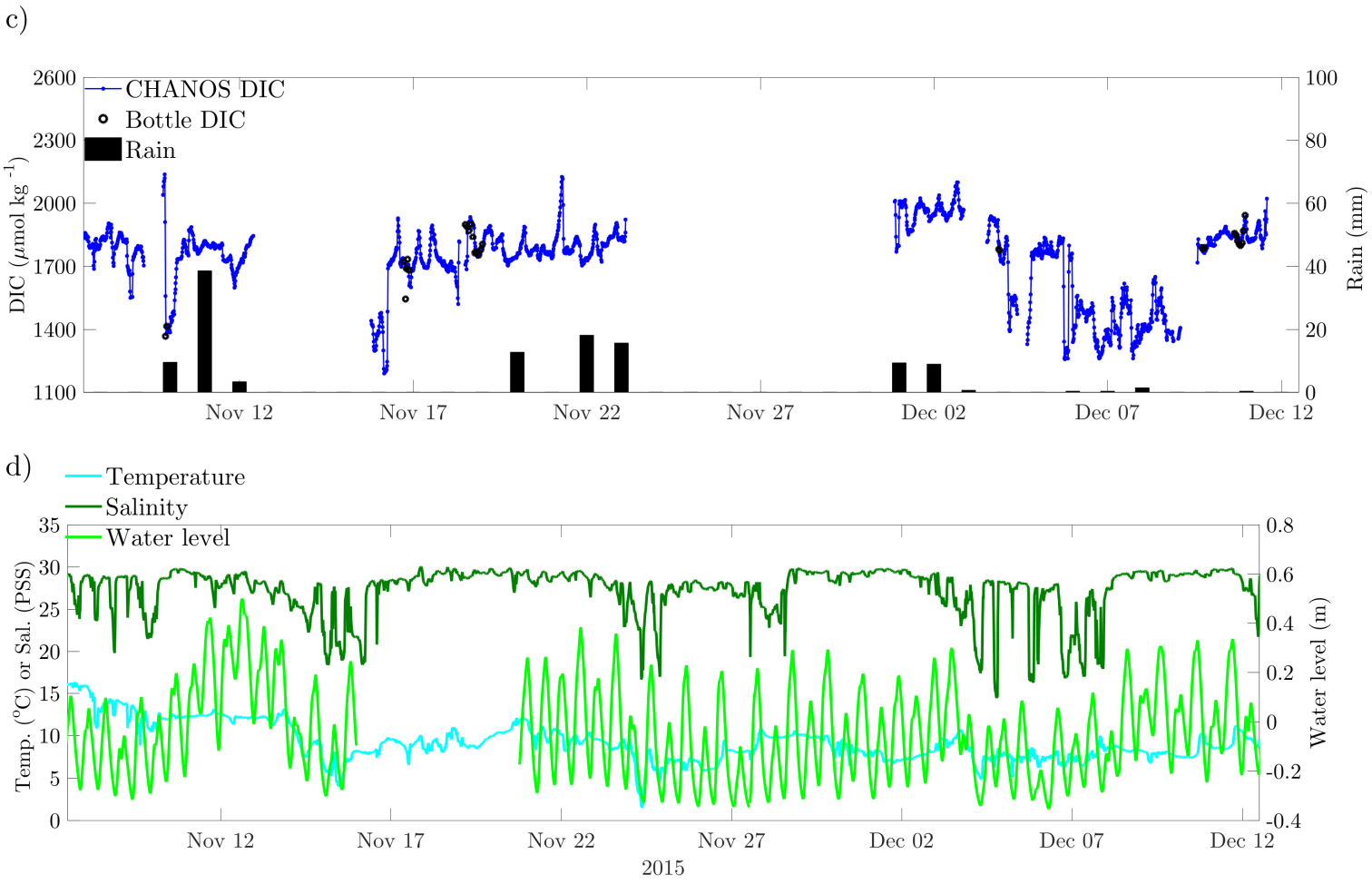

**Figure 4.** Average tides show DIC concentration, water flux, DIC flux, and water level from summer (blue) and late fall (red). Shaded areas show standard deviation of averages.

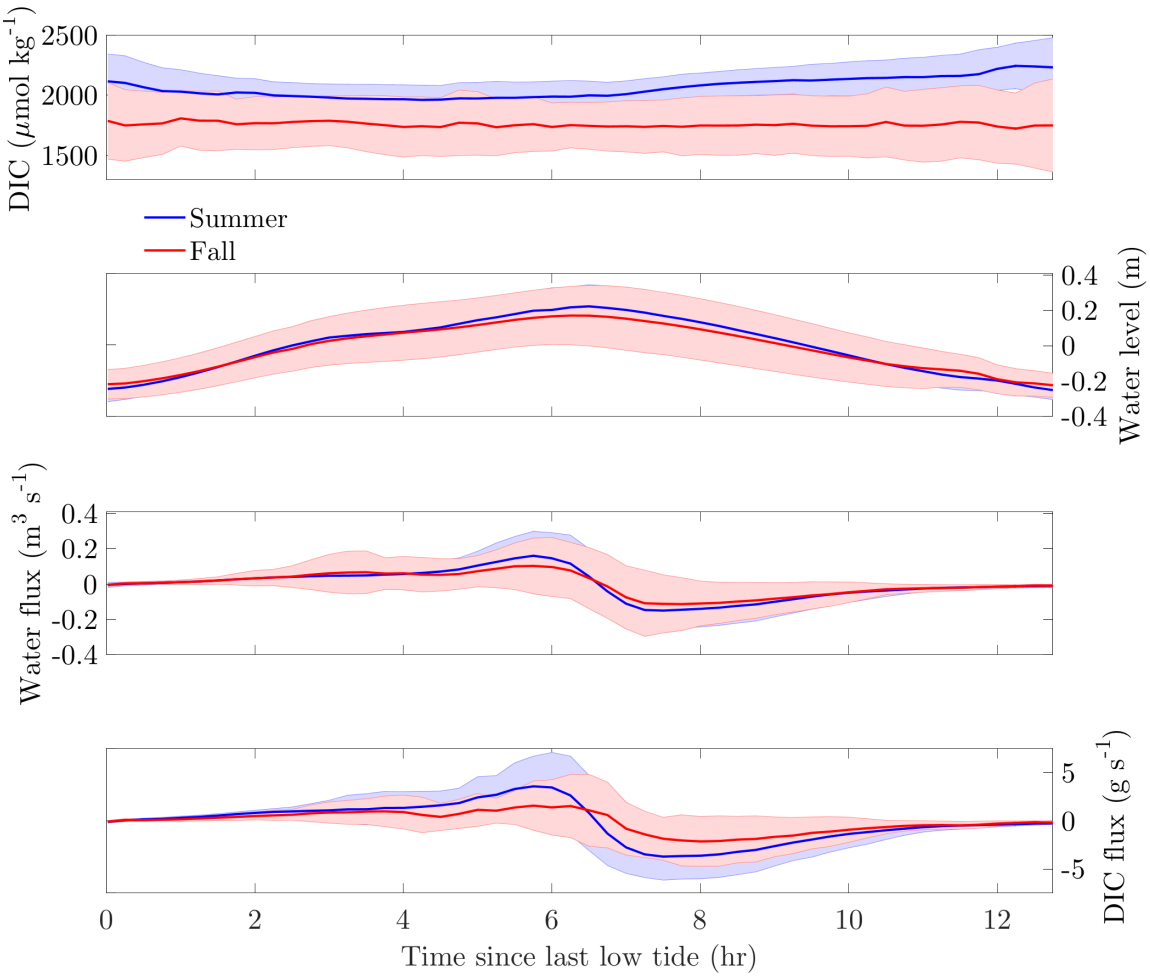

**Figure 5.** Sampling time period before and after high tide required to capture the total flux.

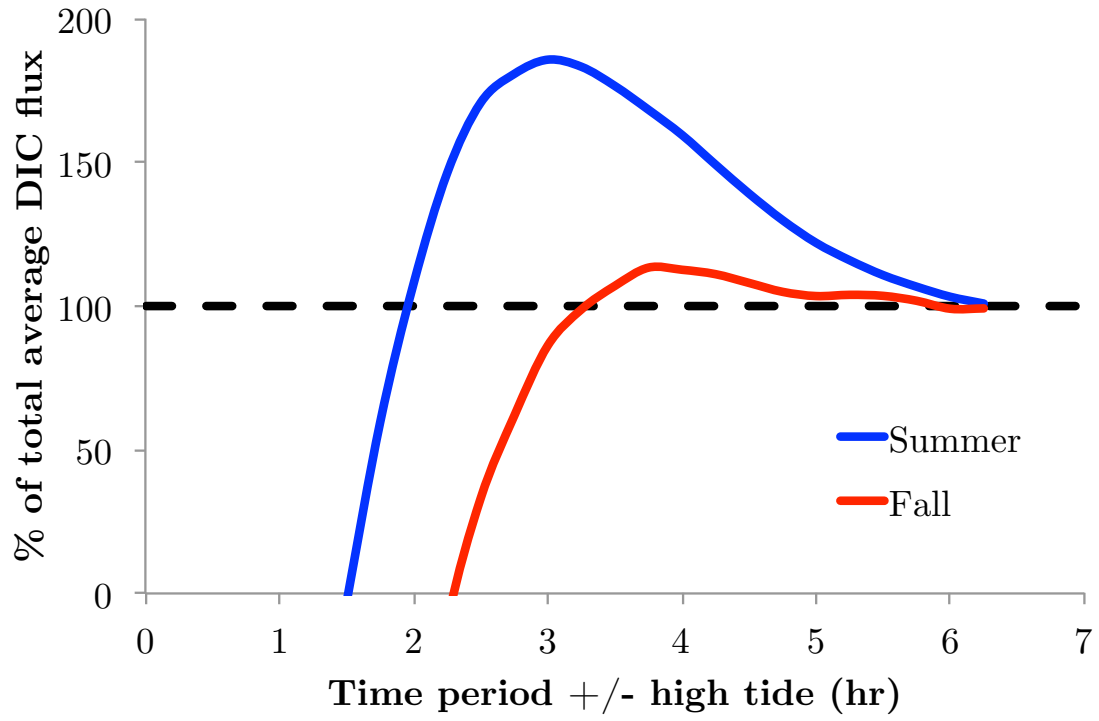

**Figure 6.** Time series of DIC flux, water level, tidal range over two tidal cycles, and accumulated flux in percent of total flux over given time period a) July 7 to August 11 and b) November 30 to December 18. Vertical lines in the 24 hr tidal range mark sections between high, middle, and low tidal ranges.

a)

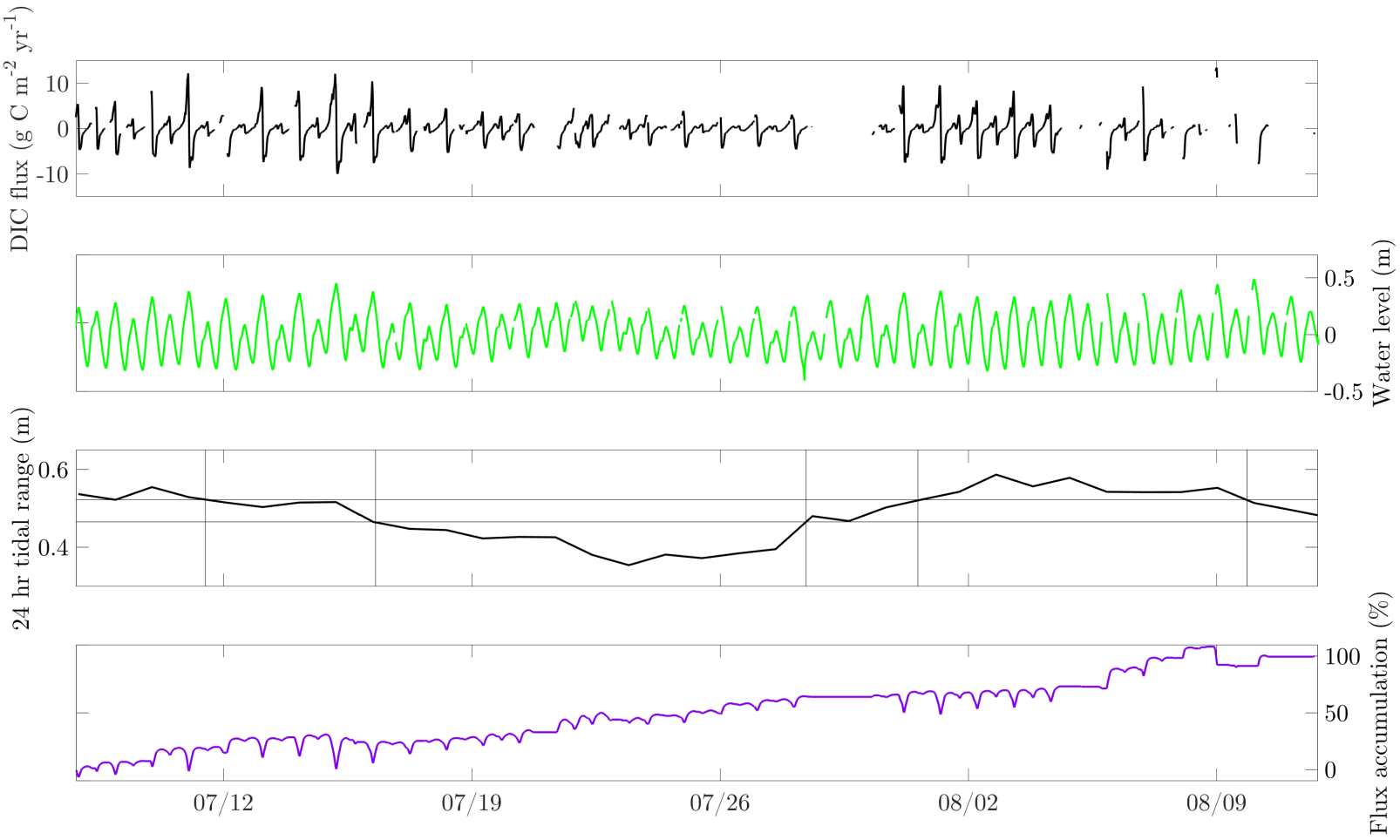

**Figure 6** (continued).
b)

**Figure 7.** Total flux exported (negative) or imported (positive) during high, middle, or low tidal ranges in summer and fall. Data presented in Table 5.

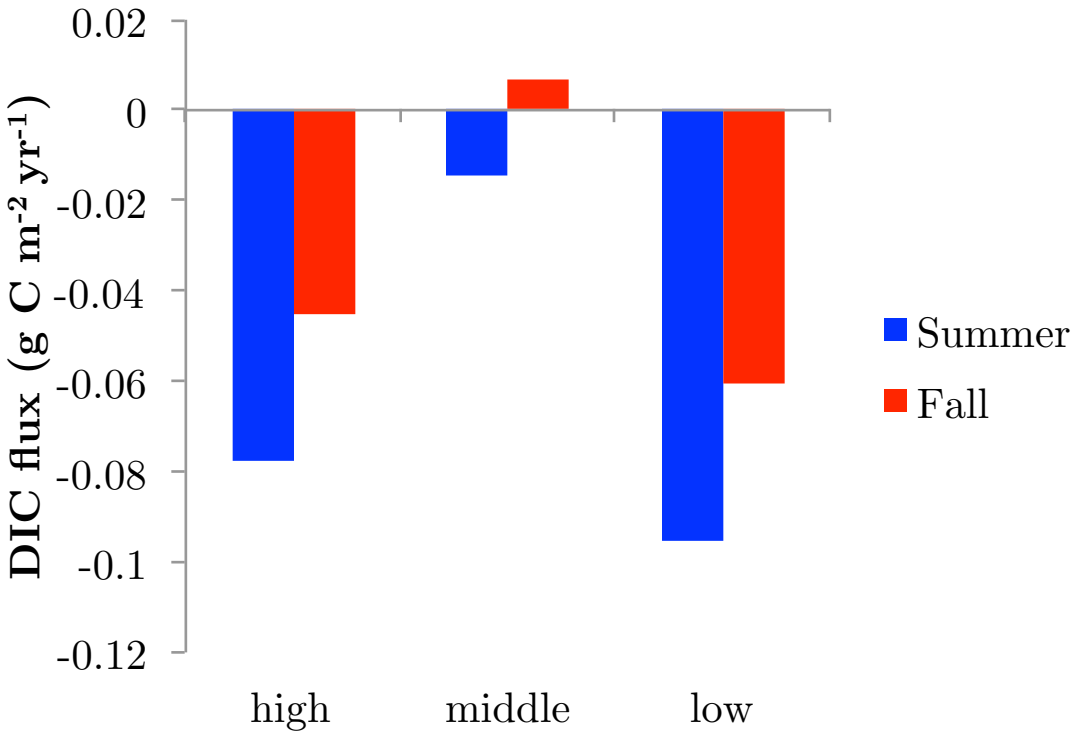

**Table 1.** Average DIC concentration and average instantaneous water fluxes over indicated time periods. Negative fluxes indicate export from the marsh and positive fluxes indicate import to the marsh from the estuary. Uncertainty in measured water fluxes is less than 5% and for DIC concentrations, is 4.6%.

| **Time period** | **DIC** ($\mu mol\ kg^{-1}$) | **Water base flux** ($m^3\ s^{-1}$) | **Water flux overland corrected** ($m^3\ s^{-1}$) | **Water flux overland and groundwater corrected** ($m^3\ s^{-1}$) |
|---|---|---|---|---|
| July 7 to August 11 | 2056 | -0.0057 | -0.0027 | -0.0028 |
| November 5 to 24 | 1764 | -0.0043 | -0.0012 | -0.0013 |
| November 30 to December 18 | 1757 | -0.002 | -0.0007 | -0.0008 |

**Table 2.** Instantaneous DIC fluxes (reported in g C $s^{-1}$ and normalized to annual flux units in g C $m^{-2}$ $yr^{-1}$ in parentheses) averaged over time period indicated. Negative fluxes indicate export from the marsh. Number of days covered refers to percentage of time that had instantaneous DIC flux for given period. Missing data was not interpolated. Uncertainty in corrected DIC fluxes is 9% (details in section 4.3.5).

| **Time period** | **DIC base flux** g C $s^{-1}$ (g C $m^{-2}$ $yr^{-1}$) | **DIC flux overland corrected** g C $s^{-1}$ (g C $m^{-2}$ $yr^{-1}$) | **DIC flux overland and groundwater corrected** g C $s^{-1}$ (g C $m^{-2}$ $yr^{-1}$) | **# of days covered** |
|---|---|---|---|---|
| July 7 to August 11 (36 days) | -0.26 (-1980) | -0.19 (-1416) | -0.19 (-1430) | 25.7 (71% of time period) |
| November 5 to 24 (19 days) | -0.07 (-535) | -0.01 (-56) | -0.01 (-68) | 8.3 (44% of time period) |
| November 30 to December 18 (19 days) | -0.14 (-1078) | -0.09 (-747) | -0.10 (-759) | 11.1 (58% of time period) |

**Table 3.** Overland and groundwater corrected DIC fluxes using different timing for sampling schemes starting at low tide and sampling once an hour or every two hours or only at low and high tide (reported in g C $s^{-1}$ and in parentheses g C $m^{-2}$ $yr^{-1}$). % of total flux compares these methods to overland and groundwater corrected fluxes reported in Table 2.

| | **Once an hour DIC flux** | | **Once every 2 hours DIC flux** | | **High/low tide DIC flux** | |
|---|---|---|---|---|---|---|
| | g C $s^{-1}$ (g C $m^{-2}$ $yr^{-1}$) | % of total flux | g C $s^{-1}$ (g C $m^{-2}$ $yr^{-1}$) | % of total flux | g C $s^{-1}$ (g C $m^{-2}$ $yr^{-1}$) | % of total flux |
| July 7 to August 11 | -0.16 (-1226) | 86 | 0.02 (185) | -13 | 0.29 (2183) | -153 |
| November 30 to December 18 | -0.11 (-831) | 109 | -0.09 (-668) | 87 | 0.45 (3432) | -450 |

**Table 4.** Percentage of tides that capture 75-125% (±25%) of total flux from testing each sampling protocol on all individual tides. 100% means that the sampling protocol matches the flux calculated from 15 min sample coverage. % Data coverage refers to the average data available for each tidal cycle. High tide-HT, low tide-LT.

| | 4 hrs centered at HT | 6.5 hrs centered at HT | Every hr starting at LT | Every 2 hrs starting at LT | % Data coverage |
|---|---|---|---|---|---|
| July 7 to August 11 | 16% | 13% | 38% | 18% | 70% of 71 tides |
| November 30 to December 18 | 5% | 10% | 11% | 8% | 58% of 37 tides |

## 4.7 Supporting Information for Chapter 4

**Figure S1.** Residual (CHANOS or CHANOS corrected – bottle) plots. Plots a, c, and e are uncorrected residuals for CHANOS temperature, YSI EXO salinity, and Date. After monthly-based corrections, CHANOS vs bottle residuals are no longer strongly biased (shown in b, d, and f.)

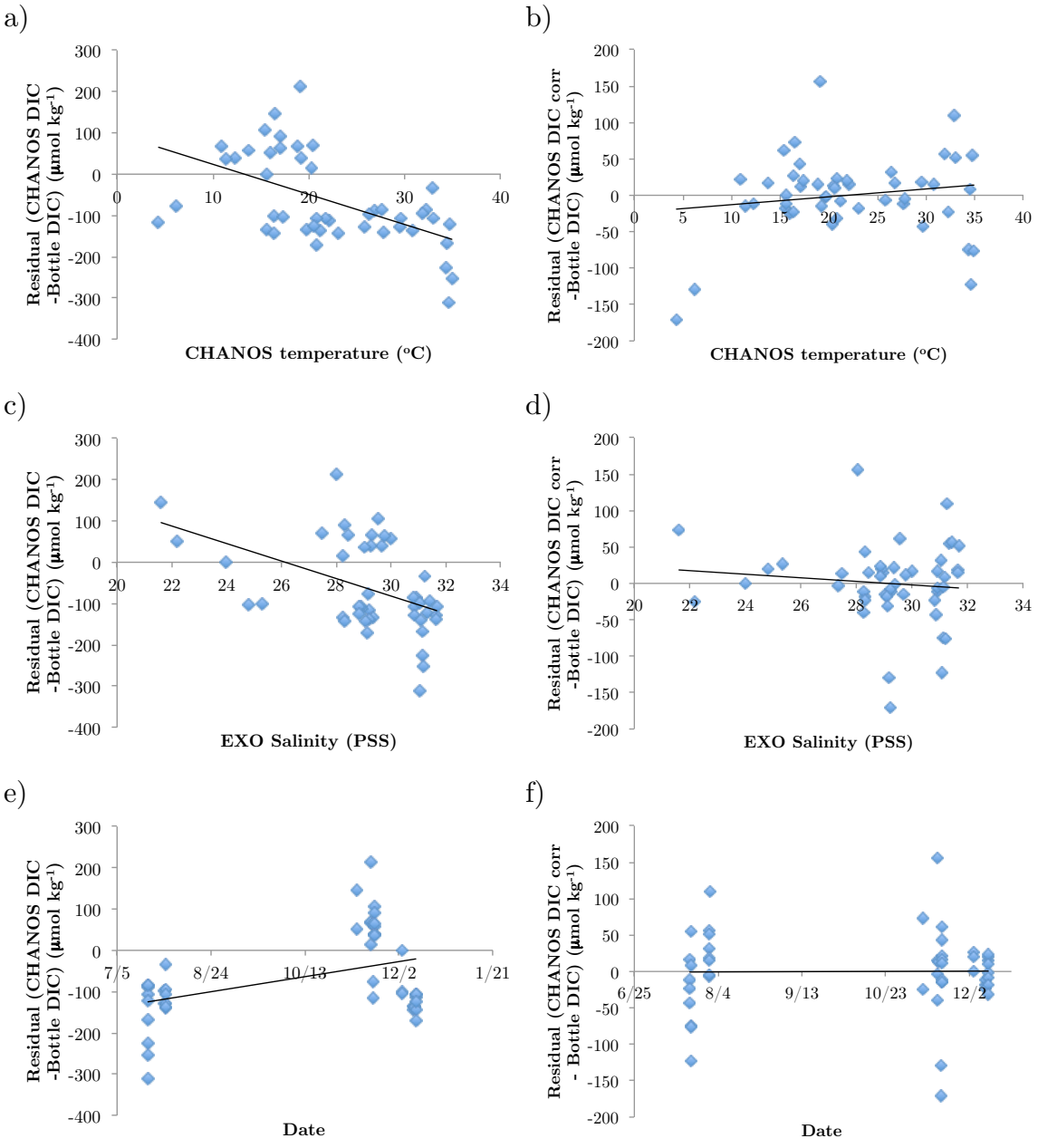

**Table S1.** High frequency DIC fluxes from Wang et al. (2016). Bolded months are relevant to comparison to this study.

| **Time period** | **DIC base flux** g C $m^{-2}$ $yr^{-1}$ | **DIC flux overland corrected** g C $m^{-2}$ $yr^{-1}$ | **DIC flux overland and groundwater corrected** g C $m^{-2}$ $yr^{-1}$ | **% of data coverage** |
|---|---|---|---|---|
| Apr | -331 | -17 | -138 | 48 |
| May | -644 | -266 | -385 | 40 |
| Jun | -1455 | -382 | -501 | 64 |
| **Jul** | **-1368** | **-391** | **-516** | **37** |
| **Aug** | **-1478** | **-425** | **-556** | **53** |
| Sep | -1281 | -511 | -645 | 58 |
| Oct | -650 | -153 | -285 | 21 |
| **Nov** | **-946** | **-385** | **-518** | **37** |
| **Dec** | **-928** | **-251** | **-376** | **44** |

**Table S2.** High, middle, low tidal range fluxes plotted in Figure 7.

| | **High tidal range DIC flux** | | **Mid tidal range DIC flux** | | **Low tidal range DIC flux** | |
|---|---|---|---|---|---|---|
| | g C $s^{-1}$ (g C $m^{-2}$ $yr^{-1}$) | # of days covered | g C $s^{-1}$ (g C $m^{-2}$ $yr^{-1}$) | # of days covered | g C $s^{-1}$ (g C $m^{-2}$ $yr^{-1}$) | # of days covered |
| July 7 to August 11 | -0.08 (-594) | 12.9 | -0.01 (-110) | 9.9 | -0.1 (-726) | 12.1 |
| November 30 to December 18 | -0.05 (-344) | 6.1 | 0.01 (50) | 5.2 | -0.06 (-463) | 6.5 |

# Chapter 5

## Conclusions

The goal of this thesis was to investigate the transport and storage of inorganic carbon species in open and coastal environments using high-resolution sampling and simple empirical modeling techniques. In Chapter 2, I analyzed changes in chemical parameters between 2001 and 2012 in the Northeast Pacific that revealed changes in circulation, deoxygenation and invasion of anthropogenic carbon dioxide in the water column. In Chapter 3, I estimated lateral alkalinity export over tidal, seasonal, and annual timescales from an intertidal salt marsh in Cape Cod, MA using a multiple linear regression approach with high frequency, in situ sensors data. These estimates let me evaluate the roles of marsh alkalinity in affecting tidal water chemistry and the coastal alkalinity budget. In Chapter 4, I used a newly developed, high frequency sensor to measure dissolved inorganic carbon and estimated DIC export from a salt marsh. I used the directly measured high-resolution flux to determine when most of the export was occurring, verify previous estimates, and derive a sampling window for how to best capture the variability of export fluxes when using discrete bottle samples.

In Chapter 2, surface waters accumulated $CO_2$ following the increase in atmospheric $CO_2$. The increase in $CO_2$ caused a decrease in pH and shoaling of the aragonite saturation horizon at the higher end of rates reported in other regions of the ocean. The Northeast Pacific is still acting as a carbon sink for anthropogenic $CO_2$ and

at a rate not statistically different than that in the Northwest Pacific but significantly lower than that in the North Atlantic at similar latitudes. However, because the Northeast Pacific is at the end of meridional overturning circulation, the waters contain high concentrations of respired products and create an already fragile condition that is exacerbated by additional anthropogenic $CO_2$. These results indicate that the Northeast Pacific is one of the most sensitive regions to changes in carbonate chemistry.

In Chapter 3, TA export was estimated using high frequency data measured by in situ sensors deployed in a salt marsh in Sage Lot Pond, MA. Alkalinity export was calculated using an empirical model of physical and chemical parameters in combination with high frequency water fluxes and chemical sensor data. Results show that water fluxes are greatest right before and right after high tide. 70% of annual alkalinity flux was exported in the summer, likely due to the increased rates of primary production and anaerobic respiration in sediments (Giblin et al., 1990; Giblin and Wieder 1992; Wang and Cai 2004). DIC export was also calculated using a similar method and found to have a similar pattern at larger magnitudes than alkalinity export over the year. Alkalinity and DIC fluxes were scaled up to global salt marsh area and found to contribute significantly to the coastal alkalinity budget.

In Chapter 4, DIC export was estimated using a new, automated DIC sensor called CHANOS, to directly measure DIC in a salt marsh at time intervals of ~15 min. Fluxes estimated from directly measured DIC during a period in July-August and December showed at least double the rates reported by Wang et al. (2016) suggesting

that the directly measured DIC fluxes may have covered processes that the model did not capture or as a result of interannual variability. I investigated export dynamics over various timescales – tidal, spring-neap, and seasonal. The results show that most of export actually occurred right before and right after high tide when water fluxes were also at maximum values. In the summer, full tidal export could be captured by sampling for every hour in the summer and fall as well as every two hours in the fall. Caveats for these sampling strategies are that these estimates are based on average seasonal signals and would likely not apply to sampling during episodic events such as rain. Our data included such an example of a rain event in November that skewed the fluxes for November. It was also found that DIC export was greater at neap tide than spring tide. During spring tides, the marsh was inundated over an area due to greater tidal amplitude and some of this water likely stayed in the sediments until the following neap tide (Nuttle 1988). Higher export was found over the summer period than the fall period as expected due to high rates of biological production and respiration in sediments as well as water column in the summer.

An accurate estimate of TA and DIC export fluxes allows for a better assessment of salt marshes as sources of buffering capacity to coastal oceans. Export of high TA and low pH water from salt marshes can act simultaneously as alkalizing and acidifying sources to the coastal ocean and this delicate balance can change tidally and seasonally. These results will help reduce uncertainty in current estimates of marsh DIC and TA export and establish a baseline export flux in order to evaluate the importance of

intertidal salt marshes in coastal carbon cycling. This thesis also helps to establish a well-constrained method for future studies to examine exports of carbon and other materials from tidal wetlands. Results from this work can help guide sampling protocols for future studies. The development and deployment of high frequency sensors are essential to providing the necessary temporal resolution needed to quantify dynamic inorganic carbon fluxes in coastal areas. These estimates of carbon and alkalinity storage and export will provide the groundwork in monitoring changes and understanding the mechanisms that control carbonate chemistry and inorganic carbon fluxes in the tidal waters of salt marshes.

**References**

Giblin, A. E., G. E. Likens, D. White, and R. W. Howarth. 1990. Sulfur storage and alkalinity generation in New- England Lake-sediments. Limnol. Oceanogr. 35: 852–869. doi:10.4319/lo.1990.35.4.0852

Giblin, A. E., and R. K. Wieder. 1992. Sulfur cycling in marine and freshwater wetlands. In R. W. Howarth, J. W. Stewart, and M. V. Ivanov [eds.], Sulphur cycling on the Continents. SCOPE.

Nuttle, W.K., 1988. The extent of lateral water movement in the sediments of a New England salt marsh. Water Resources Research, 24(12), pp.2077-2085.

Wang, Z. A., and W. J. Cai. 2004. Carbon dioxide degassing and inorganic carbon export from a marsh-dominated estuary (the Duplin River): A marsh CO2 pump. Limnol. Oceanogr. 49: 341-354.

Wang, Z. A., Kroeger, K. D., Ganju, N. K., Gonneea, M. E. and Chu, S. N. 2016. Intertidal salt marshes as an important source of inorganic carbon to the coastal ocean. Limnol. Oceanogr., 61: 1916–1931. doi:10.1002/lno.10347